

## **ABSTRACT**

CROUCH, JUSTIN A. Multi-season Observational Study of the Thermodynamic, Kinematic and Precipitation Structures within Flooding and Typical Storms in the Oregon Cascades. (Under the direction of Dr. Sandra E. Yuter).

During the winter months, extra-tropical cyclones develop over the Pacific Ocean and move across the U.S. Pacific Northwest. The Coastal and Cascade mountain ranges modify the precipitation patterns of these storms leading to enhanced precipitation.

Winter storms affecting the Oregon Cascades from 2003 to 2008 are analyzed. Portland, Oregon operational WSR-88D radar data is utilized to examine the spatial patterns and distributions of precipitation structures over the windward slope of the Cascade Mountains. Data from operational soundings at Salem, Oregon and a vertically pointing MicroRainRadar in Portland are used to analyze the environmental characteristics upwind of the Cascades. Extreme storm events are associated with flooding and mudslides.

The precipitation persistence and intensity were calculated for radar subsets  $\pm 6$  hours of operational sounding launches based on the observed flow characteristics. The sensitivity of precipitation patterns to downslope flow and changing flow characteristics with altitude, as well as the strength of the cross-barrier flow, freezing level altitude, and atmospheric stability is tested. The cross-barrier flow is the most important factor in determining the magnitude of precipitation persistence and intensity along the Cascade windward slope. Two precipitation ‘hotspots’ occurring within our study domain are investigated further and we find that low-level flow convergence due to flow deflection by the Cascades is associated with the precipitation enhancement at both locations.

The conditional probability of flooding is examined based upon the values of single parameters and the combination of multiple parameters. All flooding storms were associated with land-falling atmospheric rivers, deep rain layers, strong cross-barrier flow, and long durations of precipitation. Flow being multi-layered with the presence of shear is shown to have a significant impact on the flooding potential by increasing the precipitation persistence and intensity along the Cascade windward slope. The lower-level flow acts to increase the effective barrier width, by forcing the mid- and upper-level flow to up and over the lower level flow regime. These criteria, however, are not sufficient to lead to flooding. 65% of time periods with these conditions flood over the course of our 5 year dataset. The spatial patterns of the precipitation persistence and intensity provide insight into why some storms with anomalously high values of certain environmental conditions lead to flooding and others do not. Flooding storms had more persistent and intense rainfall occurring upstream of the Cascades compared to non-flooding storms.

Multi-season Observational Study of the Thermodynamic, Kinematic  
and Precipitation Structures within Flooding and  
Typical Storms in the Oregon Cascades

by  
Justin Alan Crouch

A thesis submitted to the Graduate Faculty of  
North Carolina State University  
in partial fulfillment of the  
requirements for the Degree of  
Master of Science

Marine, Earth, and Atmospheric Sciences

Raleigh, North Carolina

2009

APPROVED BY:

---

Matthew Parker

---

Anantha Aiyyer

---

Sandra Yuter  
Chair of Advisory Committee

## **ACKNOWLEDGEMENTS**

I would like to thank my advisor Dr. Sandra Yuter for the opportunity to be a part of this research project. I have learned a tremendous amount, not only about orographic precipitation, but of how to a better research scientist. Thanks to Paul Neiman of NOAA/ESRL for providing dates from his database of land-falling Atmospheric Rivers. I would like to thank Matthew Miller for help with MATLAB programming. Thanks to David Stark, Clay McGee, Kate Rojowsky, and Jay Bozeman for their help processing radar data from the NCDC. I would also like to thank Dr. Matthew Parker and Dr. Anantha Aiyyer for providing feedback on this work and for their instruction in the classroom. This work was funded by National Science Foundation grants ATM-0544766 and ATM-0450444

## TABLE OF CONTENTS

<b>List of Tables</b> .....	vii
<b>List of Figures</b> .....	viii
<b>1 Introduction and Background</b> .....	1
1.1 Motivation .....	1
1.2 Relationship to Previous Work .....	2
1.3 Objectives .....	10
<b>2 Data and Methods</b> .....	12
2.1 Operational Radar Data.....	12
2.2 Operational Sounding Data .....	13
2.3 Terrain Data .....	16
2.4 Domain Selection .....	16
2.5 Radar Calculations– Z Frequencies and Z Frequency Volumes .....	17
2.6 Significance Testing .....	19
2.7 Atmospheric Rivers .....	20
2.8 Flooding Events .....	21
2.9 Vertically Pointing Micro Rain Radar and Derived Rain Layer Depth .....	22
2.10 Visualizations.....	23
2.10.1 Contoured Frequency by Distance Diagrams (CFDDs) .....	23
2.10.2 Cross-Section 75 <sup>th</sup> Percentile Plot .....	25
<b>3 Orographic Precipitation Processes</b> .....	26
3.1 Environmental Parameters .....	26
3.2 Single and Combined Parameter Variability .....	29
3.2.1 Low-Level Down Slope Flow.....	30
3.2.2 Multiple and Single Layer Flows.....	31
3.2.3 Cross-Barrier Wind Speed and Freezing Level Sensitivity .....	35
3.2.4 Cross-Barrier Wind Speed and Stability Sensitivity .....	38
3.3 Local Precipitation ‘Hot Spots’ .....	41
3.3.1 The Lewis River Valley .....	41
3.3.2 Kelso, Washington .....	43
<b>4 Flood Events</b> .....	47
4.1 Storm Scale .....	47
4.2 Combined Conditional Probabilities.....	48
4.3 Spatial Patterns of Precipitation Persistence and Intensity .....	53

<b>5 Conclusions</b> .....	56
<b>Bibliography</b> .....	102
<b>Appendices</b> .....	111
Appendix A.....	112
Appendix B.....	113
Appendix C.....	115

## LIST OF TABLES

Table 1. Total number of winter flooding events reported by the Portland, Oregon National Weather Service forecast office for each winter month from 2003 to 2008 .....	63
Table 2. The 25 <sup>th</sup> , 50 <sup>th</sup> (median), 75 <sup>th</sup> percentiles and mean values of variables calculated from 487 wintertime SLE soundings from 2003 to 2008 .....	64
Table 3. Calculated correlation coefficients of environmental parameters calculated from SLE soundings and radar statistics .....	65
Table 4. The calculated and derived variables from two SLE soundings used to contrast differences in two layer and one layer flow in Figures 13 and 14. The two layer flow case variables are from SLE sounding released March 3, 2007 00Z. The one layer flow case variables are from SLE sounding released March 20, 2007 00Z .....	66
Table 5. Calculated and derived variables from two SLE soundings used to illustrate precipitation hotspots in Figures 19 and 20. The variables are determined from SLE soundings released January 8, 2007 00Z and October 31, 2005 12Z. ....	67
Table 6. Single and combined conditional probabilities of flooding. Number of 12-hour periods meeting certain criteria which flooded and did not flood. The critical success index (CSI) is a skill score used to determine the skill of the flooding probability for each combination of environmental parameters .....	68

## LIST OF FIGURES

- Figure 1. Topography of Portland, Oregon and its surrounding areas (in km altitude). Locations of Coastal and Cascade Ranges, Portland NEXRAD (KRTX) radar, Salem sounding (triangle), Kelso Washington, the Lewis River Valley (LRV), the Willamette Valley, and significant mountain peaks are labeled. The 120 km radar range ring from KRTX is shown in blue. Red box indicates Cascade windward slope study domain.....69
- Figure 2. Conceptual model of the orographic precipitation mechanisms active in MAP cases of (a) unstable unblocked low-level flow, (b) stable blocked low-level flow. The diagrams show the types of hydrometeors present in each case, along with the flow behavior. The dashed box in (a) indicates the position of the embedded convective precipitation. Adapted from Medina and Houze (2003) and Rotunno and Houze (2007). .....70
- Figure 3. Schematic diagram of Alpine-scale orographic flow modifications illustrating (a) the importance of weak stability enabling depicted southerly flow to surmount the tall Alpine barrier instead of flowing around (to the left in the Northern Hemisphere) and (b) effects of Alpine shape in directing southerly flow towards the concavity. Adapted from Rotunno and Houze (2007). .....71
- Figure 4. Average annual precipitation (in inches) for thirty-year (1961 – 1990) climatology of the U.S. Pacific Northwest. The diagram shows enhanced precipitation associated with Coastal (left side) and Cascade (right side) Ranges in the analysis area (From Daly et al. 1994). .....72
- Figure 5. Meridional (North-South) 25<sup>th</sup>, 50<sup>th</sup>, 75<sup>th</sup> percentiles and maximum values of gridded terrain elevation within study domain. Significant terrain features along the Cascade windward slope are indicated. The horizontal lines correspond to the 25<sup>th</sup>, 50<sup>th</sup>, and 75<sup>th</sup> percentiles of the freezing level altitude. ....73

Figure 6. Vertically integrated water vapor (IWV) in mm as measured by SSM/I instruments carried onboard the DMSP series of polar orbiting satellites. Land regions are colored gray where measurements are not valid. The areas colored black is where the satellite did not pass over and no data were collected, areas where data were collected but were determined to be bad, coastal areas, or areas affected by sun glint. (a) IWV measured by SSM/I overpass on November 7, 2006 at 20:30 local time, illustrating a land-falling atmospheric river along the Oregon coast. (b) IWV measured by SSM/I overpass on November 6, 2005 at 08:30 local time, illustrating a possible land-falling atmospheric river with a satellite data gap occurring along the Oregon coast. Images from the Remote Sensing Systems ([www.remss.com](http://www.remss.com)). .....74

Figure 7. Contoured Frequency by Distance Diagram (CFDD) explanation. (a) Persistence ( $Z > 13$  dBZ frequency) horizontal cross-section at 2 km altitude. (b) Histogram of persistence data within the 2 km wide box in 3a. (c) Histogram in 3b in 3-dimensional space with respect to distance from the crest. X-axis is distance from crest, Y-axis is the persistence values, Z-axis is the normalized percent occurrence. (d) Histograms of all data across the study domain in 3a placed into the 3-dimensional variable space. Red histogram is the same as 3c. (e) Histograms colored color-coded by their normalized percent occurrence (Z-axis). (f) Values of Z-axis contoured similar to a topographic map. Color scale indicates the contoured normalized percent occurrence (Z-axis) values. ....75

Figure 8. Scatter plots of environmental variables layer-averaged from the surface to 2.2 km AMSL from all SLE winter storm soundings (487) from 2003 to 2008. Blue lines indicate the 25<sup>th</sup> and 75<sup>th</sup> percentiles of the plotted variable (see Table 1). 12-hour periods when the wind direction was between the 25<sup>th</sup> and 75<sup>th</sup> percentile of the wind direction ( $202^{\circ}$ - $242^{\circ}$ ) are indicated by circular points. Wind directions outside this subset are shown by crosses. Blue markers indicate times when the flow was multi-layered, red shows flooding time periods which were multi-layered, and magenta indicates time periods when the flow was not multi-layered but resulted in flooding. (a) Average wind direction versus average cross-barrier wind speed. (b) Average squared moist Brunt-Vaisala Frequency versus average cross-barrier wind speed. (c) Average cross-barrier wind speed versus freezing level altitude (AMSL). (d) Average wind direction versus IWV. (e) Average cross-barrier wind speed versus average IWV. (f) IWV versus freezing level altitude (AMSL). ....77

Figure 9. Scatter plots of moisture flux and other environmental variables layer-averaged from the surface to 2.2 km AMSL from all SLE winter storm soundings (487) from 2003 to 2008. Blue lines indicate the 25<sup>th</sup> and 75<sup>th</sup> percentiles of the plotted variable (see Table 1). 12-hour periods when the wind direction was between the 25<sup>th</sup> and 75<sup>th</sup> percentile of the wind direction (202°-242°) are indicated by circular points. Red indicates flooding events. (a) Average cross-barrier wind speeds versus moisture flux. (b) Average squared moist Brunt-Vaisala Frequency versus moisture flux. (c) IWV versus moisture flux. (d) Freezing level altitude (AMSL) versus moisture flux. ....79

Figure 10. (a) Scatter plot of SLE sounding derived freezing level and MRR-derived storm maximum rain layer depth. Thin blue lines indicated 25th and 75th percentiles for each variable. (b) Freezing level altitude for all 12 hourly soundings during each storm. Each line is an individual storm. (c) IWV for all 12 hourly soundings during each storm. Each line is an individual storm. Shades of blue indicate not flooding events. Red indicates flooding storms in (a), (b), and (c).....80

Figure 11. Histogram of all storm durations binned in 6 hour increments. Blue indicates non-flooding storms, red indicates flooding storms. ....82

Figure 12. Radar composite of 12-hour periods with average downslope flow. Blue lines indicate 35 km and 65 km distance from the crest. Median terrain elevation is shown for reference. (a) Horizontal cross-section of precipitation persistence at 2 km altitude. (b) CFDD of persistence at 2 km altitude. (c) Cross-section of 75<sup>th</sup> percentile values of persistence. (d) Horizontal cross-section of precipitation intensity at 2km altitude. (e) CFDD of intensity at 2 km altitude. (f) Cross-section of 75<sup>th</sup> percentile values of intensity. ....83

Figure 13. (a) Average cross-barrier wind speed from the surface to 1.2 km altitude versus average cross-barrier wind speed from 1.2 km to 2.2 km altitude measured by SLE soundings. Red markers indicate flooding events. The black line shows the 1-to-1 relationship. (b) Histogram of the differences between the average cross-barrier wind speed below 1.2 km and between 1.2 km and 2.2 km. Blue line indicates the 80th percentile of the distribution at 10 m/s. All samples to the right of the blue line are defined as two-layered flow regimes.. ....84

Figure 14. Layer averages of cross-barrier wind speed using 500 m thick and near 1000 m thick layers. (a) Cross-barrier wind speed averages for 500 m thick layers from the surface to 2.2 km for soundings that do not have defined multi-layered flow. This highest layer average is only 200 m thick. (b) Cross-barrier wind speed average for two layers, bottom layer is from the surface to 1.2 km, and the upper layer is from 1.2 km to 2.2 km altitude, for soundings that do not have defined multi-layered flow. (c) Same as (a) for soundings that do have defined multi-layered flow. (d) Same as (b) for soundings that do have defined multi-layered flow .....	85
Figure 15. (a) Histogram of the average Brunt Vaisala Frequency from the surface to 1.2 km AMSL. Red indicates multi-layered flow cases. (b) Layer average differences in average Brunt-Vaisala Frequency from the surface to 1.2 km AMSL and 1.2 km to 2.2 km AMSL. Red indicates multi-layered flow cases .....	86
Figure 16. Radar composite of 12-hour period illustrating patterns associated with 2 layer flow. Data from the period $\pm$ 6 hours from the SLE released March 3, 2007 00Z. (a) Horizontal cross-section of precipitation persistence at 2 km altitude. (b) CFDD of persistence at 2 km altitude. (c) Cross-section of 75 <sup>th</sup> percentile values of persistence. (d) Horizontal cross-section of precipitation intensity at 2km altitude. (e) CFDD of intensity at 2 km altitude. (f) Cross-section of 75 <sup>th</sup> percentile values of intensity .....	87
Figure 17. Radar composite of 12-hour period illustrating patterns associated with single layer flow. Data from the period $\pm$ 6 hours from the SLE released March 20, 2007 00Z. (a) Horizontal cross-section of precipitation persistence at 2 km altitude. (b) CFDD of persistence at 2 km altitude. (c) Cross-section of 75 <sup>th</sup> percentile values of persistence. (d) Horizontal cross-section of precipitation intensity at 2km altitude. (e) CFDD of intensity at 2 km altitude. (f) Cross-section of 75 <sup>th</sup> percentile values of intensity .....	88

Figure 18. Radar composites of 12 hour periods  $\pm$  6 hours from SLE soundings testing the sensitivity of precipitation persistence on derived freezing level and cross-barrier wind speed values. The median terrain elevation is shown for reference. (a) Horizontal cross-section at 2 km altitude for 12-hour periods with freezing level and cross-barrier wind speed greater than their 75<sup>th</sup> percentiles. (b) CFDD at 2 km altitude using same 12-hour periods as (a). (c) Cross-section of 75<sup>th</sup> percentiles using same 12-hour periods as (a). (d) Horizontal cross-section at 2 km altitude for 12-hour periods with freezing level less than the 25<sup>th</sup> percentile and cross-barrier wind speed greater than the 75<sup>th</sup> percentile. (e) CFDD at 2 km altitude using same 12-hour periods as (d). (f) Cross-section of 75<sup>th</sup> percentiles using same 12-hour periods as (d). (g) Horizontal cross-section at 2 km altitude for 12-hour periods with freezing level greater than the 75<sup>th</sup> percentile and cross-barrier wind speed less than the 75<sup>th</sup> percentile (h) CFDD at 2 km altitude using same 12-hour periods as (g). (i) Cross-section of 75<sup>th</sup> percentiles using same 12-hour periods as (g). .....89

Figure 19. Same as figure 15 with calculated precipitation intensity. ....91

Figure 20. Radar composites of 12 hour periods  $\pm$  6 hours from SLE soundings testing the sensitivity of precipitation persistence on derived squared moist Brunt-Vaisala frequency and cross-barrier wind speed values. The median terrain elevation is shown for reference. (a) Horizontal cross-section at 2 km altitude for 12-hour periods with the squared moist Brunt-Vaisala frequency and cross-barrier wind speed greater than their 75<sup>th</sup> percentiles. (b) CFDD at 2 km altitude using same 12-hour periods as (a). (c) Cross-section of 75<sup>th</sup> percentiles using same 12-hour periods as (a). (d) Horizontal cross-section at 2 km altitude for 12-hour periods with the squared moist Brunt-Vaisala frequency less than the 25<sup>th</sup> percentile and cross-barrier wind speed greater than the 75<sup>th</sup> percentile. (e) CFDD at 2 km altitude using same 12-hour periods as (d). (f) Cross-section of 75<sup>th</sup> percentiles using same 12-hour periods as (d). (g) Horizontal cross-section at 2 km altitude for 12-hour periods with the squared moist Brunt-Vaisala frequency greater than the 75<sup>th</sup> percentile and cross-barrier wind speed less than the 75<sup>th</sup> percentile (h) CFDD at 2 km altitude using same 12-hour periods as (g). (i) Cross-section of 75<sup>th</sup> percentiles using same 12-hour periods as (g). .....92

Figure 21. Same as figure 17 with calculated precipitation intensity. ....94

Figure 22. Radar composite of single 12-hour period  $\pm$  6 hours from the SLE released January 8, 2007 00Z illustrating precipitation enhancement over the Lewis River Valley. Black box indicates area of the Lewis River Valley (a) Horizontal cross-section of the median radial velocity at 1 km altitude. The red arrows indicate airflow direction. (b) Horizontal cross-section of precipitation persistence at 1 km altitude. (c) Horizontal cross-section of precipitation intensity at 1 km altitude. ....95

Figure 23. Radar composite of single 12-hour period  $\pm$  6 hours from the SLE released October 31, 2005 12Z illustrating precipitation enhancement over Kelso, Washington. Black box indicates area of Kelso, Washington (a) Surface winds (knots) at 15Z on October 31, 2005 in the Pacific Northwest (b) Horizontal cross-section of the median radial velocity at 1 km altitude. The red arrows indicate airflow direction. (c) Horizontal cross-section of precipitation persistence at 1 km altitude. (d) Horizontal cross-section of precipitation intensity at 1 km altitude. ....96

Figure 24. Scatter plots of SLE cross-barrier wind speed and freezing level versus storm volumes per hour. 12-hour periods when the wind direction was between the 25<sup>th</sup> and 75<sup>th</sup> percentile of the wind direction (202°-242°) are indicated by circular points. Wind directions outside this subset are shown by crosses. Red markers indicate times when flooding occurred. (a) Cross-barrier wind speed versus storm volume per hour of Z > 13 dBZ. (b) Freezing level versus storm volume per hour of Z > 13 dBZ. (c) Same as (a) with storm volume per hour of Z > 25 dBZ. (d) Same as (b) with storm volume per hour of Z > 25 dBZ. ....97

Figure 25. Single and combined conditional probabilities of flooding. Each point is associated with a pie chart, the darker shade of grey and number indicate the probability of flooding with that condition. Each pie chart at a vertex indicates the probability of flooding when the single variable it represents exceeds the stated threshold. The top vertex represents periods when the cross-barrier flow is greater than its 75<sup>th</sup> percentile (10.5 m/s). The bottom left vertex represents periods when the freezing level is greater than its 75<sup>th</sup> percentile (2130 m). The bottom right vertex represents periods when the storm duration is greater than 24 hours. Each side represents the probability of flooding when both conditions of the adjacent vertices are true. The center pie chart represents the probability of flooding when all three conditions are met. The bottom outlying vertex represents the probability when all three conditions are met and flow measured by the SLE sounding is two-layered.....98

Figure 26. Same as Figure 25, showing critical score index (CSI) for environmental condition .....99

Figure 27. Radar composite of 12-hour periods that did not flood and were associated with cross-barrier winds and freezing level greater than their 75<sup>th</sup> percentiles and having storm durations greater than 24 hours. The median terrain elevation is shown for reference. (a) Horizontal cross-section of precipitation persistence at 2 km altitude. (b) CFDD of precipitation persistence at 2 km altitude. (c) Cross-section of 75<sup>th</sup> percentile values of persistence. (d) Same as (a) for precipitation intensity. (e) Same as (b) for precipitation intensity. (f) Same as (c) for precipitation intensity .....100

Figure 28. Same as Figure 23, for 12-hour periods that did flood and were associated with cross-barrier winds and freezing level greater than their 75<sup>th</sup> percentiles and having storm durations greater than 24 hours. The median terrain elevation is shown for reference. ....101

# Chapter 1

## Introduction and Background

### 1.1 Motivation

During the winter months, extra-tropical cyclones form over the Pacific Ocean and move across the Western United States. When these extra-tropical cyclones make land-fall along the West Coast their kinematic and microphysical structures are modified by the mountainous terrain. In the states of Washington and Oregon in the U.S. Pacific Northwest, the windward slopes of the Coastal and Cascade mountain ranges enhance storms, and lead to prolonged precipitation events in the region. Narrow channels of moisture in the lower troposphere associated with land falling cyclones, often called atmospheric rivers (ARs), transport large amounts of moisture to the West coast, playing a critical role in precipitation climatology in the region. ARs form due to local moisture convergence along baroclinic fronts and sometimes transport moisture from the tropics to the mid-latitudes (Bao et al. 2006; Neiman et al. 2008). The large influx of moisture associated with an AR can initiate and fuel orographic precipitation along the Coastal and Cascade Mountains (Zhu and Newell 1998; Neiman et al. 2008; Smith et al. 2009).

This study focuses on the Portland, Oregon area in the Willamette Valley of the Pacific Northwest (Fig. 1) which is prone to orographic precipitation and landfalling ARs (Stoelinga et al. 2003; Neiman et al. 2008). Some precipitation events in the Oregon

Cascades can become very intense and lead to heavy rainfall with flooding and mudslides. Accurate heavy precipitation forecasts for single-storm flood events and water resource management have far reaching socio-economic impacts. If a forecaster is better equipped to recognize the environmental variables that are more likely to lead to flooding, the public and local governments can be better prepared. It is also important to understand the potential impacts of future climate change on long-term regional precipitation patterns and hydrology. By examining precipitation events over multiple seasons, this study provides insight into the environmental controls of orographic precipitation during intense and more typical storms.

### 1.2.1 Relationship to Previous Work

In orographic flow studies, the atmospheric stability is an important parameter, usually measured by calculating the squared Brunt-Väisälä frequency (Durrán and Klemp 1982). The Brunt-Väisälä frequency indicates at what frequency a displaced air parcel will oscillate when subjected to an infinitesimal perturbation in a stably stratified atmosphere. For this study we assume the atmosphere is saturated (RH=100) because it is precipitating and use the squared moist Brunt-Väisälä frequency ( $N_m^2$ ) equation from Durrán and Klemp (1982):

$$N_m^2 = \frac{g}{T} \left( \frac{dT}{dZ} + \Gamma_m \right) \left( 1 + \frac{Lq_s}{RT} \right) - \frac{g}{1+q_w} \frac{dq_w}{dz} \quad (1)$$

where  $g$  is gravitational acceleration ( $9.8 \text{ ms}^{-2}$ ),  $T$  is the sensible temperature,  $Z$  is the altitude,  $\Gamma_m$  is the moist adiabatic lapse rate,  $L$  is the latent heat of vaporization,  $q_s$  is the saturation mixing ratio,  $R$  is the ideal gas constant, and  $q_w$  is the total water mixing ratio. In orographic flow applications, it is convenient to think of the stability as a measure of how easily an air parcel can be displaced vertically when it encounters a barrier. Negative  $N_m^2$  values indicate unstable flow, positive values indicate stable conditions, and values near zero are neutrally stable. The more stable an environment, the more energy it takes to vertically displace an air parcel. Multiple layered flows can have different stabilities at different altitudes (Rotunno and Ferretti 2001; Houze and Medina 2005).

The Froude number is a non-dimensional parameter used to determine if a flow has enough energy to rise over a barrier. It takes into account the atmospheric stability ( $N_m$ ), cross-barrier wind speed ( $U$ ), and mountain height ( $h$ ).

$$F_r = \frac{U}{N_m h} \quad (2)$$

The Froude number measures to what extent terrain blocking will occur, and does not exist for unstable flows ( $N_m^2 < 0$ ). A high Froude number ( $F_r > 1$ ) indicates flow will more easily rise over the barrier, while  $F_r < 1$  flows will tend to be blocked and deflected around the obstacle. Flows can be blocked to different extents with complete blockage and deflection possible or only minor deflection occurring depending on the Froude number. Flow at different levels can have different Froude numbers depending on the vertical

profile of the cross-barrier wind speed and stability, leading to blockage occurring to different degrees at different altitudes. Low-level flow with  $F_r < 1$  can have a higher Froude flow aloft causing possible flow reversal at lower altitudes, and cross barrier flow above (Fig. 2). The region between the two flow regimes can have intense shear and turbulence (Houze and Medina 2005). The Froude number is also an indicator if a mountain gravity wave will form (Colle 2008, Reinecke and Durran 2008). Higher wind speeds and more static stability ( $Fr > 1$ ) will favor the development of a mountain wave.

The California Land-Falling Jet Experiment (CALJET) and the Pacific Land-Falling Jet Experiment (PACJET) examine the impacts of landfalling ARs on the precipitation along the U.S. West Coast (Neiman et al. 2002; Neiman et al. 2004; Ralph et al. 2003; Ralph et al. 2004; Ralph et al. 2005; Bao et al. 2006; Smith et al. 2009). Neiman et al. (2002) found a linear relationship between the upslope flow and the magnitude of the rain rate, or intensity of rainfall, over California's coastal mountain ranges during landfalling ARs. This correlation was more evident when flow was unblocked. Blocking caused the low-level flow to become deflected from cross-barrier to barrier parallel, decreasing the cross-barrier component of the wind, and limiting orographic enhancement. Neiman et al. (2008) used the polar orbiting Special Sensor Microwave Image (SSM/I) satellite and the NCEP-NCAR reanalysis dataset to examine eight years of water vapor transport along the U.S. West Coast. Pacific Northwest climatology indicates that most precipitation falls during the winter months (Guirguis and

Avissar 2008a,b). Strong extra-tropical cyclones during the winter, with saturated low-levels and strong cross-barrier flow, lead to greater moisture flux and more precipitation in the region (Neiman et al. 2008).

Two recent field campaigns have addressed the issue of orographic precipitation: The Mesoscale Alpine Programme (MAP) (Bougeault 2001; Medina and Houze 2003 [MH2003 from here]; Medina et al. 2005; Rotunno and Houze 2007) and the Improvement of Microphysical Parameterization through Observational Verification Experiment II (IMPROVE-2) (Stoelinga et al. 2003; Colle et al. 2005; Garvert et al. 2005; Medina et al. 2007). Case studies and simulations of events during these field campaigns have increased the understanding of the physical mechanisms associated with orographic precipitation, and refined orographic precipitation theory.

The MAP field campaign took place along the southern windward slope of the Alps, in the Lago Maggoire Region. Storms in this area tend to have environments that range from stable to slightly unstable (Houze et al. 2001). MH2003 examined two MAP intense observation periods (IOP). IOP8 was characterized by strong stability and upstream blocking, while IOP 2b was unstable with strong cross-barrier flow at all levels. During IOP 2b, the unblocked flow resulted in convective precipitation over the first ridge with large amounts of cloud liquid water and graupel, as confirmed by dual-polarimetric radar. Embedded convective cells during IOP 2b, led to heavy precipitation. IOP 8 had flow reversal at the lowest levels, effectively changing the shape of the barrier.

The stratiform precipitation occurring along the windward slope extended upstream of the barrier due to the low level blocking (MH 2003; Rotunno and Houze 2007) (Fig. 2). Above the layer of down slope winds, unblocked, strong cross-barrier flow easily rose over the terrain. The turbulent overturning in the shear region between the two flows enhanced precipitation upstream of the barrier along the windward slope (Houze and Medina 2005).

The IMPROVE-2 field study focused on the US Pacific Northwest, and examined frontal-systems making landfall during the winter season. The campaign utilized an extensive set of observational platforms. An intense storm during the field campaign on December 13-14, 2001 had anomalously high precipitation falling over the Cascades and has been the subject of several case studies (Colle et al. 2005; Garvert et al. 2005ab; Woods et al. 2005). Gravity waves along the Cascades were indicated by upwind tilting of maximum reflectivity structures preceding a dip in potential temperatures. Gravity waves enhance vertical motions and precipitation along the windward slope (Medina et al. 2007; Colle 2008). Precipitation along the windward slope was also enhanced by warm air advection aloft, friction, blocking, and non-linear interactions between the flow and topography during the December 13-14 storm (Garvert et al. 2007). These mechanisms can play varying roles in precipitation enhancement and be present to different degrees during any given storm (Garvert et al. 2007).

Rotunno and Ferretti (2001) used an idealized 3-D simulation to understand the role of airflow convergence during a flooding orographic precipitation event along the Southern Alps. The shape of the southern edge of the Alpine barrier resembles the letter ‘L’ and flow will tend to converge into the concave structure (Rotunno and Ferretti 2001; Rotunno and Houze 2007) (Fig. 3). The moisture content of the flow will affect the degree of deflection ahead of a barrier due to the impacts of saturation on stability (Durran and Klemp 1982; Rotunno and Ferretti 2001). When flow is blocked, it slows and deflects to the left in the Northern Hemisphere due to a decrease in the Coriolis force. The case studied by Rotunno and Ferretti (2001) had a moisture gradient along the windward slope. Saturated flow lifted over the barrier with minimal deflection because of increased latent heating destabilizing the atmosphere. The unsaturated air deflected to the left, undercutting the non-deflected air, affectively changing the shape of the barrier. The two flows converge at the focal point of the terrain concavity, creating additional atmospheric lift along the windward slope (Fig. 3). The location of the convergence coincided with higher rain rates and a longer duration of rainfall in radar observations and simulations.

Colle (2004) conducted 2-D idealized numerical simulations to study the effects of mountain width and height, ambient flow, moist static stability, and freezing level height on orographic precipitation. Increasing the wind speed caused heavier precipitation upwind of the mountain, and enhanced the signature of a gravity wave near

the peak. Colle (2004) also found that freezing level plays an important role in precipitation production along the windward slope. Higher freezing levels produced less precipitation spill-over into the leeside, and thus higher precipitation efficiency within liquid phase (warm rain) precipitation processes. On the windward slope precipitation production increases more rapidly with increasing wind speeds for higher freezing levels. Simulations with low freezing levels had precipitation maximums closer to the crest compared to the higher freezing level simulations.

Colle (2008) examined the affects of small scale ridges on precipitation distribution along a broad mountain slope using idealized 2-D simulations. Past studies (Medina and Houze 2003; Garvert et al. 2007) have indicated that narrow ridges can enhance precipitation locally along a windward slope. Increasing the number of small ridges increases the net precipitation because gravity waves develop over each ridge and increase the local vertical motion. More precipitation was produced during unstable simulations since. Increasing the number of ridges had a greater impact when the freezing level was high because precipitation growth occurred through the efficient mechanism of collision-coalescence over a greater area of the windward slope. These simulations use a finer grid resolution than Colle (2004). Both studies agree that low freezing levels yield precipitation maximums close to the crest for a single ridge. As the number or ridges along the windward slope were increased, the precipitation maximum shifted lower on

the windward slope. The addition of ridges lower on the windward slope depletes moisture from the flow and less moisture is available for precipitation further upslope.

Panziera and Germann (2009)[PG2009 from here], examined the importance of the upstream dynamic and thermodynamic conditions on orographic precipitation in the same study region as MAP using multi-year observations from the Monte Lema radar. Low level wind velocity, compared to stability and upper level flow, was the most significant factor in regulating the intensity of rainfall ahead of the barrier. The mid-level flow velocity regulated the rainfall intensity along the windward slope. Yuter et al. (2009) conducted sensitivity tests using a multi-year observational dataset along the Cascades. Using a narrow wind direction subset, within  $33^\circ$  azimuth, the sensitivity of precipitation patterns to a range of flow characteristics (freezing level, stability, and cross-barrier wind speed) were examined. In the Cascades, cross barrier wind speed had the greatest impact on the persistence of precipitation, while the freezing level impacted the intensity of precipitation (Yuter et al. 2009). Rainfall frequencies were larger over the Alpine terrain in unstable and neutral conditions compared to stable flow (PG2009), but such a pattern was not as evident along the Oregon Cascades (Yuter et al. 2009). In both studies, the stability played a minor role in upstream precipitation enhancement, different from the MH2003 schematic derived from MAP (PG2009; Yuter et al. 2009).

Flooding in the Pacific Northwest during the winter months is of particular concern. Neiman et al. (2008) discussed the impacts ARs on flooding along the

mountains of the US West Coast. ARs are associated with higher temperatures because of their location within the warm-sector of storms (Bao et al. 2006, Neiman et al. 2008). The warmer temperatures lead to a higher flooding potential related to a higher freezing level and rain, instead of snow, falling over a greater area. Nearly twice as much rain fell when ARs made landfall along the West Coast compared to non-AR rain events (Neiman et al. 2008). Storms which are warmer and have a deeper rain layer produce rainfall over a larger geographic area, especially in mountainous areas. More rainfall at higher elevations produces more runoff, and a higher flooding potential. Although it is raining upon snow at high elevations, the fate of the rain and snowpack is a function of temperature (Lundquist et al. 2008). Direct observations in the Sierra Nevada Mountains by the U.S. Army Corps of Engineers (1956) show that for surface temperatures above 3.0° C the likelihood that rain will melt a snowpack is greater than 60%. Between 0° C and 3.0° C, the rainfall will either filter through the snowpack and runoff, or freeze and add to the snowpack. The closer the temperature is to freezing, the higher probability the rain falling on snow will freeze (Lundquist et al. 2008).

### **1.3 Objectives**

Case studies of orographic precipitation events may not be representative of more typical characteristics over extended periods of time (Neiman et al, 2002, Yuter et al. 2009). This study examines a multi-year dataset of winter storms and their environmental conditions along the windward slope of the Oregon Cascades. Our goal is to:

- (1) Examine the impacts of changing flow characteristics on the spatial patterns and distributions of precipitation persistence and intensity along Cascade windward slope.
- (2) Investigate why certain regions in the Willamette Valley preferentially experience precipitation enhancement.
- (3) Demonstrate that high values of certain environmental variables and the combination of variables increase the probability flooding. Use physical reasoning to explain why certain environmental conditions are more favorable for heavy rainfall and flooding to occur.

## Chapter 2

### Data and Methods

Over 2.5 m of precipitation falls along the Cascade and Coastal ranges in the Pacific Northwest annually (Daly et al. 1994). Portland, Oregon is located in the Willamette Valley, which stretches from north to south between the Coastal Range (0.8-1.0 km crest elevation) to the west and the Cascade Range (1.5-3.0 km crest elevation) to the east (Fig. 1). The majority of Portland's annual rainfall occurs during the winter months (Cayan and Roads 1984, Guirguis and Avissar 2008). This study will focus on precipitation events during the period between 1 November and 31 March (with a few exceptions occurring a few days before or after).

#### 2.1 Operational Radar Data:

A storm day is defined as a day that the Portland airport received at least 5 mm of precipitation or a day that surrounds a 5 mm rainfall day and received at least 2.5 mm, a method similar to James and Houze (2005). We define 329 storm days between November 2003 and March 2008 for the Portland region.

For each storm day, operational radar data from the Portland Next Generation Radar (NEXRAD) (Fig. 1) Weather Surveillance Radar 88-Doppler (WSR-88D)(KRTX) located at 45.710° N -122.959° W and 0.479 km elevation were obtained from the National Climatic Data Center (NCDC). The WSR-88D Level II data were converted to

Universal Format (Barnes 1980), and quality control was applied to reduce non-meteorological echo such as ground clutter and anomalous propagation. Data were then processed to dealias radial velocities (James and Houze 2001) and interpolated to a 3-D Cartesian grid utilizing NCAR Earth Observing Laboratory's REORDER software with Cressman weighting (radius of influence settings: azimuth radius 1.1 degrees and z radius = 1 km). The interpolation grid was 120 km x 120 km x 16 km with 2 km spatial resolution in the horizontal and 1 km resolution in the vertical. The data were converted into Unidata's Network Common Data Format (NetCDF) for display in MountainZebra (James et al. 2000) and statistical analysis in Matlab. MountainZebra was used to refine the storm start and end times to the nearest 15 minutes by determining when storm echo entered and exited the radar domain. The duration of each storm was recorded. Using this technique, 193 storms were identified over the five year period with 49,885 (~6 minutes) radar volumes processed. Individual storm durations ranged from a few hours to several days.

## **2.2 Operational Sounding Data:**

Operational upper air soundings are released every 12 hours (0 UTC and 12 UTC) from Salem, OR (SLE) which is located 75 miles south of Portland in the Willamette Valley (Fig. 1). Soundings were evaluated during defined storm time periods and used to represent the periods  $\pm 6$  hours from the sounding launch time. The layer averages (Reinecke and Durran 2008) of sounding parameters (cross-barrier wind speed, wind

direction, stability) were calculated from the 1010-770 mb, which corresponds to the surface elevation at Salem of 0.061 km AMSL to 2.2 km AMSL. The freezing level altitude and vertically integrated water vapor were also calculated for each sounding.

The Froude number (eqn. 2) is calculated using an average crest height ( $h$ ) of 1.8 km. The cross barrier wind speed ( $U$ ) is defined as the component of the wind from the 270° azimuth, roughly perpendicular to the barrier.

The vertically integrated water vapor (IWV) is calculated for the entire column of the atmosphere measured by the sounding. Most (~75%) of moisture in the atmosphere is confined to the lowest 2.5 km (Neiman et al. 2008). The IWV is calculated using:

$$IWV = \frac{1}{g} \int_{p_1}^{p_2} q_w dp \quad (3)$$

Where  $g$  is the gravitational acceleration,  $p_1$  and  $p_2$  are the pressure layer bounds,  $q_w$  is the mixing ratio, and  $p$  is the pressure.

The layer moisture flux is calculated by using equation (3) from Smith et al. (2009):

$$Q_{flux} = \frac{1}{g} \int q_v V_n dp \quad (4)$$

Where  $g$  is the gravitational acceleration,  $q_v$  is the layer average water vapor mixing ratio,  $V_n$  is the layer average cross-barrier wind component, and  $p$  is the pressure.

Our layer averages of variables assume a single flow regime impinging upon the Cascade windward slope. To examine the implications of a multi-layered flow, we calculated the stability, wind direction, cross-barrier wind speed, and Froude number for the SLE soundings below 1.2 km AMSL, and above 1.2 km AMSL up to 2.2 km AMSL. We determine if a flow is two layered by looking at the distributions of the differences of values between the lower altitude and upper altitude sounding variables. If the difference is greater than the 80<sup>th</sup> percentile of all differences for that variable, we define the sounding as a two-layered flow regime. A single layer flow has a difference less than the 20<sup>th</sup> percentile of all differences for that particular variable.

The freezing level of the atmosphere was calculated by determining the first altitude within the sounding when the temperature fell below 0°C, and then linearly interpolating to 0°C using the temperature measurement at the next lowest altitude to the sub-freezing reading. The assumption of a linear lapse rate holds well over short vertical distances in the atmosphere.

In a method similar to Yuter et al. (2009), the 2003-2008 winter storms were subdivided into 487 twelve hour periods  $\pm$  6 hours from the sounding times of 0 UTC and 12 UTC. The periods were grouped into subsets by wind direction, cross-barrier wind speed, stability, freezing level height, moisture content, and whether the 12 hour period was associated with a flooding event or not. If a storm did not persist for the entire 12

hours, only the portion with radar echo was used in the associated calculations. Little over half (52%) of the 12 hour periods had radar echo for the entire 12 hour period.

### **2.3 Terrain Data**

We use thirty second digital elevation data from the Defense Mapping Agency and National Aeronautics and Space Administration (NASA) to provide a reference for precipitation enhancement to terrain features. Using terrain data cropped to a 120 km by 120 km square centered on KRTX, we calculate the meridional (north-south) 25<sup>th</sup>, 50<sup>th</sup>, 75<sup>th</sup> percentiles, and maximum values to determine how the terrain changes from west to east across the Coastal Range, Willamette Valley, and along the Cascades (Fig. 5). This provides information on how much the terrain varies at a given location.

### **2.4 Domain Selection:**

The study domain corresponds to the windward slope of the Cascades and overlaps with the northern portion of the IMPROVE-II study area. Domain selection is based on the need to use the highest quality radar observations. WSR-88D radar data beyond 120 km range has an effective beam width greater than 2 km and is larger than our interpolated grid resolution. This distance will be the maximum data range considered from KRTX. Some mountain peaks in the region cause radar beam blockage and subsequent loss of data. The median terrain elevation peaks about 100 km east of KRTX, and corresponds to the location of the Cascade crest. The crest will be defined as

the eastern boundary of our domain because beyond the crest there is significant beam blockage. The Coastal Range also significantly blocks the radar beam beyond 30 km west of KRTX, and this distance will define the western extent of our domain. The east-west extent of the domain is 130 km (123.36° W to 121.66° W) and the north-south extent is 240 km (46.76° N to 44.6° N) (Fig. 1).

## **2.5 Radar Calculations – Z Frequencies and Z Frequency Volumes**

During any given storm affecting the Pacific Northwest, the altitude of the freezing level can vary by more than 1.5 km, especially when there is a frontal passage (Medina et al. 2007). The changing altitude of the bright band makes accurately estimating rain-rate from reflectivity when the freezing level is shallow highly uncertain (Yuter 2003). Previous studies (Houze et al. 2001; James and Houze 2005; Medina et al. 2007) have used mean reflectivity of storms. The high reflectivity values of the bright band would skew means to higher values and could be misinterpreted as terrain enhancement of precipitation (Yuter et al. 2009). Following Yuter et al. (2009), this study uses exceedence frequencies of reflectivity to limit the affects of the bright band on our analysis. James and Houze (2005) used a 13 dBZ threshold to examine the frequency and intensity of precipitation in Northern California. This study will use 13 dBZ (rain rate of  $\sim 0.2 \text{ mmhr}^{-1}$ ) and 25 dBZ (rain rate of  $\sim 1.3 \text{ mmhr}^{-1}$ ) as exceedence frequency thresholds (Hagen and Yuter, 2003).

Matlab is used to calculate the exceedence frequency of radar reflectivity ( $Z$ ), using afore mentioned thresholds of  $Z \geq 13$  dBZ ( $Z_{13}$ ) and  $Z \geq 25$  dBZ ( $Z_{25}$ ). The exceedence frequencies are calculated by examining each data pixel and determining the ratio of occurrences that the measured dBZ values exceeded the threshold to the total number of radar volumes. Each ratio was multiplied by 100 to obtain the exceedence frequency percentage. Pixels with  $Z_{13} < 20\%$  are set to missing in all calculations and cross-sections. These regions have small sample sizes due to terrain blockage, lack of adequate radar coverage, or do not experience much echo.

Rainfall accumulation in the Willamette Valley and surrounding mountains is important for hydrological applications. Rainfall accumulation ( $A$ ) can be represented as the summation of rain rates ( $R$ ) and duration ( $t$ ) at a given location (Rotunno and Ferretti 2001; Yuter et al. 2009)

$$A = \sum_i R_i t_i \quad (5)$$

$R$  is typically not steady state and in the Portland region we cannot obtain  $R$  directly from radar measurements. We use the exceedence frequency of  $Z \geq 13$  dBZ to represent the duration, or persistence, of rainfall for a given period (PG2009, Yuter et al. 2009).

The  $Z_{25}$  values are used in conjunction with the  $Z_{13}$  values as a ratio ( $Z_{25}:Z_{13}$ ) to represent the relative precipitation intensity (Yuter et al. 2009). The calculation provides a number between zero and one; 0 meaning that for the times that a pixel had  $Z$

$\geq 13$  dBZ, it never exceeded  $Z \geq 25$  dBZ, and 1 meaning that for every time the pixel had  $Z \geq 13$  dBZ it also always exceeded  $Z \geq 25$  dBZ.

Using radar data within our defined study domain, we created composites of Z13, and the Z25:Z13 ratio. The 12 hour periods and their associated radar volumes were further subsetted based on IWV, freezing level, cross-barrier wind speed, and stability measured by the associated sounding. Radar radial velocity statistics were not able to be calculated due to an error with the KRTX radar during the 2006-2007 winter season. Each composite is radially masked within 25 km of the radar location, and beyond 120 km. The scan geometry of the WSR-88D causes data gaps within 25 km of the radar. Each composite is also cropped to the dimensions of the study domain defined above.

To measure storm scale, the storm precipitation volume per hour (Yuter et al. 2009) within the defined study domain was calculated. The total number of pixels of Z13 and Z25 for each 12 hour set of radar volumes was calculated, summed, and divided by the number of hours of radar echo. The number was multiplied by 4 (each radar pixel is 2 km x 2km x 1km) to represent the storm total volume in  $\text{km}^3$  per hour.

## **2.6 Significance Testing**

Kelso, WA, located due north of KRTX, and the Lewis River Valley, situated northeast of KRTX, frequently experience persistent and intense precipitation (Fig. 1). Two 12-hour periods with enhanced precipitation over these locations were selected to

investigate the underlying physical mechanisms leading to the precipitation. This is further discussed in Chapter 3.3. To determine to what extent the high values of precipitation persistence and intensity during these 12-hour periods are significant, a Monte Carlo simulation was run. A box 20 km by 20 km over Kelso, and another box 22 km (east-west) and 20 km (north-south) over the Lewis River Valley were selected within the radar domain. For the 2 twelve hour periods, the median persistence and intensity were calculated at each location at 2 km altitude. The Monte Carlo simulation was run with 10,000 iterations of 12-hour periods within our radar dataset. Each of the iterations calculated the median persistence and intensity at 2 km altitude within each box.

## **2.7 Atmospheric Rivers**

Atmospheric rivers making landfall along the Pacific Northwest have important implications on rainfall in the region and the potential for flooding. Neiman et al. 2008, defines a landfalling atmospheric river (AR) as being a narrow (<1000 km wide) and long (>~2000 km) plume of moisture, with IWV > 2 cm, making contact with the coast for both the morning and evening overpass of the SSM/I satellite sensor. Paul Neiman provided dates from his dataset of land-falling atmospheric rivers along the US Pacific Northwest and British Columbia (41.0°N to 52.5°N) during the 2003-2008 water years. Some of the ARs described by Neiman make landfall north or south of our domain, and do not directly affect our region of study. We examine all 12-hour periods which had IWV > 2 cm from the SLE sounding site. Nearly half agreed with Neiman's list of ARs

making landfall in the Pacific Northwest (Fig. 6a). To investigate the discrepancy, we examined the daily SSM/I imagery using the Remote Sensing System's (REMSS) online satellite data viewer. Almost all (98%) of the periods with IWV > 2 cm were associated with a plume of moisture appearing to make landfall along the Pacific Northwest coast. Neiman's rigorous criterion of an AR making landfall excludes many plumes of moisture. The most common cause of the discrepancy is data gaps occurring over the US West Coast due to the orbit path and swath width of the SSM/I IWV measurement. In the cases with IWV > 2 cm at SLE and a data gap over the region, plumes of moisture over the ocean can be visually interpolated to the coast (Fig. 6b). In these cases, Neiman erred on the side of caution and did not include these events in his dataset. Some other reasons found for the discrepancy: some plumes do not continuously make landfall for the morning and evening SSM/I overpass, some plumes are wider than the 1000 km width criteria, and IWV values at SLE can remain high after an AR has dissipated over the ocean.

## **2.8 Flooding Events**

Eleven winter flooding events from 2003-2008 were identified by the National Weather Service office located in Portland within their county warning area. A flooding event was reported when significant flooding occurred in urban regions, and several rivers/streams had flows above their flood stage. We designate a twelve hour period as flooding if it overlaps with a day that the NWS reported as a flooding event. 43 (8%) of

the 12-hour periods were identified as flooding. Most (73%) occurred during November and December, early in the winter season (Table 1).

## **2.9 Vertically Pointing Micro Rain Radar and Derived Rain Layer Depth**

Data are utilized from a deployed METEK Micro Rain Radar (MRR) at the Portland National Weather Service forecast office, next to the Portland airport (Fig. 1). MRR information is available after November 2005. The MRR is a vertically pointing Ku-band Doppler radar and provides information on reflectivity and velocity of falling precipitation (Peters et al. 2005). The MRR measurements are averaged every minute, with vertical resolution of 150 m up to 5 km altitude. The velocity of falling precipitation provides information on the phase (frozen vs. liquid) of the hydrometeors. The gradient in Doppler velocity as measured by the MRR, associated with change in particle fall speed, indicates the altitude of the melting layer (White et al. 2002). For each storm we define the MRR-derived storm maximum rain layer depth. The storm maximum rain-layer depth is associated with all 12-hour periods within that storm. In the rare case when there was not any radar echo above the MRR for a storm, the maximum rain layer depth was assumed to be equal to the maximum freezing level height from the SLE sounding during the storm.

## **2.10 Visualizations**

Two statistical visualization tools were employed to aid the analysis of the radar data and calculations performed on the radar data.

### **2.10.1 Contoured Frequency by Distance Diagrams**

Vertical cross-sections through radar volumes have been used in many past studies to provide insight into the vertical structure of orographic precipitation. This method provides a 2-D representation of 3-D terrain and storm structures. The information gathered from cross-sections is highly dependent on the location of the cross section (Yuter and Houze 1995; Yuter et al. 2009).

To overcome shortcomings of vertical cross-sections, we use a statistical tool to visualize the horizontal distributions of precipitation persistence and relative intensity across the study domain. The diagrams are called contoured frequency by distance diagrams (CFDD) and were first described by Guarente (2007). CFDDs are similar to CFADs, described by Yuter and Houze (1995), which look at the distribution of reflectivity in the vertical. CFDDs visualize the frequency distribution of the precipitation persistence and intensity as a function of distance from the Cascade crest at a constant altitude. Since the geographic features of the Willamette Valley and the Cascades are oriented north and south, the distributions from west to east can indicate where along the windward slope precipitation enhancement is most likely to occur. By examining the full

distribution of these values, we gain more information than by examining just a single statistic such as the mean (Yuter and Houze 1995).

To create a CFDD, we use a method similar to Yuter and Houze (1995), to examine the distributions of precipitation persistence and intensity values. The Cascade crest is set as the initial distance, with a value of zero. A histogram of the radar-derived values is created at each 2 km distance across the 130 km domain (Fig. 7a,b), resulting in 65 individual distributions. The histogram bin size used is 2.5%. Each distribution is normalized by the number of non-zero data points at that distance, resulting in frequency distributions. The 65 frequency distributions are arranged according to distance from crest into a 3-dimensional figure. (Fig. 7c,d) The x-axis is the distance from crest, the y-axis the value of the parameter being plotted, and the z-axis the frequency of occurrence. Each histogram point is color coded based upon its value of frequency occurrence on the z-axis (Fig. 7e). To simplify, we replace Figure 7e by contouring the z-axis values similar to the topographic map of a mountain elevation. (Fig. 7f) The CFDD visualizes the spread, skewness, and modal frequency of values with respect to location along the Cascade windward slope. CFDDs are created with radar composite values of precipitation persistence and intensity calculated using the 12-hour radar subsets depending on the sounding derived flow characteristics.

## **2.11 Cross-Section 75<sup>th</sup> Percentile Plot**

Another statistical tool was developed to examine enhancement in both the horizontal and vertical. Similar to the method used in the development of the CFDDs, we calculate the distribution of the persistence and relative intensity at each distance from the crest. From each distribution, we record the 75<sup>th</sup> percentile value. The 75<sup>th</sup> percentile value is chosen to represent persistence and intensity values within the distribution that are most likely associated with enhancement. We repeat this for each altitude level of the interpolated radar data from 1 km up to 6 km altitude. These plots will help indicate both the locations with respect to the crest and in the vertical where enhancement is occurring.

## Chapter 3

### Orographic Precipitation Processes

#### 3.1.1 Environmental Parameters

Scatter plots of the layer average environmental parameters are shown in Figure 8. The 25<sup>th</sup>, 50<sup>th</sup>, and 75<sup>th</sup> percentiles of the calculated variables are used to describe flow characteristics because most do not exhibit a Gaussian distribution (Yuter et al. 2009) (Appendix B). Percentile values are given in Table 2 and the correlation coefficients for pairs of environmental parameters are given in Table 3.

Figure 8a shows the relationship between the wind direction and cross-barrier wind speed. The highest cross barrier wind speeds occur when the wind direction is from the southwest. The SW flow is usually associated with the warm-sector of extra-tropical cyclones and this region of a storm tends to have strong wind speeds (Neiman et al. 2008).

Figure 8b shows that the Brunt-Vaisala frequency and cross-barrier wind speed are also nearly independent. The Froude number (eqn. 2), is a function of these two atmospheric variables. We decompose the Froude number into its components to examine them separately. For the Portland region, the atmosphere tends to be more stable when the cross-barrier wind component is near zero and the wind direction is not within the

SW subset. In these cases, the flow is originating from the continent and not from the typically more unstable environment over the ocean.

The cross-barrier wind speed and freezing level relationship is shown in Figure 8c. The scatter plot indicates that these parameters are also nearly independent. The impacts of these values and the potential for flooding will be discussed in Chapter 4.

The relationship between the IWV and the wind direction is shown in Figure 8d. The highest values in IWV are associated with wind directions from the southwest. Winds from the SW originate over the ocean and transport moisture on shore. This wind direction is commonly associated with land-falling atmospheric rivers that transport large amounts of moisture into the Willamette Valley.

The cross-barrier wind speed and the moisture (IWV) for SLE soundings are shown in Figure 8e. Moisture flux, is defined as the rate of moisture transported through a unit area, and is a function of the moisture content of the atmosphere and the cross-barrier wind speed. Moisture flux is used in past orographic precipitation studies (Neiman et al. 2008; Smith et al. 2009) to understand the amount of moisture impinging upon the barrier. For this study we decompose the moisture flux into its components and investigate them separately.

The freezing level and the IWV are highly positively correlated for SLE soundings (Fig. 8f). A warmer atmosphere will have a higher freezing level altitude and

can hold more moisture throughout its depth. The freezing level altitude and IWV of flooding events tend to have higher values for both parameters.

Figure 9 illustrates the relationship between the environmental parameters and the layer moisture flux. The cross-barrier wind speed and the moisture flux are highly positively correlated (Fig 9a), while the IWV and moisture flux are less correlated (Fig. 9c) (Table 3). This indicates that the moisture flux is more sensitive to the cross-barrier flow than the atmospheric moisture. The stability and moisture flux appear to be nearly independent (Fig. 9b). The freezing level and moisture flux have a slight positive correlation (Fig. 9d). The higher the freezing level, more moisture would be available in the atmosphere.

Twice daily observational soundings do not always capture the storm maximum rain layer depth. Storm structure, especially the rain layer depth, can change drastically over the course of a storm and 12 hour period (Medina et al. 2007). We compare the storm maximum rain layer depth measurement by the MRR to the 12-hour operational SLE sounding derived freezing level (Fig. 10a). The MRR-derived storm maximum rain layer depth is used to represent all 12-hour periods during a given storm. The relationship is highly positively correlated, with the MRR derived storm maximum rain layer depth tending to have higher values compared to the sounding-measured values. A few cases have sounding measured freezing levels greater than the storm maximum rain layer depth measured by the MRR. In these cases the time period when the storm had the maximum

rain depth there was no echo over the MRR. Figure 10b shows how the freezing level varies for each storm within our dataset. Both the twelve hour freezing level and the storm maximum rain depth are important storm characteristics. The sounding-derived freezing level is important to how portions of a storm will affect the near term precipitation patterns and will be discussed further in Chapter 4.2. The storm maximum rain depth is important because the portion of a storm with the deepest rain layer has the highest potential for widespread heavy rainfall and significant runoff (Colle 2004; Colle 2008; Lundquist 2008). Figure 10c shows how the IWV varies over the course of each storm. The observed trend of IWV is very similar to the observed trend of the freezing level altitude. The relationship between the flooding events and the storm maximum rain layer depth will be discussed in section in Chapter 4.2.

The distribution of storm durations is shown in Figure 11 with flooding storms shown in red. Most storms lasted between 12 and 24 hours, with some storms lasting over 3 days. It is important to note that all flooding events were associated with storms lasting at least 24 hours, but not all storms lasting this long produced flooding.

### **3.2 Single and Combined Parameter Variability**

We examine the impacts of the environmental conditions on the spatial distributions of precipitation persistence and intensity. Radar composites are created using only time periods meeting specific criteria from the SLE soundings. The impact of

variations within single variables and a combination of variables are explored in this section

### **3.2.1 Low-Level Down Slope Flow**

When the cross-barrier wind component is less than zero, the winds flow down the windward slope of the Cascades. We look at the average cross barrier wind speed below 1.2 km altitude to determine the impacts of having low-level downslope flow on the spatial distribution of precipitation persistence and intensity. Low-level downslope flow is defined by having cross-barrier wind component less than -1.0 m/s. Forty-six 12-hour periods had low level downslope flow.

Radar composites of cases with low-level downslope flow have precipitation preferentially occurring over the Willamette Valley with decreasing precipitation persistence and intensity approaching the Cascade crest (Fig. 12). Figure 12b shows the distribution of the precipitation persistence with decreasing values across the domain approaching the crest. The cross-section of 75<sup>th</sup> percentiles of persistence shows greater depth (up to 6 km altitude) of relatively higher persistence occurring over the western portion of the study domain and the Coastal Range with not as much enhancement in the vertical over the Cascades (Fig. 12c). The precipitation intensity mode has a decrease of nearly 50% along the windward slope (Fig. 12e). The cross-section of 75<sup>th</sup> percentile values of intensity also peak over the Willamette Valley with the highest values occurring at 1 km altitude from 130 km to 40 km from the crest (Fig. 12f).

When precipitation enhancement is not occurring over the terrain we expect a pattern similar to what is shown in Figure 12. Upslope flow creates orographic precipitation enhancement. During conditions with downslope flow no enhancement occurs over the windward slope. The increase in the precipitation persistence closer to the western extent of the domain could be driven by flow being forced up the eastern slope of the Coastal Range. The relatively higher persistence values also extend vertically deeper over the western portion of the Willamette Valley. These increases are slight, so there might also be other factors controlling this feature.

### **3.2.2 Multiple and Single Layer Flows**

In this section, we explore the impacts of having single and multiple layered flows on the spatial pattern and distribution of precipitation persistence and intensity. The lower layer variables from the SLE soundings are defined below 1.2 km AMSL (mid-slope) and the upper layer is between 1.2 km and 2.2 km AMSL. The altitude of 1.2 km AMSL was selected as the location to determine if flow was multi-layered because it is near the midpoint of the full layer calculated averages.

The largest spread in differences between the upper and lower layers occurred for  $N_m^2$  values (Fig. 15b). These differences did not produce significant impacts on the flooding potential. The sensitivity of the precipitation patterns to changing stability and cross-barrier flow strength is discussed in section 3.2.4, and the results of that section are used as further justification to use the difference in cross-barrier flow strength in defining

flow as multi-layered. Figure 8b indicates that for SLE soundings, there is also greater variability in the full layer average of cross-barrier flow strength than stability. Soundings with two distinct layers of cross barrier wind did have a significant impact on probability of flooding. Ninety-six soundings were identified as having two layers of cross-barrier winds and twenty four (25%) were associated with flooding. Figure 13a shows the relationship between the lower and upper level cross-barrier wind speeds. The 80<sup>th</sup> percentile of differences for the two layers of cross-barrier wind speed is 10 m/s (Fig. 13b). This difference implies significant shear between the two flow layers, either directional shear, speed shear, or a combination of both. Soundings with two layered flow tend to occur when the cross-barrier wind speed for the full layer average had a higher value. The median cross-barrier wind speed when the flow was two-layered flow is 11.6 m/s, compared to the median cross-barrier wind speed of 7.1 m/s for all 487 soundings.

To examine the impacts of choosing 1.2 km AMSL as the inflection point to determine if flow is multi- or single- layered, a sensitivity plot of using 2 vertical layers was compared to using 5 layers of the average cross-barrier wind component. Figure 14 shows the cross-barrier wind component averaged for 500 m thick layers from the surface up to 2.2 km, with the highest altitude layer only averaged over 200 m for both multi- and single- layered flow. Figure 14d indicates that for multi-layered flow the largest change in the cross-barrier wind speed tends to occur across the 1 km to 1.5 km layer. This provides evidence that the use of the 1.2 km altitude as the dividing point for estimating

if flow is multi-layered is a reasonable assumption. This altitude allows both the low-level and upper-level flow to be sampled and represented in our calculation.

The two layers of cross-barrier flow can be driven by low-level flow deflection, the presence of an along-barrier jet, or background shear associated with the extratropical cyclone. The along-barrier jet and low-level flow deflection are not mutually exclusive, with the development of a jet typically associated with low-level stability and blockage. To determine if the multiple layers of cross-barrier flow were associated with changes in stability or background shear, we examined the soundings with multi-layered flow. It was found that 43% (41 of 96), of the soundings with multiple layers of cross-barrier flow were also associated with a difference in stability between the two layers greater than  $6.7 \times 10^{-5} \text{ s}^{-1}$  (50<sup>th</sup> percentile of all differences of  $N_m^2$  for the two layers). This provides evidence that over half of the cases when the cross-barrier flow has multiple levels it might be associated with the environmental background shear, while the rest of the time periods it is associated with low-level flow deflection. Figure 15a shows the distribution of stability for the lower altitude layer (surface to 1.2 km) and Figure 15b shows the distribution of differences of stability for the two layers for both the single and multiple level flow regimes.

To compare the impacts of multi-layered flow on the patterns of precipitation persistence and intensity, we chose two 12-hour cases to examine further March 3, 2007  $\pm$  6 hours of the 00Z sounding and March 20, 2007  $\pm$  6 hours of the 00Z sounding. The

two cases had similar environmental conditions (Table 4). All environmental conditions for both cases are between their 25<sup>th</sup> and 75<sup>th</sup> percentiles, except for IWV. Both soundings have IWV slightly greater than the 75<sup>th</sup> percentile. Figures 16 and 17 show the spatial patterns of the persistence and intensity for these two cases. The horizontal cross-sections shown are from 1 km altitude to limit the impacts of the bright band since the freezing level was ~1.8 km altitude. The multi-layer flow case has high persistence and intensity located along the mid-slope, with smaller values over the Willamette Valley and along the upper slope (Fig. 16a,b,d,e). The higher intensity values are confined to the lowest levels, and do not extend very deep (Fig. 16f). The single-layer flow case has lower persistence over much of the domain except north of KRTX (Fig. 17a,b,c). The intensity is high over the valley but decreases along the mid and upper slope (Fig. 17d,e,f). Colle and Yuter (2007) showed that a friction induced shear layer can enhance upstream precipitation by increasing the effective barrier width and deepening the boundary layer. Our dataset has insufficient vertical resolution to determine if the shear of the multi-layered flow is producing turbulent overturning and subsequent precipitation growth as described by Medina et al. 2007. These two contrasting cases for Portland provide evidence of more precipitation enhancement when there is significant shear at low levels.

### 3.2.3 Cross-Barrier Wind Speed and Freezing Level Sensitivity

The cross-barrier wind speed ( $U$ ) and the freezing level altitude as measured by the SLE soundings are nearly independent (Fig. 8c) (Table 3). Cases with strong cross-barrier flow and deep freezing levels have a high occurrence of flooding and will be discussed in Chapter 4.2. High freezing levels will lead to more rainfall over a larger area with more potential runoff (Neiman et al. 2008; Lundquist et al. 2008) In this section we explore both the impacts of freezing level and cross-barrier flow in greater detail. We look at 3 variations of atmospheric conditions all which have typical wind direction values (between 25<sup>th</sup> and 75<sup>th</sup> percentiles) (Table 2). The three subsets used for the calculations are:

- Freezing Level and  $U > 75^{\text{th}}$  percentile (Figures 18a-c, 19a-c)
- Freezing Level  $< 25^{\text{th}}$  percentile and  $U > 75^{\text{th}}$  percentile (Figure 18d-f, 19d-f)
- Freezing Level  $> 75^{\text{th}}$  percentile and  $U < 25^{\text{th}}$  percentile (Figure 18g-i, 19g-i)

The cases when the freezing level and  $U$  are both greater than their 75<sup>th</sup> percentiles, the precipitation persistence and intensity are both high across most of the domain (Figs. 18a,b and 19a,b). Figures 18b and 19b show distributions of persistence and intensity which are bimodal across the Willamette Valley. The northern portion of the valley experiences more persistent and intense precipitation compared to south of KRTX (Figs. 18a, 19a). The persistence peaks near 40 km from the crest, and has a modal value of 90 % up to the crest (Fig. 18b). The intensity peaks near the same location to 0.8, but drops within the nearest 15 km of the crest (Fig. 19b). The cross-section of 75<sup>th</sup>

percentiles shows high persistence and intensity extending upwards to 5 km and 3 km, respectively, along the upper portions of the windward slope (Figs. 18c, 19c)

When the freezing level is less than the 25<sup>th</sup> percentile and the cross-barrier wind is greater than the 75<sup>th</sup> percentile, the persistence and intensity has lower magnitude across the domain (Figs. 18d, 19d). The persistence has a wide distribution over the domain with only a faint signal of a mode (Fig. 18e). The intensity values decrease along the upper portion of the slope (Fig. 19e). The cross-section of 75<sup>th</sup> percentiles of persistence shows that highest values occurring along the lower and mid slope, with values dropping near the crest (Fig. 18f). The most persistent precipitation occurs at lower elevations when the freezing level is low compared to when the freezing level is high (Fig. 18e,f).

When the freezing level is greater than the 75<sup>th</sup> percentile and the cross-barrier wind speed is less than the 25<sup>th</sup> percentile the persistence of the precipitation has a similar magnitude compared to when the freezing level was low and the cross-barrier flow was strong, but the highest values are occurring at a different location along the slope (Fig. 18g). The maximums are shifted further to the south along the terrain. The distribution of persistence is multi-modal over the Willamette Valley, with increasing values along the lower and mid-slope, and decreasing near the crest (Fig. 18h). The intensity has a nearly constant distribution across the Willamette Valley and windward slope, with a slight drop

near the crest (Fig. 19h,i). For these cases the localized region of precipitation enhancement north of KRTX at Kelso is not present (Fig. 19g).

These sensitivities indicate that both the freezing level and the cross-barrier wind speed are important components for orographic precipitation enhancement along the Cascade windward slope. When both are greater than their 75<sup>th</sup> percentiles, heavy and persistent rainfall is common. Given the relationship between the IWV and freezing level (Figure 8f) this combination would lead to a greater moisture flux upon the Cascades. The moisture flux calculation used by Smith et al. 2009 (eqn. 4) during a land-falling atmospheric river in California was used to determine that the minimum moisture flux impinging upon the Cascade windward slope is 210 kg m/s when the IWV and cross-barrier wind speed are both greater than their respected 75<sup>th</sup> percentiles (Table 2). If these conditions are met, the probability of that storm being associated with an atmospheric river is also high (Figure 8e). High freezing level cases would have more rain compared to snow over the domain (Lundquist 2008). However, rain is associated with a higher reflectivity compared to snow, and this artifact could lead to the smaller intensity values for cases with low freezing levels. The persistence would not be as affected. High cross-barrier wind leads to stronger upslope flow and the potential for orographic effects leading to greater precipitation enhancement (Neiman et al. 2002; Colle 2004). High cross-barrier flow will also advect more preexisting precipitation cells over the slope, increasing the rainfall across the domain (Yuter et al. 2009). Figure 9 and Table 3 also

indicate that the moisture flux is more highly correlated with the cross-barrier wind speed than with the IWV and subsequently the freezing level height. This provides additional insight into why the precipitation intensity is more sensitive to the cross-barrier wind speed compared to the freezing level altitude.

### 3.2.4 Cross-Barrier Wind Speed and Stability Sensitivity

To test the sensitivity of the precipitation patterns to flow blocking, we examine the impacts of changing the input variables to the Froude number (stability and cross-barrier wind speed, eqn. 2) on the precipitation persistence and intensity. We only look at time periods when the freezing level and wind direction have typical values (between 25<sup>th</sup> and 75<sup>th</sup> percentiles) (Table 2) to limit the impacts of other processes. The three subsets used for the calculations are:

- $N_m^2$  and  $U > 75^{\text{th}}$  percentile (Figures 20a-c, 21a-c)
- $N_m^2 < 25^{\text{th}}$  percentile and  $U > 75^{\text{th}}$  percentile (Figures 20d-f, 21d-f)
- $N_m^2 > 75^{\text{th}}$  percentile and  $U < 75^{\text{th}}$  percentile (Figures 20g-i, 21g-i)

When  $N_m^2$  and  $U$  are greater than the 75<sup>th</sup> percentile the environment is stable with strong cross-barrier flow. The persistence has a wide distribution and slowly increasing mode across the Willamette Valley with a peak in the mode occurring 30 km from the crest (Fig. 20b). The cross-section of 75<sup>th</sup> percentile of persistence has the highest values between 10 km and 40 km from the crest, with values near 60% occurring up to 3 km altitude (Fig. 20c). The modal intensity values do not change much over the Willamette Valley and peaks in the same location as the persistence (Fig. 21b). The

values in the cross-section of 75<sup>th</sup> percentiles occur in the lowest 2 km 40 km from the crest (Fig. 21c).

In the second subset,  $Nm^2$  is less than the 25<sup>th</sup> percentile and  $U$  is greater than the 75<sup>th</sup> percentile. These values would lead to a high Froude number and unblocked flow (eqn. 2) (Medina and Houze 2003). The persistence increases across the Willamette Valley with a strong modal peak 30 km from the crest (Fig. 20e). The cross-section of 75<sup>th</sup> percentiles also has a peak in the same location extending up to 4 km altitude (Fig. 20f). The spatial pattern of the intensity is very similar to the case when both the stability and the cross-barrier flow are greater than their respected 75<sup>th</sup> percentiles (Fig. 21d-f).

The last subset examined in this series had  $Nm^2$  greater than the 75<sup>th</sup> percentile and  $U$  less than the 25<sup>th</sup> percentile. In these cases, the Froude number would be low and flow would be blocked (eqn. 2) (Medina and Houze 2003). The persistence of rainfall is less than 20% over most of the high terrain (Fig. 20g,h). The highest persistence values occur over the Northern Willamette Valley and west of most terrain (Fig. 20g). The intensity values are low for the entire domain, with zero values within 30 km of the crest (Fig 21g-i).

These composites indicate that the cross-barrier wind speed is more important in determining the magnitude of the precipitation enhancement over the entire windward slope compared to atmospheric stability, similar to PG2009. When the flow is unblocked, the highest precipitation persistence and intensity occurs near the first

significant terrain along the slope, similar to what observed during IOP 2b of MAP (MH2003) (Figs. 20d, 21d). Periods when the cross-barrier flow is strong and the atmosphere is stable, the mode of the precipitation persistence is ~15% higher over the Willamette Valley compared to when the atmosphere was unstable. The combination of stable conditions and high cross-barrier flow is associated with a greater magnitude of upstream persistence compared to when the cross-barrier flow was weaker and the atmosphere was stable. The upstream enhancement resembles radar observations for IOP 8 of MAP (MH2003). The horizontal cross-sections at 2 km show that the highest intensity values are occurring at different locations along the terrain for varying atmospheric stabilities (Fig. 21a,d). The unstable cases have high intensity values over more locations, while the stable cases have the highest intensities confined to the Lewis River Valley. The CFDD and cross section of 75<sup>th</sup> percentiles of precipitation intensity show no significant difference with varying atmospheric stabilities and a strong cross-barrier flow.

In the case of a stable atmosphere and low cross-barrier flow (Froude <1), the precipitation is confined to the Willamette Valley. This indicates that the flow was not able to make it far up the windward slope, and no orographic enhancement occurred. The upstream precipitation persistence and intensity is also smaller in magnitude compared to when the cross-barrier flow was above the 75<sup>th</sup> percentile with stable conditions.

The sensitivity of the precipitation persistence and intensity is most sensitive to changes in the cross-barrier wind speed and least sensitive to atmospheric stability. The cross-barrier wind speed has a greater range of variability for SLE soundings (Fig. 8b). Changes in the cross-barrier flow strength and the freezing level altitude lead to the changes in the location of the precipitation enhancement along the windward slope.

### **3.3 Local Precipitation ‘Hot Spots’**

Two areas within our study domain have a high incidence of relatively large magnitude precipitation persistence and intensity when compared to the rest of the domain- the Lewis River Valley northwest of KRTX and Kelso, Washington directly north of KRTX (Fig. 1). The Lewis River Valley is situated along the southern foothills of Mount St. Helens. Kelso, Washington is located to the west of Mount Saint Helens near the confluence of the Willamette and Columbia rivers.

#### **3.3.1 The Lewis River Valley**

The Lewis River Valley (LRV) is situated in a prime location for upslope precipitation enhancement. The northern wall of this small valley extends out into the larger Willamette Valley and is nearly perpendicular to southerly and south-southwesterly flow. This leads to an optimal amount of lift for typical storm wind directions. The location of the valley in proximity to the rest of the Cascades also makes it subject to low level convergence under certain atmospheric conditions. When flow upon the Cascades is blocked, it is deflected to the left. This left deflection makes air

flow more southerly towards the LRV. The radar composite for stable conditions and strong cross-barrier flow (Figures 20a, 21a) illustrates this phenomenon. Both the precipitation persistence and intensity are enhanced most over the LRV. The role of convergence in Alpine terrain similar in shape to the Lewis River Valley is discussed by Rotunno and Ferretti (2001) and Rotunno and Houze (2007) When flow is deflected to more southerly ahead of the Cascade barrier, it converges with the more westerly flow coming across the Willamette Valley. These flows converge at the LRV and lead to low-level atmospheric lift and increased precipitation persistence and intensity for a range of atmospheric conditions.

The twelve hour period represented by the sounding on January 8, 2007 00Z has significant enhancement occurring over the LRV. The environmental conditions are given in Table 5. Figure 22 shows the median radial velocity, precipitation persistence, and intensity at 1 km altitude. The median radial velocity field (Fig. 22a) shows more westerly wind to the north of KRTX and more south-westerly wind to the south. To the south of KRTX, the air flow is deflected due to terrain blocking, to the north of KRTX the flow is uninterrupted. These two flows converge near the LRV leading to the enhancement of precipitation persistence and intensity during this twelve hour period. Using a Monte Carlo simulation the high precipitation persistence over LRV for this case is significant to 99%, and the strong precipitation intensity is significant to 95%.

In cases when the flow is not blocked, the LRV still experiences significant precipitation enhancement. The typical wind direction from the SW leads to flow impinging directly upon the terrain of the valley. The unblocked flow will rise over the terrain of the valley and lead to persistent and intense rainfall. Figures 20d and 21d show that for unstable cases with high cross-barrier wind speed there is high persistence and intensity over the LRV. The high persistence and intensity are also occurring at more locations along the windward slope when the atmosphere is more unstable.

### **3.3.2 Kelso, Washington**

Kelso, Washington is located to the northwest of the LRV (Fig. 1). This location also tends to be a hotspot of precipitation enhancement but not usually as intense or as frequently as the LRV. The 2 km horizontal cross sections of precipitation persistence and intensity from the multi-variable sensitivity testing (Chapters 3.2.3 and 3.2.4) show a region of locally enhanced precipitation over Kelso, WA for a range of atmospheric stability, cross-barrier flow, and freezing level. The magnitude of the enhancement varies little with changing stability (Figs. 20 and 21).

For cases when the freezing level is low and the cross-barrier wind is strong, the magnitude of intensity and persistence is not as high over Kelso, but it is still relatively higher compared to the rest of the domain (Figures 18d, 19d). Figures 18d and 19d show the strong cross-barrier flow preferentially leads to the enhancement, and the freezing level altitude dictates the magnitude of the persistence and intensity.

To further examine this phenomenon we selected a 12-hour period when Kelso, WA experienced high persistence and intensity of rainfall. The SLE sounding used was from October 31, 2005 12Z. A Monte Carlo simulation shows the high persistence and intensity values for this case are both significant to 99%. Figure 23 shows the surface winds at 15Z and the horizontal cross-sections of median radial velocity, precipitation persistence and intensity for the twelve hour period at 1 km altitude. The atmospheric conditions are shown in Table 5. The sounding indicated a high freezing level and strong cross-barrier flow. The Kelso-Longview airport had wind directions consistently from the south and southeast (Fig. 23a). These southerly winds are mostly likely driven flow deflection by the Cascades. The Astoria airport to the west of Kelso, at the mouth of the Columbia River, experienced a range of wind directions for this time period. The few hours before and after the 12Z soundings were dominated by westerly winds and winds eventually turned more southwesterly (Fig. 23a) later in the period. The median radial velocity field shows slight speed convergence occurring to the south of Kelso over the Columbia River Gorge (Fig. 23b). This area of convergence corresponds to the edge of a large area of high persistence and intensity (Fig. 23c,d). The southerly wind direction reported at Kelso and the radial velocity at 1 km shows that the wind direction is changing substantially over a short distance in the vertical at this location. The westerly winds reported at Astoria and westerly winds shown in the radial velocity field, along with the southerly winds reported at Kelso, provide evidence of flow convergence occurring at the surface near Kelso. Unfortunately, just to the west, terrain blockage of

the radar beam is occurring and does not allow us to see the full picture of the localized enhancement.

Mass (1981) and Whitney et al. (1993) examined the Puget Sound Convergence Zone in Washington State which is driven by flow channeling through the Chehalis Gap and Strait of Juan de Fuca. The channeled flow is deflected by the Cascades and converges over the southern Puget Sound leading to increased cloudiness and precipitation. Both studies note that only marginal stability is needed to create the flow deflection and convergence zone. The wind directions observed in Astoria and the radial velocity signature (Fig. 23a,b) indicate that flow is possibly being channeled through the Columbia River Gorge and converging with the more southerly flow over Kelso leading to this precipitation hotspot. An additional radar situated to the west along the coast would provide a clearer picture of what processes are leading to this area of enhancement.

There is also a small ridge (~900 m elevation) near Kelso within the Willamette Valley. This ridge could be an additional factor in producing the localized precipitation enhancement, along with the low level flow convergence. Colle (2008) showed that strong cross-barrier flow over a small ridge with a high freezing level altitude produced localized high precipitation amounts. The combination of atmospheric phenomenon creates a precipitation hotspot over Kelso, WA and further analysis is needed to

understand to what extent each factor leads to the increased occurrence of high persistent and intense rainfall at this location.

## Chapter 4

### Flood Events

#### 4.1.1 Storm Scale

The scale of a storm is important in determining the flooding potential. The Z13 and Z25 volume per hour for each 12 hour period with respect to the freezing level and cross-barrier wind are shown in Figure 24. Flooding events tend to have a larger precipitation volume. However, having a large scale storm is not sufficient for flooding, as some large storms did not flood. Sixty-three percent of flooding events have a Z13 volume greater than the 75<sup>th</sup> percentile of all Z13 volumes, and seventy percent of flooding events have Z25 volumes greater than the 75<sup>th</sup> percentile of all Z25 volumes (Table 2). There is a slight positive correlation between the cross-barrier wind speed and the Z13 volume (Fig. 24a). A strong cross-barrier flow would prolong precipitation development over the slope, and increase the Z13 volume of a storm. Similar relationships are true for the Z25 volumes (Fig. 24c). With respect to the Z25 volume, storms with a large scale and strong-cross barrier flow or high freezing level have a high occurrence of flooding (Fig. 24c,d). A high percentage of large Z25 storm volumes (> 200,000 km<sup>3</sup>/hour) are associated with flooding. There is also a positive relationship of the Z25 volume and the freezing level height (Fig. 24d). Values in the lower left portion of Figure 24d, which represent storms with low freezing levels and low Z25 volumes, should be disregarded. A storm with a low freezing level would have more ice which

returns a lower reflectivity value than liquid precipitation due to a lower dielectric constant. Storms in this portion of the plot could still be large in scale with a significant amount of precipitation.

#### **4.2 Combined Conditional Probabilities of Flooding**

In this section, we explore the probabilities of flooding when single and combinations of variables have anomalously high values.

Figure 11 shows that all flooding storms lasted longer than 24 hours, but not all storms that lasted longer than 24 hours lead to flooding. Two hundred sixty 12-hour periods were associated with storms that lasted longer than a day, and forty three of those lead to flooding. Long duration is a necessary but not sufficient criterion for a storm to flood.

Land-falling ARs are associated with deep rain layers and significant low-level moisture (Neiman et al. 2008, Bao et al. 2006). The typical location of ARs making land-fall along the Pacific Northwest coast within the warm-sector of large extra-tropical cyclones leads to strong surface winds from the south and southwest (Neiman et al. 2008). The combination of significant moisture, a deep rain layer, and strong cross-barrier flow leads to land-falling ARs often being associated with flooding. In this portion of the study, we examine the environmental characteristics often associated with land-falling ARs separately to identify which factors are more important in determining when flooding will occur.

IWV values greater than the 75<sup>th</sup> percentile (2 cm) indicate that there is land-falling AR along the Oregon/Washington Coast. Figures 8e-f show that when the IWV is greater than 2 cm the probability of flooding is 25%. Every flooding storm in our dataset has a land-falling AR for at least a portion of the time period it precipitated. But only a quarter of the 12-hour periods associated with a land-falling AR lead to flooding. Land-falling ARs are a necessary but not sufficient condition for flooding.

Rain layer depth is also an important factor in determining whether flooding will occur. Figure 10 indicates that all flooding events have storm maximum rain layer depths greater than 2 km. Only 30% of all storms with a maximum rain layer greater than 2 km do flood. Similar to IWV and storm duration, having a storm maximum rain layer depth greater than 2 km is a necessary but not sufficient criterion for flooding to occur. As discussed in Chapter 3.1, any given storm can have a wide range of freezing levels. Some flooding events have individual soundings when the freezing level was below 2 km (Fig. 10b). Twenty four percent of the time when the sounding derived freezing level was observed to be higher than the 75<sup>th</sup> percentile (Table 2) there was flooding (Fig. 8c,f). Given the positive correlation of the freezing level altitude and IWV (Fig. 8f), the freezing level altitude will be used a proxy for IWV in the following discussion. Given that the atmosphere is saturated or nearly saturated during the storms analyzed, a deepening of the rain layer would also indicate an increase in the IWV. Also, by using the freezing level in our flooding analysis we gain insight into the surface precipitation

type along the Cascade windward slope and whether liquid or frozen phase precipitation growth processes are occurring within the precipitating cloud.

Time periods when the cross-barrier wind speed is greater than 10.5 m/s (75<sup>th</sup> percentile), flooding occurs 18% of the time (Fig. 8c). High cross-barrier wind speeds lead to more moisture flux, upslope flow, and advection of preexisting precipitation cells (Neiman et al. 2002; Yuter et al. 2009). Multi-layered flow also increases the probability that flooding will occur. A quarter of time periods when flow has 2 layers, flooding was observed.

For each of these single parameters, the likelihood that they will lead to flooding increases for time periods when the wind directions are from the SW. Most (91%) flooding storms were associated with winds within the SW storm subset for at least a single sounding.

Certain combinations of factors increase the probability of flooding. Figure 25 visualizes these probabilities based upon the values of single parameters and the combination of those parameters. Each vertex of the triangle shape represents a single environmental condition and the probability of flooding resulting when that variable is higher than the given threshold. The edges of the triangle indicate the joint conditional probability of flooding when the criteria defined by the adjacent single parameters intersect. The center shows the probability of flooding when all three parameters are combined. Lastly, the outlying vertex shows the increased probability when all other

criteria are met and the flow is two layered. In Figure 25, the freezing level is also used to represent the IWV, since both are positively correlated (Fig. 8f). Skill is added to the probability of flooding when freezing level is used instead of the IWV. Using IWV as a proxy for freezing level (opposite of what was actually done), the probability of flooding slightly decreased. Figure 10c shows how the IWV changes over the course of a storm, and the trend is very similar to how the freezing level changes over the course of a storm (Fig. 10b).

When the storm duration is greater than 24 hours and the cross-barrier wind speed is greater than 10.5 m/s (75<sup>th</sup> percentile), flooding results 28% of the time. When storms have long duration and the freezing level is higher than 2130 m (75<sup>th</sup> percentile), the occurrence of flooding is 40%. The combination of high freezing level and strong cross-barrier flow leads to flooding 48% of the time. The combination of all variables has a probability of flooding 56% of the time. In addition, if the sounding indicates multi-layered flow, the flooding occurrence increases to 65% (Table 6).

To take into account the missed flooding events for each of the criteria described in Fig. 26, we calculated the critical success index (CSI):

$$CSI = \frac{HITS}{HITS + MISSES + FALSE ALARMS} \quad (6)$$

A CSI of 1 would indicate a perfect score and a CSI of 0 would indicate no skill. The CSI diagram is shown in Fig. 26. The CSI score for each criterion is lower than the

probability scores in Fig. 25, this is because the probability scores do not take into account the misses, only the false alarms. It is important to take into account the misses to know how many flooding events occurred outside specific environmental conditions. For the purposes of knowing the probability of flooding given certain environmental conditions, the probability scores are sufficient.

High freezing levels and strong cross-barrier flow results in more moisture flux. For cases when the moisture flux was greater than the 75<sup>th</sup> percentile, flooding occurred 58% of the time. The high freezing level also results in the efficient mechanism of precipitation growth of collision-coalescence occurring over a greater vertical depth in the atmosphere. The high freezing level would also lead to more rainfall occurring over a larger spatial extent, instead of snow, leading to increased water runoff (Lundquist et al. 2008). The combination of long storm duration increases the probability of flooding because the above processes occur for a longer time period. The increased probability of flooding with two-layered flow is possibly due to several factors: the presence of a turbulence within the shear layer enhancing precipitation growth (Medina et al. 2007); friction of the flow along the terrain deepening the boundary layer and air being lifted up and along the shear layer (Colle and Yuter 2007), or lower level flow increasing the size of the affective barrier causing parcels to reach their lifting condensation level further upstream (Rotunno and Ferretti 2001). Each mechanism would lead to a larger spatial extent of high precipitation persistence over the windward slope. In the latter two, parcels

will also be lifted to higher altitudes when lifted above the shear layer than they would be with the underlying terrain alone. This would result in more condensation and more intense rainfall along the windward slope. Our dataset has insufficient resolution to resolve which of the mechanisms are occurring or to what degree, but we do find more persistent and intense precipitation when flow is multi-layered.

### **4.3 Spatial Patterns of Precipitation Persistence and Intensity**

To investigate why some storms with high freezing levels, strong cross-barrier flow, and last longer than 24 hour flood and others with the same characteristics do not flood, we created radar composites and the associated distribution visualization plots. Sixteen periods met the above criteria and flooded, while 10 did not flood.

The distribution of the persistence for non-flooding events has a distinct bimodal distribution across the Willamette Valley (Fig. 27b). The Kelso hotspot has highly persistent precipitation, while the southern Willamette Valley does not (Fig. 27a). Along the slope the mode increases and peaks around 80%, and remains high to the crest (Fig. 27b). The cross-section of 75<sup>th</sup> percentiles of persistence shows high values across most of the domain, with the highest values above the mid and upper slope (Fig. 27c). The high persistence values extend up to 5 km altitude over the crest (Fig. 27c). The intensity also has a bimodal distribution across the valley due to the Kelso hotspot (Fig. 27d,e). The intensity peaks near 30 km from the crest and decreases closer to the crest (Fig 27e,f).

The Kelso precipitation hotspot appears to be active for the flooding cases, but there is also very persistent precipitation over the southern portions of the Willamette Valley (Fig. 28a). The flooding cases have a distribution of persistence that is narrower across the domain, with a single mode over the Willamette Valley (Fig. 28b) compared to the bimodal distribution of the non-flooding cases (Fig. 27b). The persistence increases over the slope, and peaks with a modal value slightly higher than the non-flooding cases (Fig. 28b). The cross-section of the 75<sup>th</sup> percentiles of the persistence shows that the high values do not extend as far west, but there is a larger area of values being greater than 90% (Fig. 28c). The intensity also has a narrow distribution across the valley with a mode similar to the higher mode of the non-flooding events (Fig. 28e). The values increase along the slope and drop off within the nearest 10 km of the crest (Fig. 28e). The drop in intensity for the flooding cases occurs much closer to the crest than for non-flooding events. The cross-section of the 75<sup>th</sup> percentiles of the intensity (Fig. 28f), show that the high values have a greater magnitude along the upper slope, stretch further across the Willamette Valley, and have higher magnitude up to 3 km altitude compared to the non-flooding equivalent figure (Fig. 27f)

The spatial distributions show that for flooding events, the precipitation was more persistent and intense over a larger area compared to the non-flooding events. The flooding events have more persistent and intense rainfall over most of the Willamette Valley where the orography would not be as much of a factor, but heavy precipitation still fell. The pattern of enhancement over the terrain was similar for both cases, meaning

the more persistent and intense precipitation over the valley is what distinguished the flooding from the non-flooding cases.

## **Chapter 5**

### **Conclusions**

This study examines orographic precipitation patterns along the windward slope of the Cascade Mountains in the Portland, Oregon region of the US Pacific Northwest. We utilize data from the WSR-88D NWS radar at Portland, twice daily operational upper-air sounding released from Salem, Oregon, and a vertically pointing Micro Rain Radar. Flow impinging upon the Cascades is characterized by the atmospheric stability, moisture content, rain layer depth, wind direction, and cross-barrier wind component. Radar data  $\pm 6$  hours from each sounding are composited based upon the observed flow characteristics. Horizontal cross sections of precipitation persistence and intensity allow qualitative analysis of the spatial precipitation structures with respect to the underlying terrain. Statistical visualization tools are utilized to provide more in-depth analysis of the distribution of precipitation structures in both the horizontal and vertical. The joint conditional probabilities of single and multiple sounding variables that result in flooding are explored in detail. The probability of flooding is highest when the rain layer is deep, cross-barrier flow is strong, a storm lasts longer than 24 hours, and the flow impinging upon the Cascades is multi-layered.

The sensitivity of orographic precipitation persistence and intensity to atmospheric stability, cross-barrier flow strength, and freezing level altitude are examined

using radar and sounding data from 487 12-hour periods between 2003 and 2008. Consistent with Lundquist et al. (2008) and Neiman et al. (2008) heavy precipitation occurred over a larger spatial extent when the freezing level was high and the cross-barrier flow was strong. These conditions are more common during land-falling atmospheric rivers and are associated with significant moisture flux ( $>210 \text{ kg m/s}$ ) impinging up on the Cascade barrier. Periods when the cross-barrier flow was weaker or the freezing level was low, the location of the precipitation enhancement shifted to different locations along the terrain. The Kelso precipitation hotspot was active during conditions with strong cross barrier flow, and experienced more intense rainfall when the rain layer was deeper compared to when it was shallow.

The atmospheric stability was shown to play less of a role compared to the strength of cross-barrier flow in enhancing precipitation over the Cascades, similar to the findings of PG2009 along the Southern Alps. More stable conditions were associated with more persistent rainfall upwind of the barrier over the Willamette Valley. When the flow was unblocked (high Froude number, eqn. 2) with strong cross-barrier flow and an unstable atmosphere, localized pockets of intense precipitation are evident over the first ridges in the terrain (Fig. 21d). This is consistent with the findings of MH2003 where convective precipitation was a result of unblocked flow rising over the first topographic ridge. When the flow was blocked with a low Froude number (weak cross-barrier flow and stable atmosphere, eqn. 2) precipitation was confined to the Willamette Valley (Fig.

20g). These sensitivity tests also indicate that the precipitation enhancement occurring in the Lewis River Valley occurs for a range of atmospheric stabilities. Enhancement during stable flows in the Lewis River Valley is more strongly associated with low level convergence while the enhancement in unstable flows is more strongly associated with direct orographic lifting.

The impacts of multi-layered versus single layered flow was illustrated by examining two 12-hour periods with similar environmental conditions, one with two layer flow and the other with single layer flow. Houze and Medina (2004) and Medina et al. (2007) discussed evidence of a shear layer between two flow regimes producing turbulent overturning and subsequent precipitation enhancement when multi-layered flows encounter the Cascade windward slope. Colle and Yuter (2007) found that a sloping shear layer and deepening boundary layer induced by surface friction helped to increase precipitation amounts ahead of smaller terrain features along Long Island and Connecticut. The ambient flow was lifted up and along the shear layer, causing moisture to be condensed into precipitation ahead of the small hills. Rotunno and Ferretti (2001) linked multi-layer flow to precipitation enhancement and low-level convergence along the Southern Alps. When flow is multi-layered, there is a clear distinction between the upper and lower flows. The lower altitude flow can undercut the upper flow, increasing the size of the affective barrier. When air flows over the larger barrier, parcels will be lifted to a higher altitude compared to just the underlying terrain alone, increasing the

amount of condensation and precipitation intensity. Parcels will also reach their lifting condensation levels further down the windward slope increasing the spatial extent of high precipitation persistence. The vertical resolution of our data is insufficient to differentiate to what degree each of these phenomenon are occurring along the Cascade windward slope in the two selected single cases, but they do indicate that precipitation enhancement occurs preferentially when the flow is multi-layered with directional and/or speed shear (Fig. 16).

The precipitation ‘hotspots’ of Kelso and the Lewis River Valley are both associated with atmospheric phenomenon similar to those which have been previously described for other regions that lead to increased precipitation production. The terrain feature along the Southern Alps described by Rotunno and Ferretti (2001) leading to low level convergence is similar to the terrain of the Lewis River Valley. A single 12-hour period examined had more south-southwesterly flow along the base of the Cascades and more westerly flow coming off the ocean (Fig. 22a). These two flows converge at the Lewis River Valley producing local precipitation enhancement. At the Kelso precipitation hotspot, there is evidence of flow channeling through the Columbia River Gorge leading to convergence with flow which has been deflected to more southerly at low levels along the Cascade barrier. Flow channeling through coastal gorges along the Pacific Northwest is fairly common and only a marginal amount of stability is needed to deflect the flow once it encounters the Cascades (Mass 1981; Whitney et al. 1993). The

position of a small ridge near Kelso might also play a role in the increased precipitation persistence and intensity at that location. The cross-barrier flow and freezing level altitude were found to be the two most important factors in the local precipitation enhancement at Kelso. Colle (2008) showed that strong cross-barrier flow and a deep rain layer lead to increased precipitation amounts over small scale ridges.

We investigated the impacts of certain environmental conditions and storm characteristics on the probability of flooding. Storms which flooded tend to have a larger spatial extent. Each storm which flooded had a storm maximum rain layer depth greater than 2 km altitude, corresponding roughly to the 75<sup>th</sup> percentile of all freezing levels sampled (Table 2). Each storm which flooded was also associated with a land-falling atmospheric river for a least a portion of the storm. This is consistent with the findings from the CALJET and PACJET field campaigns (Neiman et al. 2002; Neiman et al. 2004; Ralph et al. 2004; Ralph et al. 2005) and land-falling atmospheric rivers in California being associated with heavy rainfall. However, not all storms that had a deep rain layer and/or a land-falling atmospheric river flooded. These conditions are necessary but not sufficient to predict when flooding will occur in the Portland area.

Figure 25 shows the single and joint conditional probabilities of key environmental conditions leading to flooding. Of the single variables, a high freezing level is the best predictor of potential flooding events, with 24% of the occurrences of a high freezing level being associated with flooding. With a high freezing level more rain

would be falling over a larger spatial area (Lundquist et al. 2008; Neiman et al. 2008). The joint probability of a deep rain layer and strong cross-barrier flow doubles the probability that flooding will occur. A high freezing level and strong-cross barrier flow is often associated with land-falling atmospheric rivers and a large amount of moisture flux ( $> 210 \text{ kg m/s}$ ) upon the Cascade windward slope. Adding the conditions of a storm lasting for longer than 24 hours and having two layered flow increases the probability of flooding to 65%. The longer duration of these conditions would lead to more rainfall accumulation along the slope and subsequently a higher potential for flooding.

When the conditions shown in Figure 25 come together, flooding is more probable. A high freezing level indicates more moisture available for precipitation production, stronger cross-barrier flow will result in more vertical motion when it encounters the terrain, two-layer flow results in a greater parcel vertical displacement, and a longer storm duration means these phenomenon are occurring for a longer time period. In the case of multi-layered flow, the mid- and upper-level flow will be forced up and over the lower level flow due to changes in wind direction and/or speed, causing the additional vertical displacement of parcels. The additional vertical displacement will lead to more parcel cooling with increased condensation of cloud liquid and more intense precipitation along the windward slope. To help differentiate between flood and non-flood events with similar storm and environmental conditions, we examine the spatial patterns and distributions of the precipitation persistence and intensity. The key

difference is evident in the 2 km horizontal cross-sections and CFDDs of the radar composites (Figs. 27a,b and 28a,b). The flooding events have more persistent rainfall over the entire Willamette Valley, while the rainfall during the non-flooding events is confined to the higher terrain and the Kelso precipitation hotspot region (Figs. 27a,b and 28a,b). Precipitation intensity values are also higher for flooding cases over a larger portion of the Willamette Valley and the higher intensity extends further up the Cascade windward slope (Figs. 27d,28d). The more persistent and intense rainfall over a larger spatial extent lead to the flooding.

The consequence of changing environmental characteristics on the precipitation patterns in the Portland, OR region determined from this study can be used to better understand the impacts of how future climate change will affect hydrology in the region. Annual average temperatures in the Pacific Northwest are predicted to warm by 3°C by 2080 (Mote and Salathe 2009). This would result in typical seasonal rain layers being deeper than present conditions. This scenario will likely increase the number of heavy precipitation events in the region if other conditions remain the same. The joint conditional probabilities found can also better equip regional forecasters to determine which storms affecting the US Pacific Northwest will lead to flooding.

Table 1. Total number of winter flooding events reported by the Portland, Oregon National Weather Service forecast office for each winter month from 2003 to 2008.

<b>Month</b>	<b>Flood Events</b>
November	2
December	6
January	2
February	0
March	1

Table 2. The 25<sup>th</sup>, 50<sup>th</sup> (median), 75<sup>th</sup> percentiles and mean values of variables calculated from 487 wintertime SLE soundings from 2003 to 2008.

<b>Variable</b>	<b>25<sup>th</sup></b>	<b>50<sup>th</sup></b>	<b>75<sup>th</sup></b>	<b>mean</b>
<b>Wind Direction (°)</b>	202	219	242	221
<b>Cross-Barrier Wind (m/s)</b>	4.2	7.1	10.5	7.5
<b>Moist Squared BV Frequency (<math>\times 10^{-4} \text{ s}^{-2}</math>)</b>	-0.0254	0.3052	0.856	0.5628
<b>Freezing Level (m)</b>	998	1408	2131	1570
<b>Froude</b>	0.2595	0.4858	0.7554	0.5785
<b>IWV (mm)</b>	12.2	15.2	19.9	16.3
<b>Moisture Flux (kg m/s)</b>	58.1	109.1	172.39	126.6
<b>Rain Depth (m)</b>	1050	1500	2100	
<b>Z13 Vol. (km<sup>3</sup>/hour)</b>	2.56E+05	4.72E+05	7.18E+05	5.19E+05
<b>Z25 Vol. (km<sup>3</sup>/hour)</b>	2.18E+04	8.11E+04	1.63E+05	1.26E+05

Table 3. Calculated correlation coefficients of environmental parameters calculated from SLE soundings and radar statistics.

<b>Variables</b>	<b>Correlation Coefficient</b>
Cross-Barrier Wind and Wind Direction	0.42
Cross-Barrier Wind and Stability	-0.27
Freezing Level Altitude and Cross-Barrier Wind	0.01
IWV and Wind Direction	-0.19
IWV and Cross-Barrier Wind Speed	0.15
Freezing Level and IWV	0.78
Cross-Barrier Wind and IWV	0.15
Freezing Level and Stability	0.34
IWV and Stability	0.19
Freezing Level and Wind Direction	-0.26
U and Z13	0.46
U and Z25	0.40
Freezing Level and Z13	0.31
Freezing Level and Z25	0.47
Moisture Flux and IWV	0.60
Moisture Flux and Cross-Barrier Wind	0.84
Moisture Flux and Stability	-0.15
Moisture Flux and Freezing Level	0.40

Table 4. . The calculated and derived variables from two SLE soundings used to contrast differences in two layer and one layer flow in Figures 13 and 14. The two layer flow case variables are from SLE sounding released March 3, 2007 00Z. The one layer flow case variables are from SLE sounding released March 20, 2007 00Z.

<b>Variable</b>	<b>2 Layer Case</b>	<b>1 Layer Case</b>
<b>Wind Direction (°)</b>	219	234
<b>Cross Barrier Wind (m/s)</b>	7.6	8.0
<b>Nm<sup>2</sup> (x10<sup>-4</sup> s<sup>-2</sup>)</b>	0.8365	0.2138
<b>Freezing Level (m)</b>	1758	1829
<b>IWV (mm)</b>	20.16	21.66
<b>Froude</b>	0.46	0.40
<b>Difference in U (m/s)</b>	12.2	1.89

Table 5. Calculated and derived variables from two SLE soundings used to illustrate precipitation hotspots in Figures 22 and 23. The variables are determined from SLE soundings released January 8, 2007 00Z and October 31, 2005 12Z.

<b>Variable</b>	<b>2007010800</b>	<b>2005103112</b>
<b>Wind Direction (°)</b>	241	217
<b>Cross Barrier Wind (m/s)</b>	14.53	15.4
<b>Nm<sup>2</sup> (x10<sup>-4</sup> s<sup>-2</sup>)</b>	1.24	0.52
<b>Freezing Level (m)</b>	1808	3153
<b>IWV (mm)</b>	21.04	30.0
<b>Froude</b>	0.7673	0.622

Table 6. Single and combined conditional probabilities of flooding. Number of 12-hour periods meeting certain criteria which flooded and did not flood. The critical success index (CSI) is a skill score used to determine the skill of the flooding probability for each combination of environmental parameters.

<b>Storm Chars</b>	<b>Flood</b>	<b>Non-Flood</b>	<b>% Flooding</b>	<b>CSI</b>
<b>ALL Storms</b>	43	444	9%	9%
<b>U &gt; 75%</b>	22	101	18%	15%
<b>Zero &gt; 75%</b>	29	93	24%	21%
<b>IWV &gt; 75%</b>	30	91	25%	22%
<b>Long Duration (&gt; 1 day)</b>	43	217	17%	17%
<b>2 Layer Flow</b>	24	72	25%	21%
<b>U and Zero &gt; 75%</b>	19	21	48%	30%
<b>U and IWV &gt; 75%</b>	20	44	31%	23%
<b>U and Duration</b>	22	58	28%	22%
<b>Zero and Duration</b>	29	44	40%	33%
<b>IWV and Duration</b>	30	73	29%	26%
<b>U, Zero, Duration</b>	19	15	56%	33%
<b>U, IWV, and Duration</b>	20	36	36%	25%
<b>U, Zero&gt;75%, 2 Layer Flow and Long Duration</b>	17	9	65%	33%
<b>U, IWV&gt;75%, 2 Layer Flow and Long Duration</b>	18	27	40%	26%

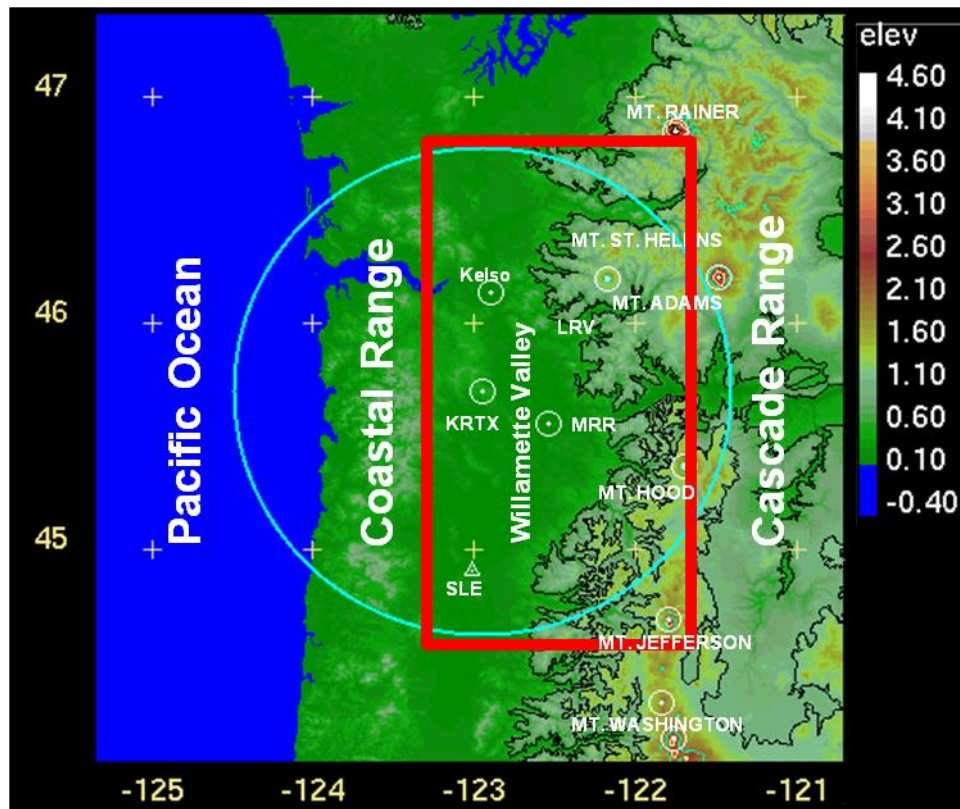


Figure 1. Topography of Portland, Oregon and its surrounding areas (in km altitude). Locations of Coastal and Cascade Ranges, Portland NEXRAD (KRTX) radar, Salem sounding (triangle), Kelso Washington, the Lewis River Valley (LRV), the Willamette Valley, and significant mountain peaks are labeled. The 120 km radar range ring from KRTX is shown in blue. Red box indicates Cascade windward slope study domain.

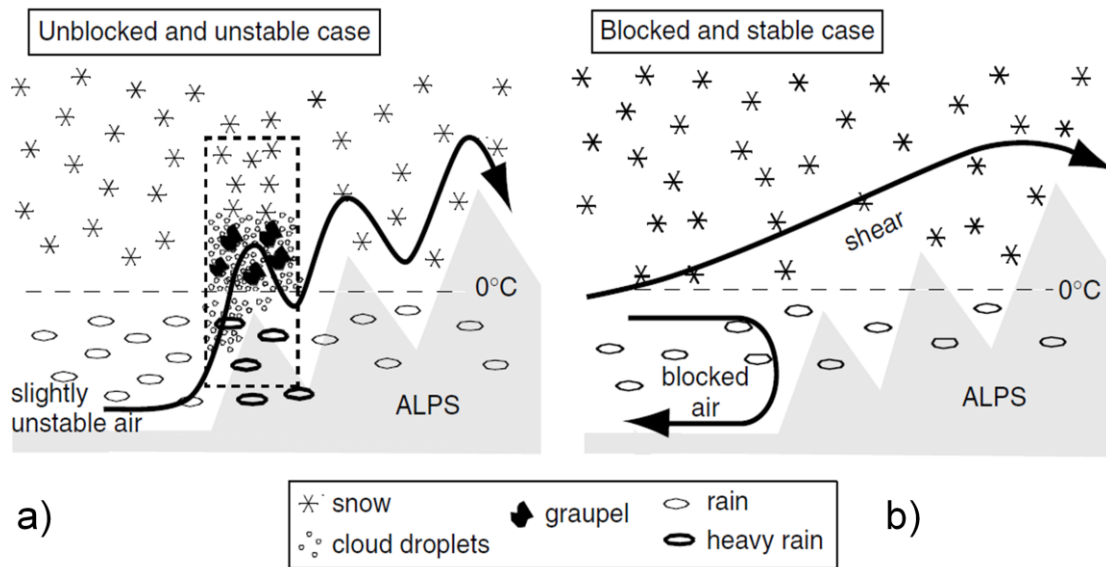


Figure 2. Conceptual model of the orographic precipitation mechanisms active in MAP cases of (a) unstable unblocked low-level flow, (b) stable blocked low-level flow. The diagrams show the types of hydrometeors present in each case, along with the flow behavior. The dashed box in (a) indicates the position of the embedded convective precipitation. Adapted from Medina and Houze (2003) and Rotunno and Houze (2007).

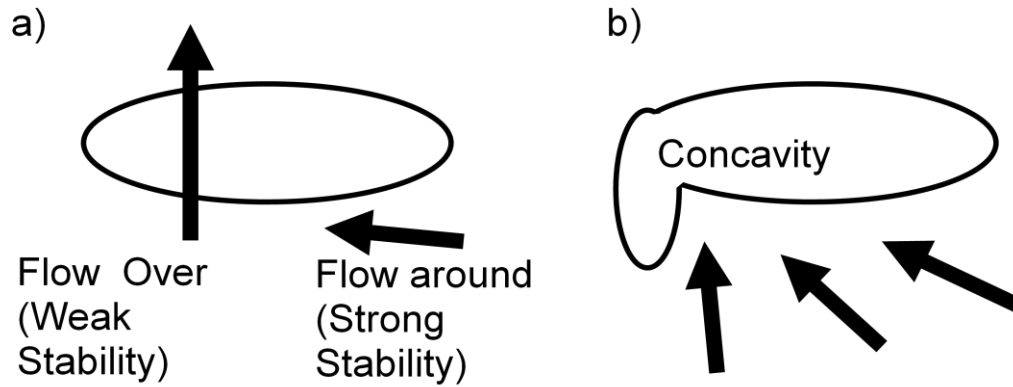


Figure 3. Schematic diagram of Alpine-scale orographic flow modifications illustrating (a) the importance of weak stability enabling depicted southerly flow to surmount the tall Alpine barrier instead of flowing around (to the left in the Northern Hemisphere) and (b) effects of Alpine shape in directing southerly flow towards the concavity. Adapted from Rotunno and Houze (2007).

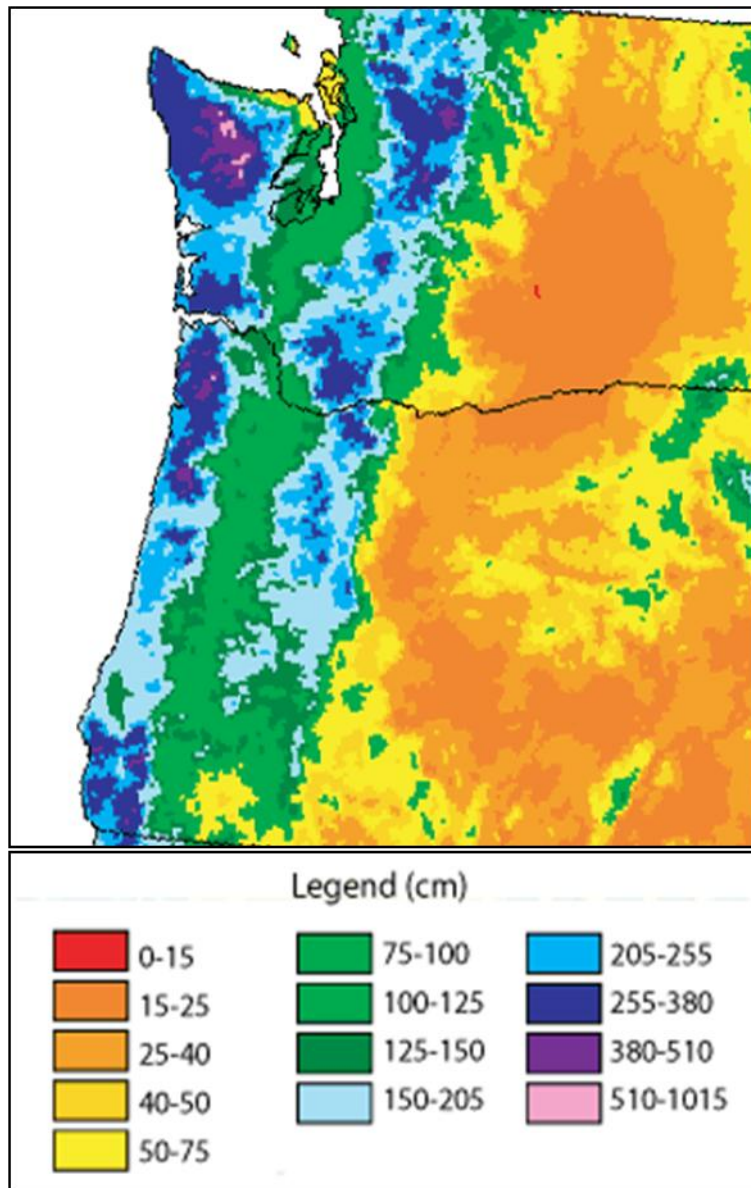


Figure 4. Average annual precipitation (in inches) for thirty-year (1961 – 1990) climatology of the U.S. Pacific Northwest. The diagram shows enhanced precipitation associated with Coastal (left side) and Cascade (right side) Ranges in the analysis area (From Daly et al. 1994).

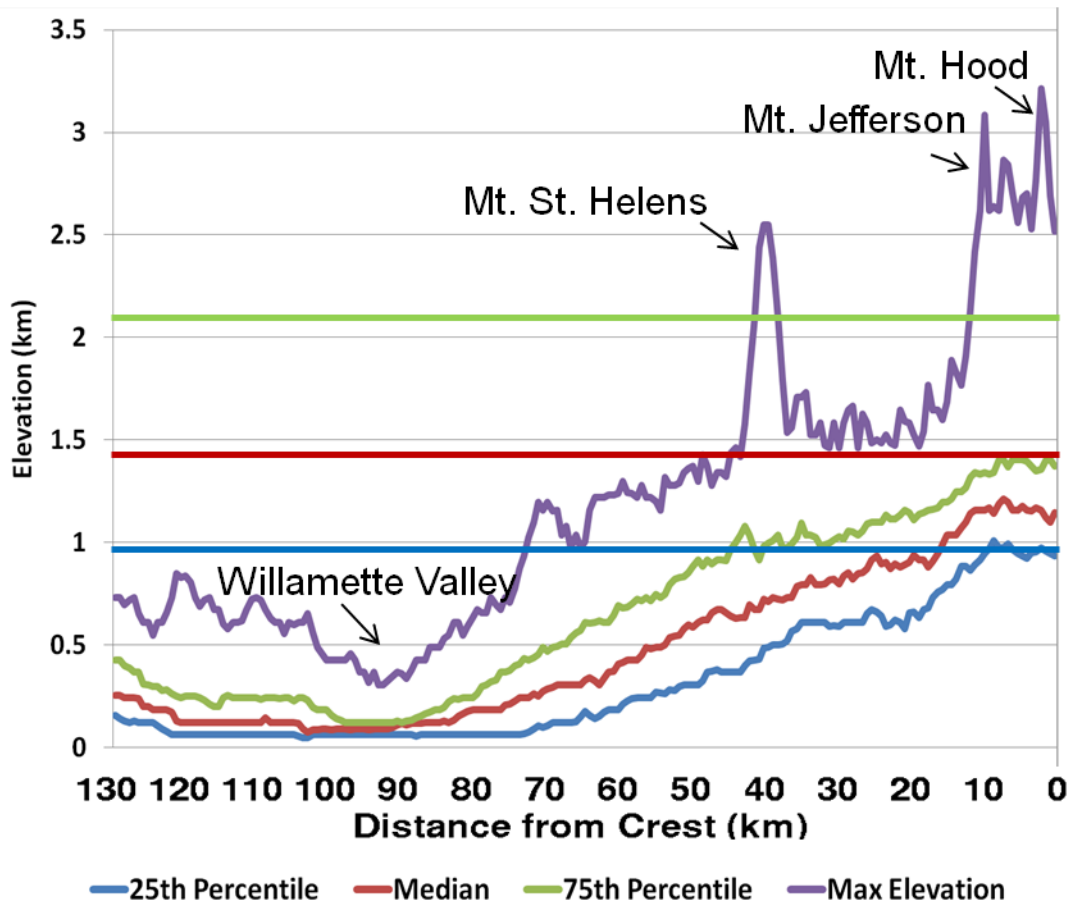


Figure 5. Meridional (North-South) 25<sup>th</sup>, 50<sup>th</sup>, 75<sup>th</sup> percentiles and maximum values of gridded terrain elevation within study domain. Significant terrain features along the Cascade windward slope are indicated. The horizontal lines correspond to the 25<sup>th</sup>, 50<sup>th</sup>, and 75<sup>th</sup> percentiles of the freezing level altitude.

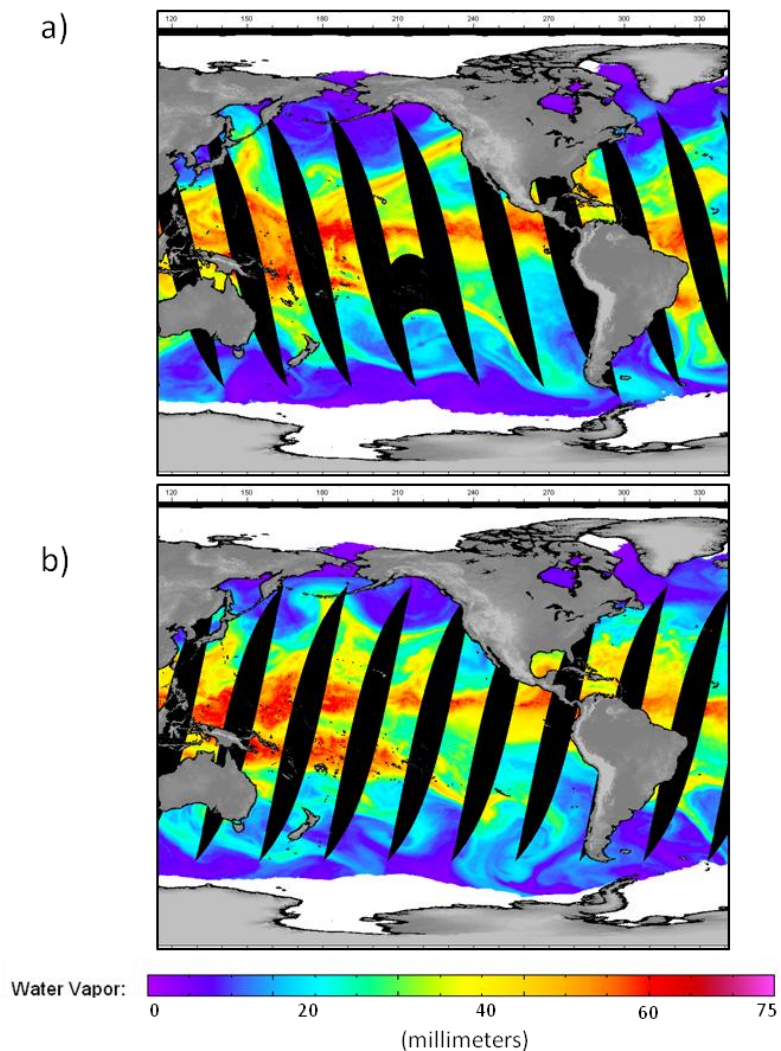


Figure 6. Vertically integrated water vapor (IWV) in mm as measured by SSM/I instruments carried onboard the DMSP series of polar orbiting satellites. Land regions are colored gray where measurements are not valid. The areas colored black is where the satellite did not pass over and no data were collected, areas where data were collected but were determined to be bad, coastal areas, or areas affected by sun glint. (a) IWV measured by SSM/I overpass on November 7, 2006 at 20:30 local time, illustrating a land-falling atmospheric river along the Oregon coast. (b) IWV measured by SSM/I overpass on November 6, 2005 at 08:30 local time, illustrating a possible land-falling atmospheric river with a satellite data gap occurring along the Oregon coast. Images from the Remote Sensing Systems ([www.remss.com](http://www.remss.com)).

Figure 7. Contoured Frequency by Distance Diagram (CFDD) explanation. (a) Persistence ( $Z > 13$  dBZ frequency) horizontal cross-section at 2 km altitude. (b) Histogram of persistence data within the 2 km wide box in 3a. (c) Histogram in 3b in 3-dimensional space with respect to distance from the crest. X-axis is distance from crest, Y-axis is the persistence values, Z-axis is the normalized percent occurrence. (d) Histograms of all data across the study domain in 3a placed into the 3-dimensional variable space. Red histogram is the same as 3c. (e) Histograms colored color-coded by their normalized percent occurrence (Z-axis). (f) Values of Z-axis contoured similar to a topographic map. Color scale indicates the contoured normalized percent occurrence (Z-axis) values.

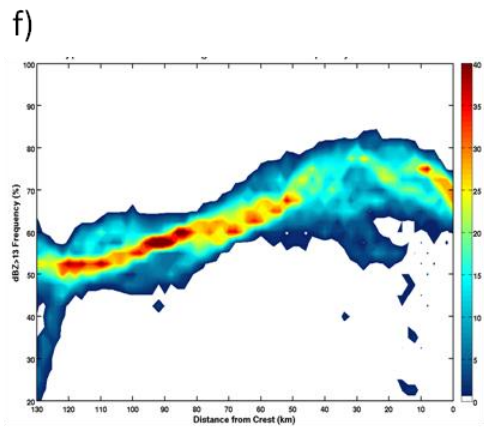
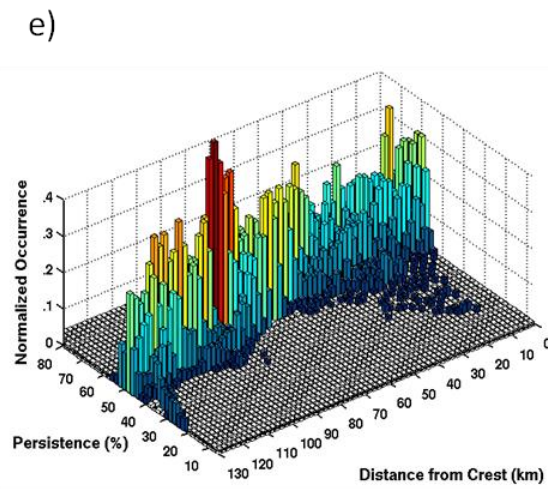
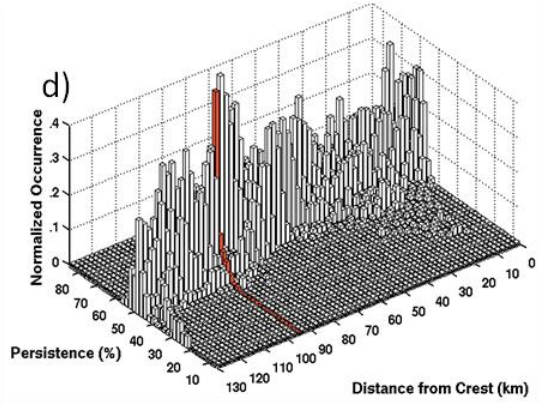
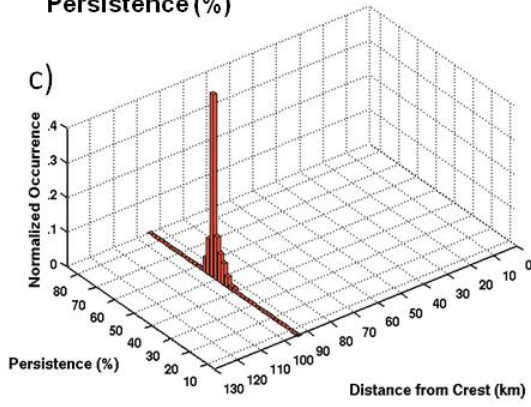
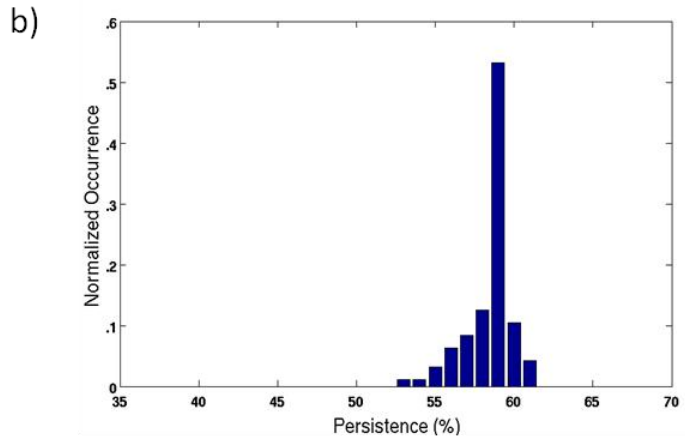
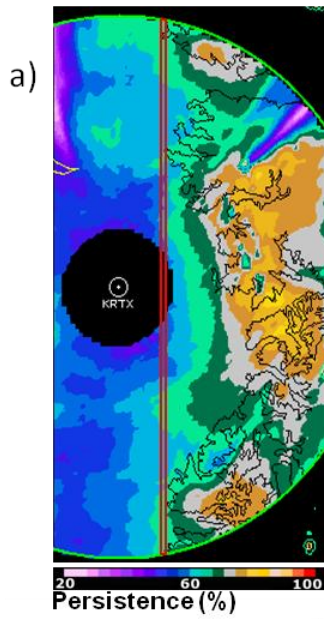
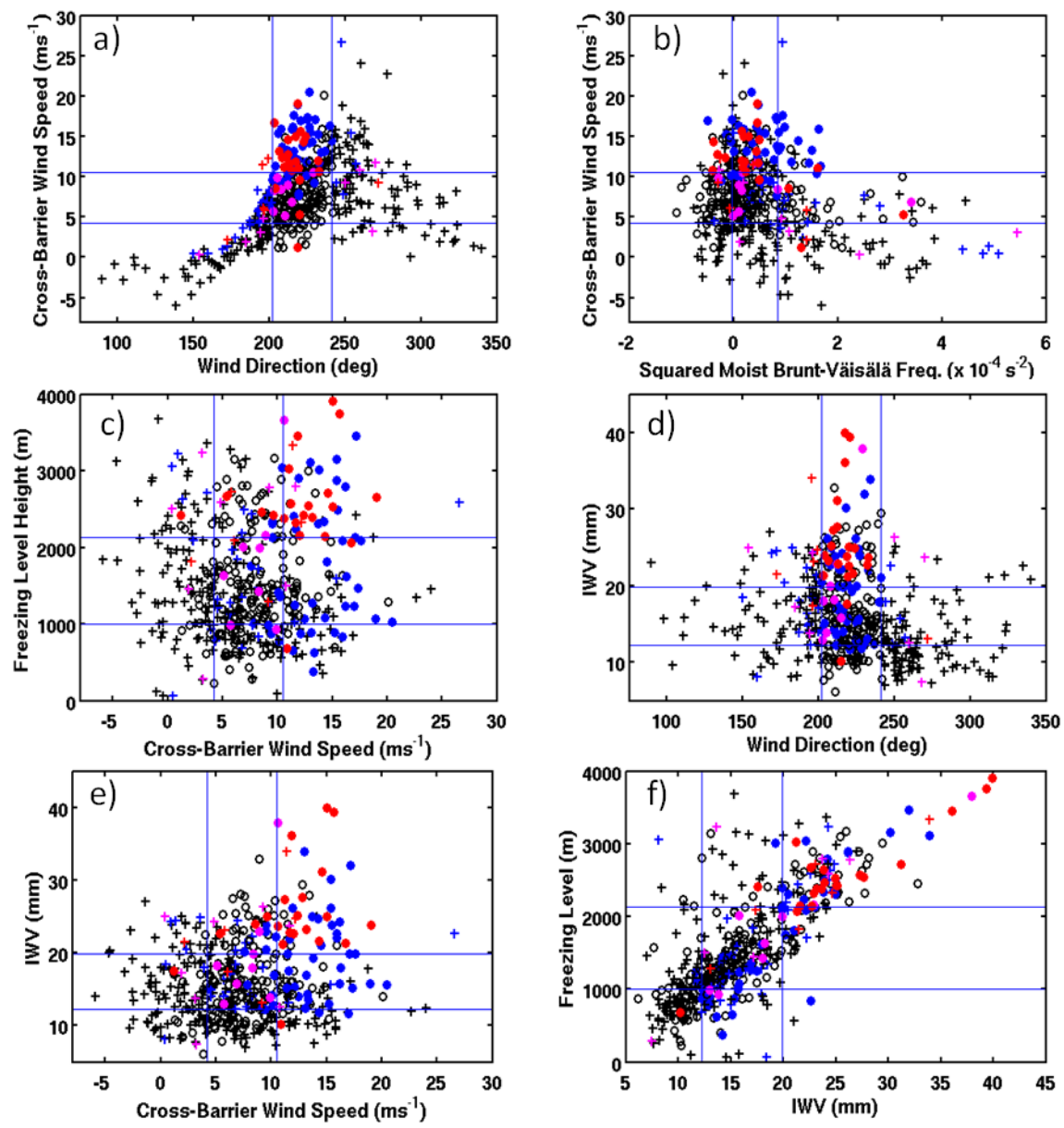


Figure 8. Scatter plots of environmental variables layer-averaged from the surface to 2.2 km AMSL from all SLE winter storm soundings (487) from 2003 to 2008. Blue lines indicate the 25<sup>th</sup> and 75<sup>th</sup> percentiles of the plotted variable (see Table 1). 12-hour periods when the wind direction was between the 25<sup>th</sup> and 75<sup>th</sup> percentile of the wind direction (202°-242°) are indicated by circular points. Wind directions outside this subset are shown by crosses. Blue markers indicate times when the flow was multi-layered, red shows flooding time periods which were multi-layered, and magenta indicates time periods when the flow was not multi-layered but resulted in flooding. (a) Average wind direction versus average cross-barrier wind speed. (b) Average squared moist Brunt-Vaisala Frequency versus average cross-barrier wind speed. (c) Average cross-barrier wind speed versus freezing level altitude (AMSL). (d) Average wind direction versus IWV. (e) Average cross-barrier wind speed versus IWV. (f) IWV versus freezing level altitude (AMSL).



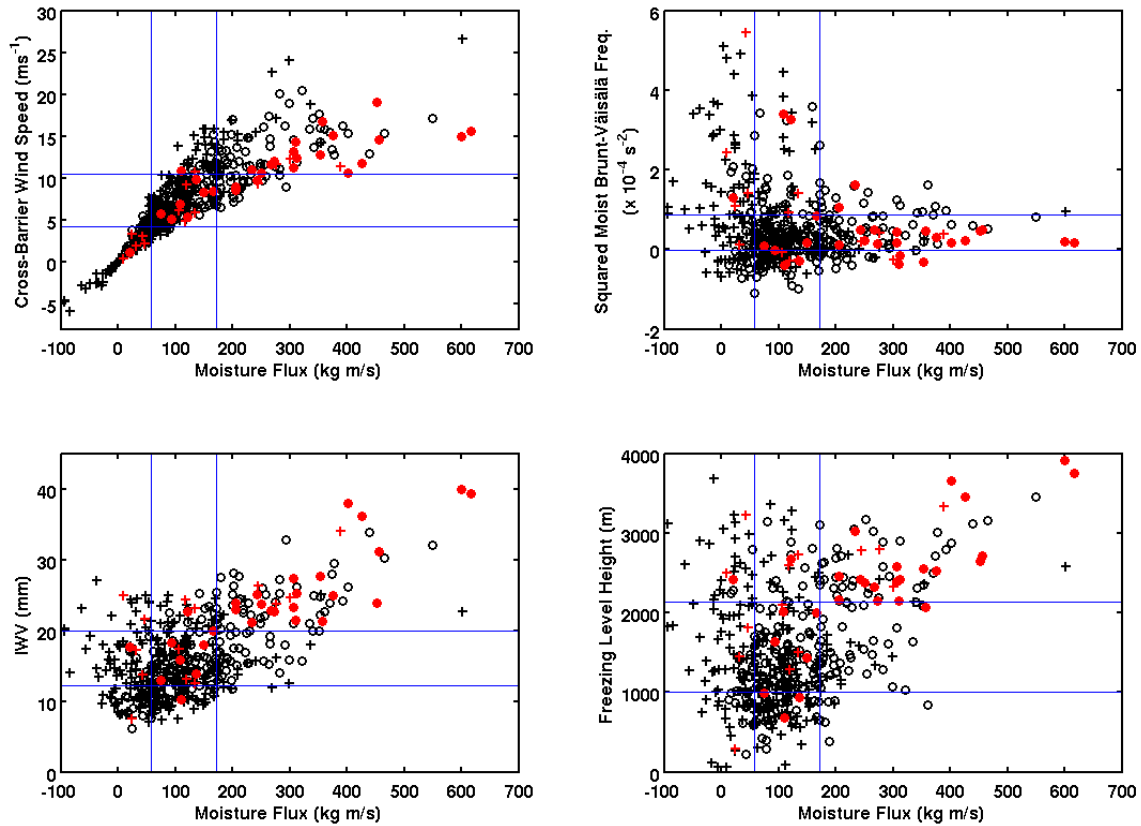
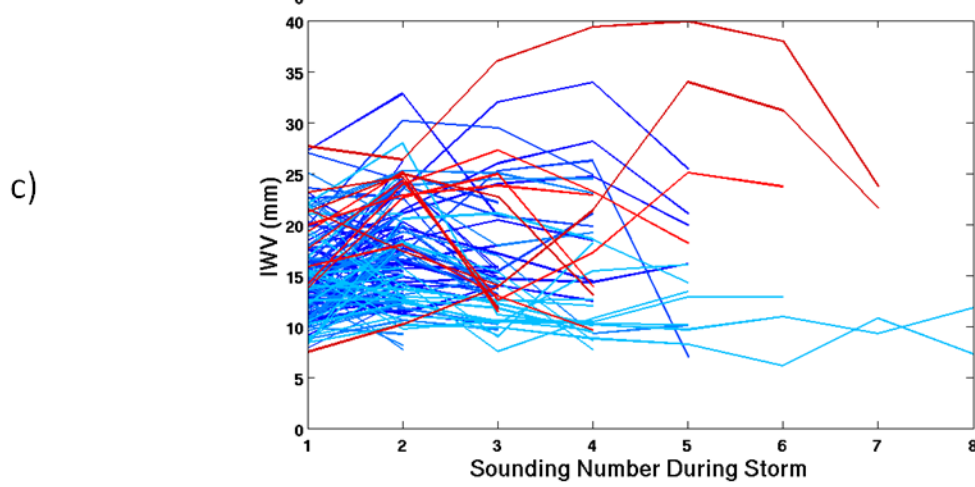
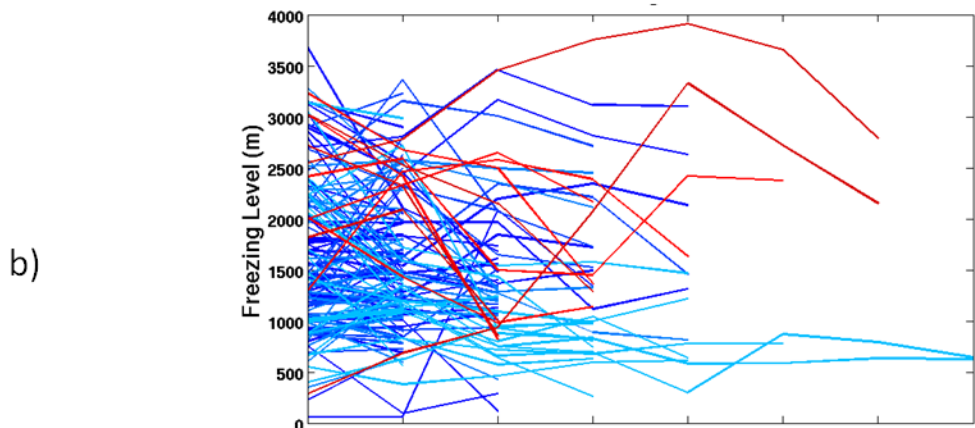
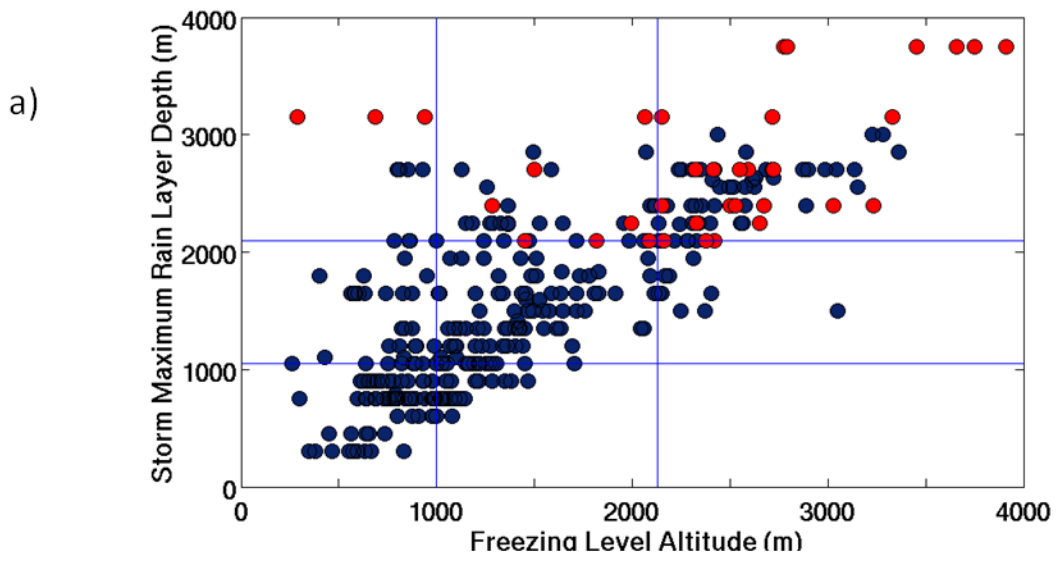


Figure 9. Scatter plots of moisture flux and other environmental variables layer-averaged from the surface to 2.2 km AMSL from all SLE winter storm soundings (487) from 2003 to 2008. Blue lines indicate the 25<sup>th</sup> and 75<sup>th</sup> percentiles of the plotted variable (see Table 1). 12-hour periods when the wind direction was between the 25<sup>th</sup> and 75<sup>th</sup> percentile of the wind direction (202°-242°) are indicated by circular points. Red indicates flooding events. (a) Average cross-barrier wind speeds versus moisture flux. (b) Average squared moist Brunt-Vaisala Frequency versus moisture flux. (c) IWV versus moisture flux. (d) Freezing level altitude (AMSL) versus moisture flux.

Figure 10. (a) Scatter plot of SLE sounding derived freezing level and MRR-derived storm maximum rain layer depth. Thin blue lines indicated 25<sup>th</sup> and 75<sup>th</sup> percentiles for each variable. (b) Freezing level altitude for all 12 hourly soundings during each storm. Each line is an individual storm. (c) IWV for all 12 hourly soundings during each storm. Each line is an individual storm. Shades of blue indicate not flooding events. Red indicates flooding storms in (a), (b), and (c).



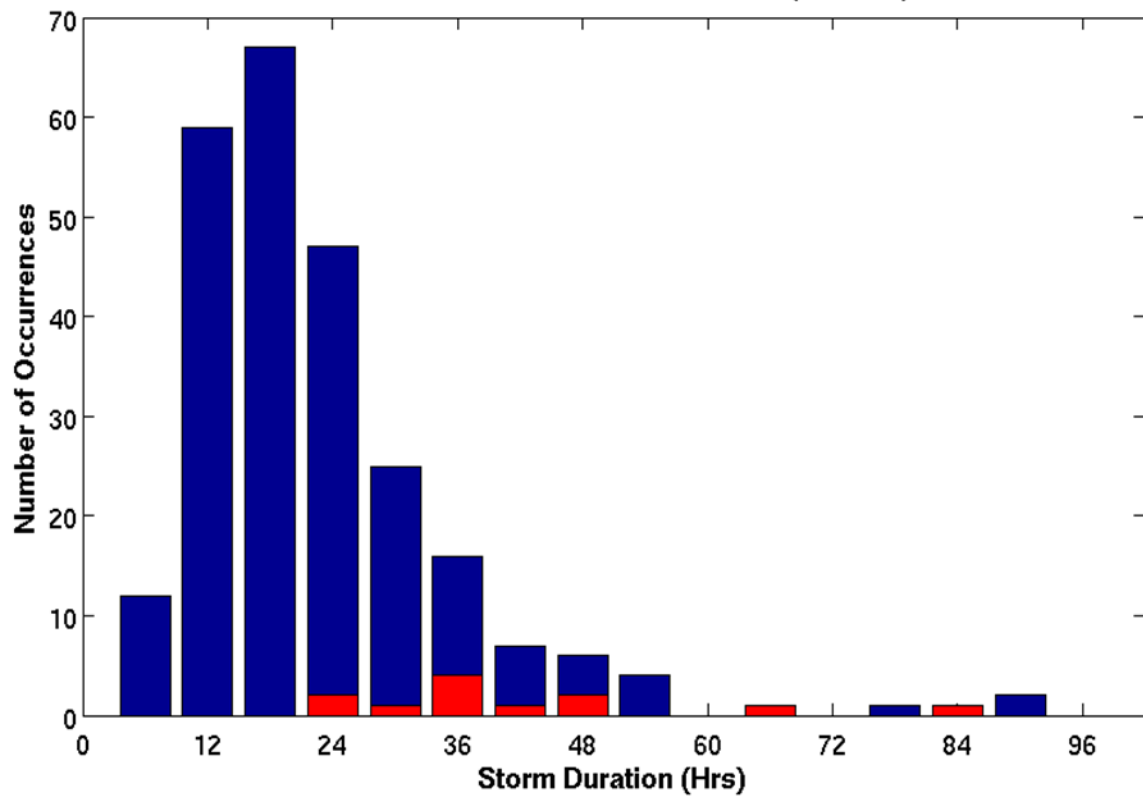


Figure 11. Histogram of all storm durations binned in 6 hour increments. Blue indicates non-flooding storms, red indicates flooding storms.

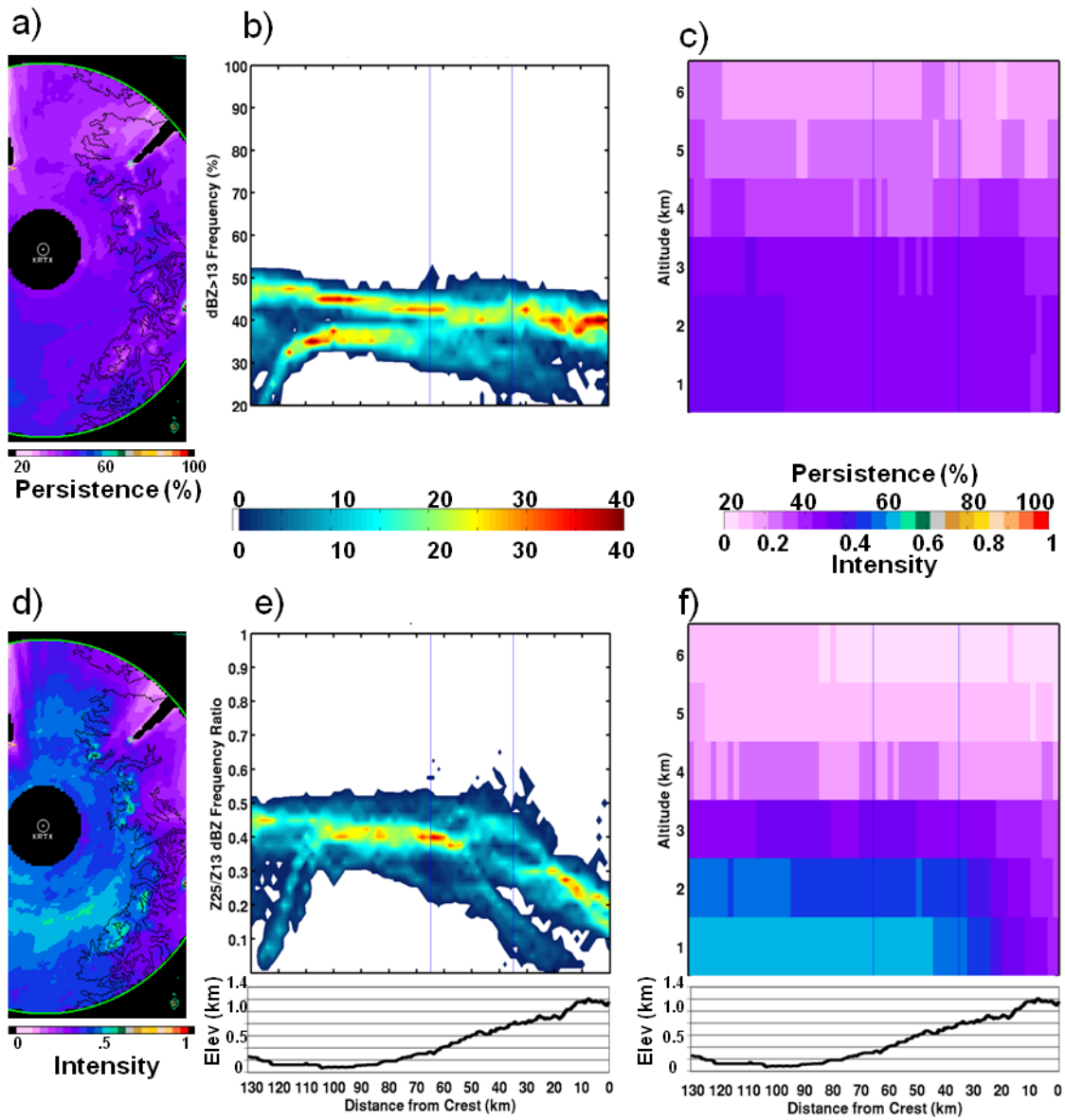


Figure 12. Radar composite of 12-hour periods with average downslope flow. Blue lines indicate 35 km and 65 km distance from the crest. Median terrain elevation is shown for reference. (a) Horizontal cross-section of precipitation persistence at 2 km altitude. (b) CFDD of persistence at 2 km altitude. (c) Cross-section of 75<sup>th</sup> percentile values of persistence. (d) Horizontal cross-section of precipitation intensity at 2 km altitude. (e) CFDD of intensity at 2 km altitude. (f) Cross-section of 75<sup>th</sup> percentile values of intensity.

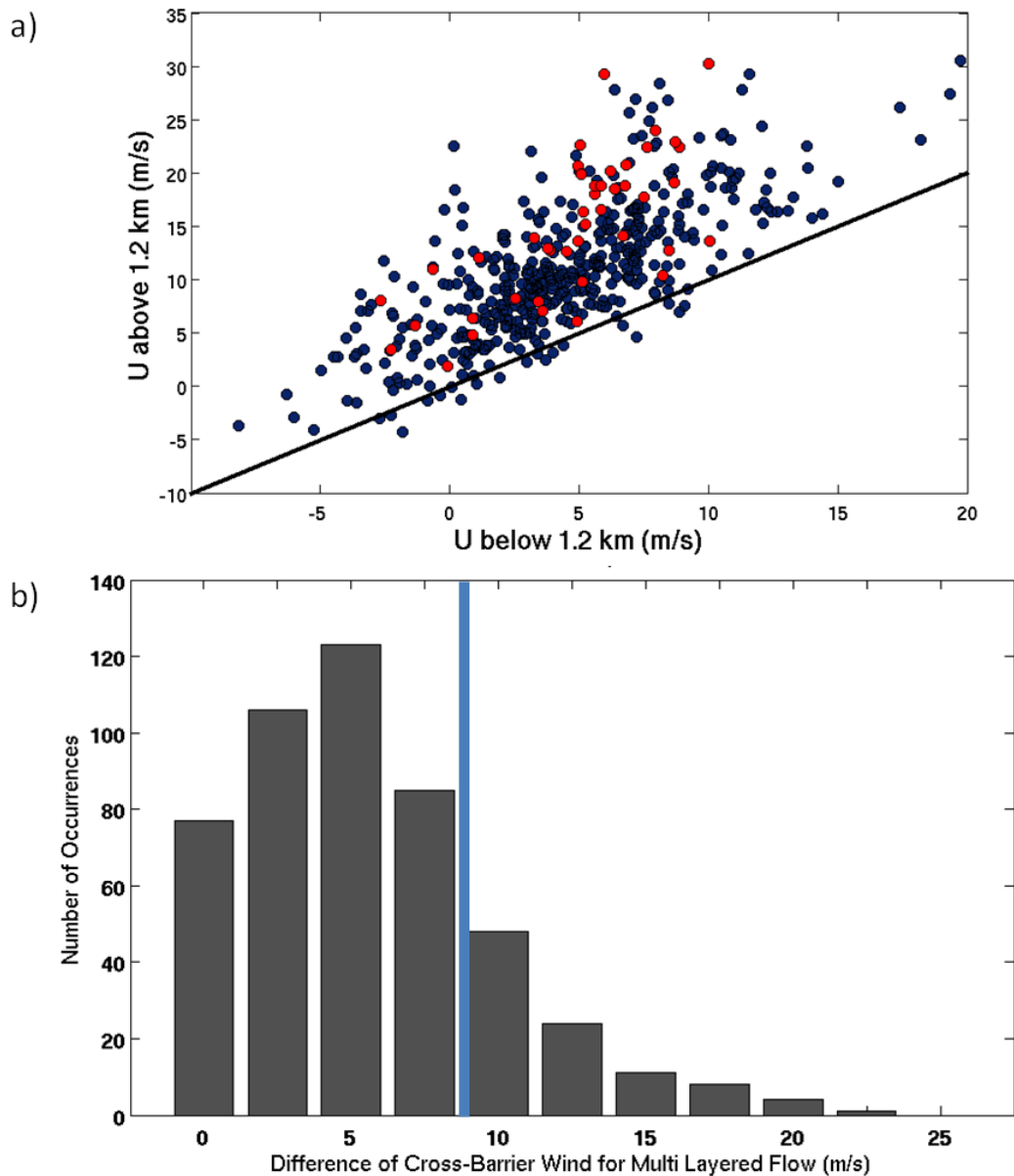


Figure 13. (a) Average cross-barrier wind speed from the surface to 1.2 km altitude versus average cross-barrier wind speed from 1.2 km to 2.2 km altitude measured by SLE soundings. Red markers indicate flooding events. The black line shows the 1-to-1 relationship. (b) Histogram of the differences between the average cross-barrier wind speed below 1.2 km and between 1.2 km and 2.2 km. Blue line indicates the 80<sup>th</sup> percentile of the distribution at 10 m/s. All samples to the right of the blue line are defined as two-layered flow regimes.

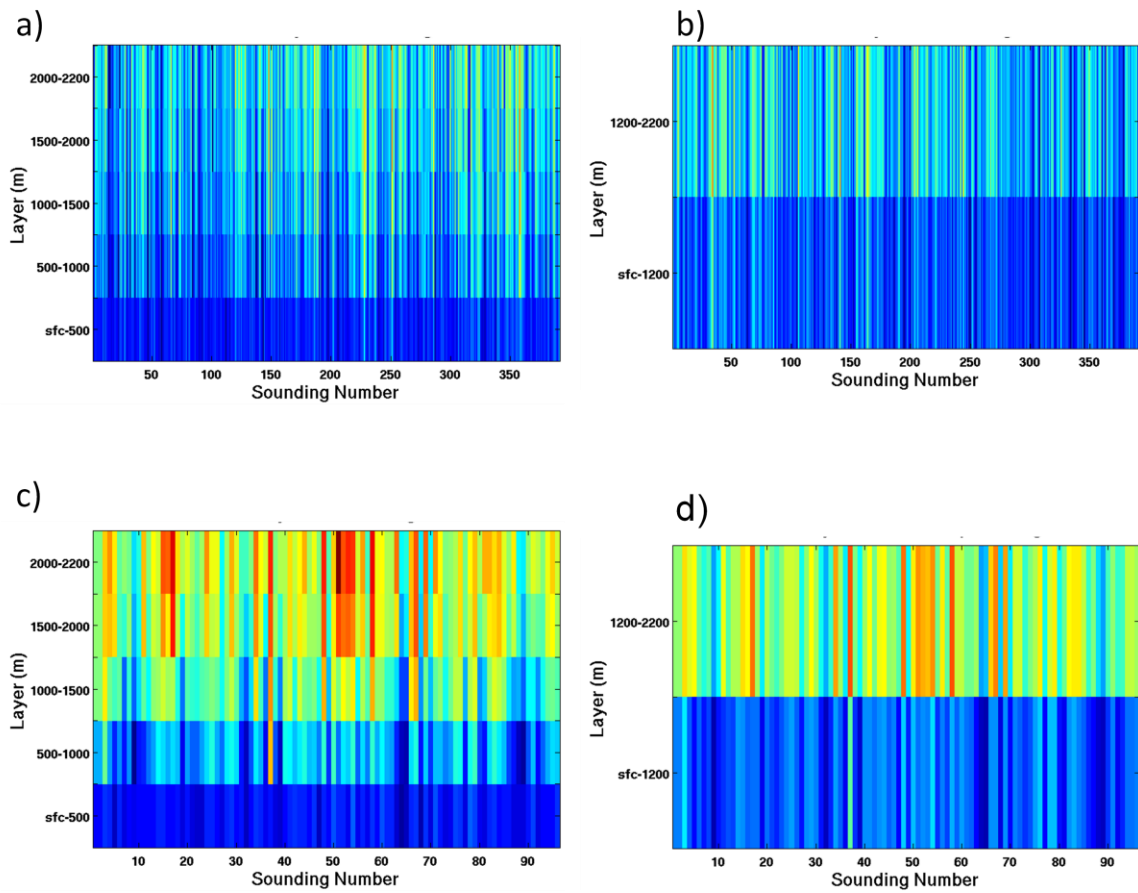


Figure 14. Layer averages of cross-barrier wind speed using 500 m thick and near 1000 m thick layers. (a) Cross-barrier wind speed averages for 500 m thick layers from the surface to 2.2 km for soundings that do not have defined multi-layered flow. This highest layer average is only 200 m thick. (b) Cross-barrier wind speed average for two layers, bottom layer is from the surface to 1.2 km, and the upper layer is from 1.2 km to 2.2 km altitude, for soundings that do not have defined multi-layered flow. (c) Same as (a) for soundings that do have defined multi-layered flow. (d) Same as (b) for soundings that do have defined multi-layered flow.

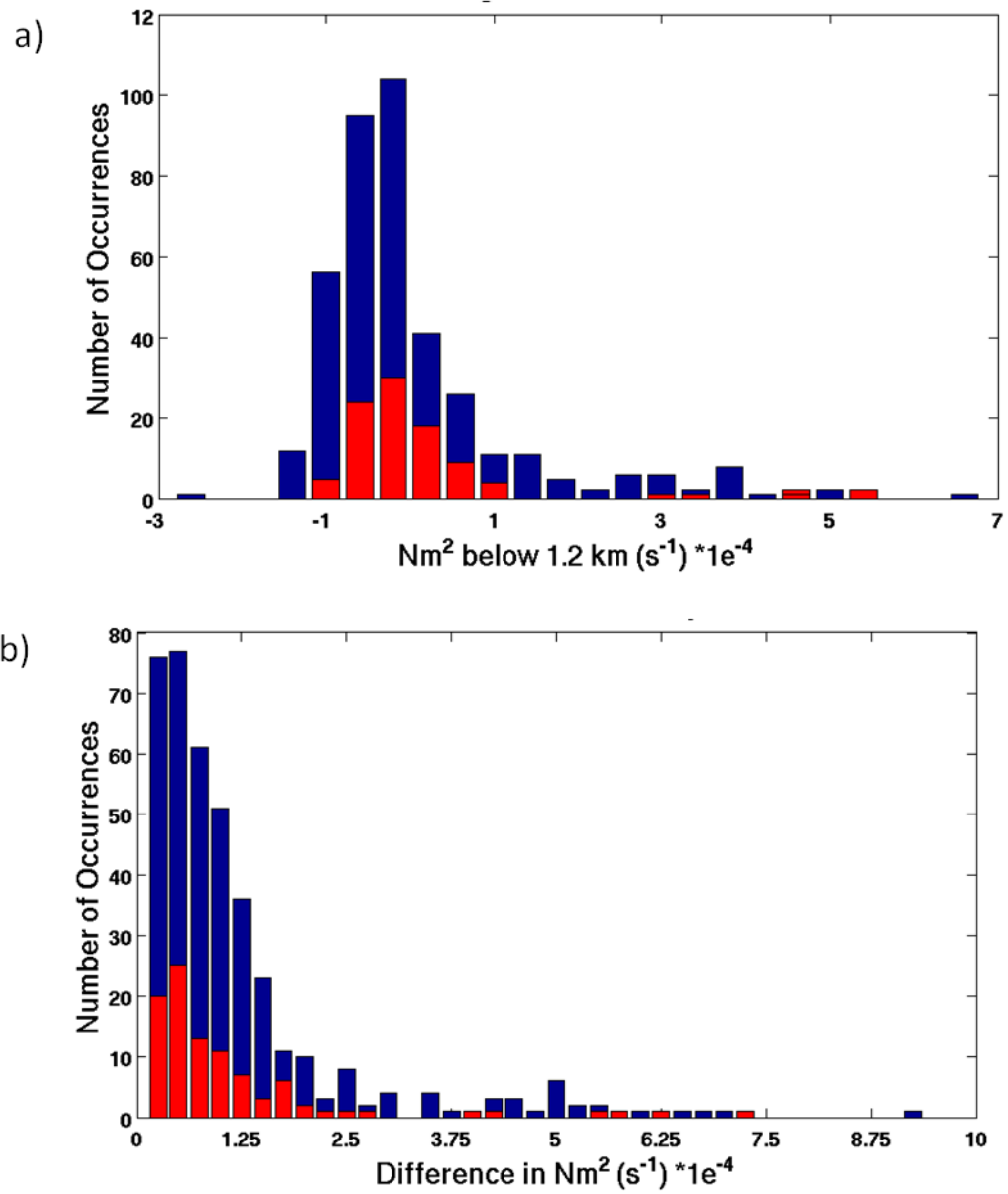


Figure 15. (a) Histogram of the average Brunt Vaisala Frequency from the surface to 1.2 km AMSL. Red indicates multi-layered flow cases. (b) Layer average differences in average Brunt-Vaisala Frequency from the surface to 1.2 km AMSL and 1.2 km to 2.2 km AMSL. Red indicates multi-layered flow cases.

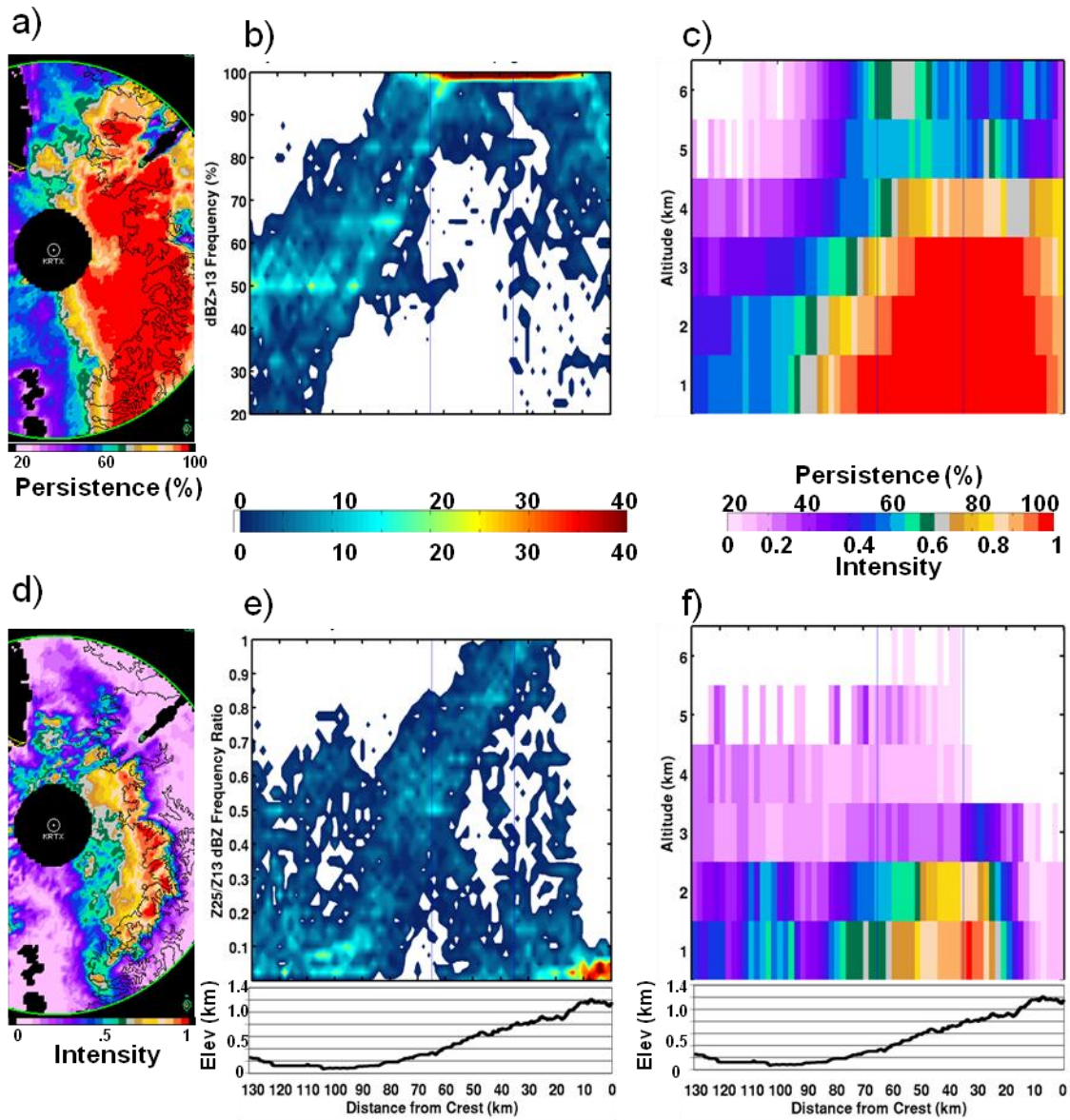


Figure 16. Radar composite of 12-hour period illustrating patterns associated with 2 layer flow. Data from the period  $\pm 6$  hours from the SLE released March 3, 2007 00Z. (a) Horizontal cross-section of precipitation persistence at 2 km altitude. (b) CFDD of persistence at 2 km altitude. (c) Cross-section of 75th percentile values of persistence. (d) Horizontal cross-section of precipitation intensity at 2km altitude. (e) CFDD of intensity at 2 km altitude. (f) Cross-section of 75th percentile values of intensity.

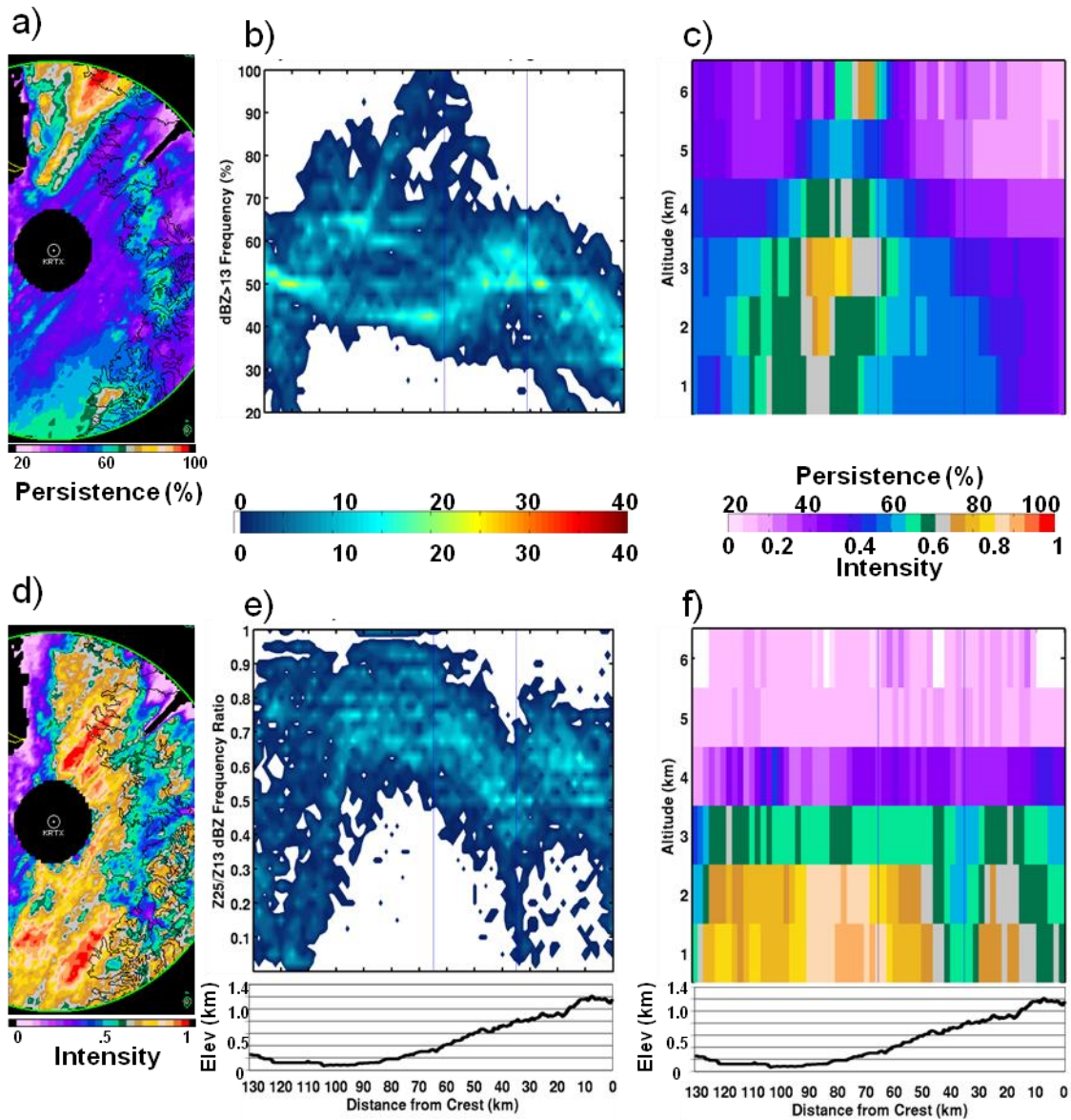
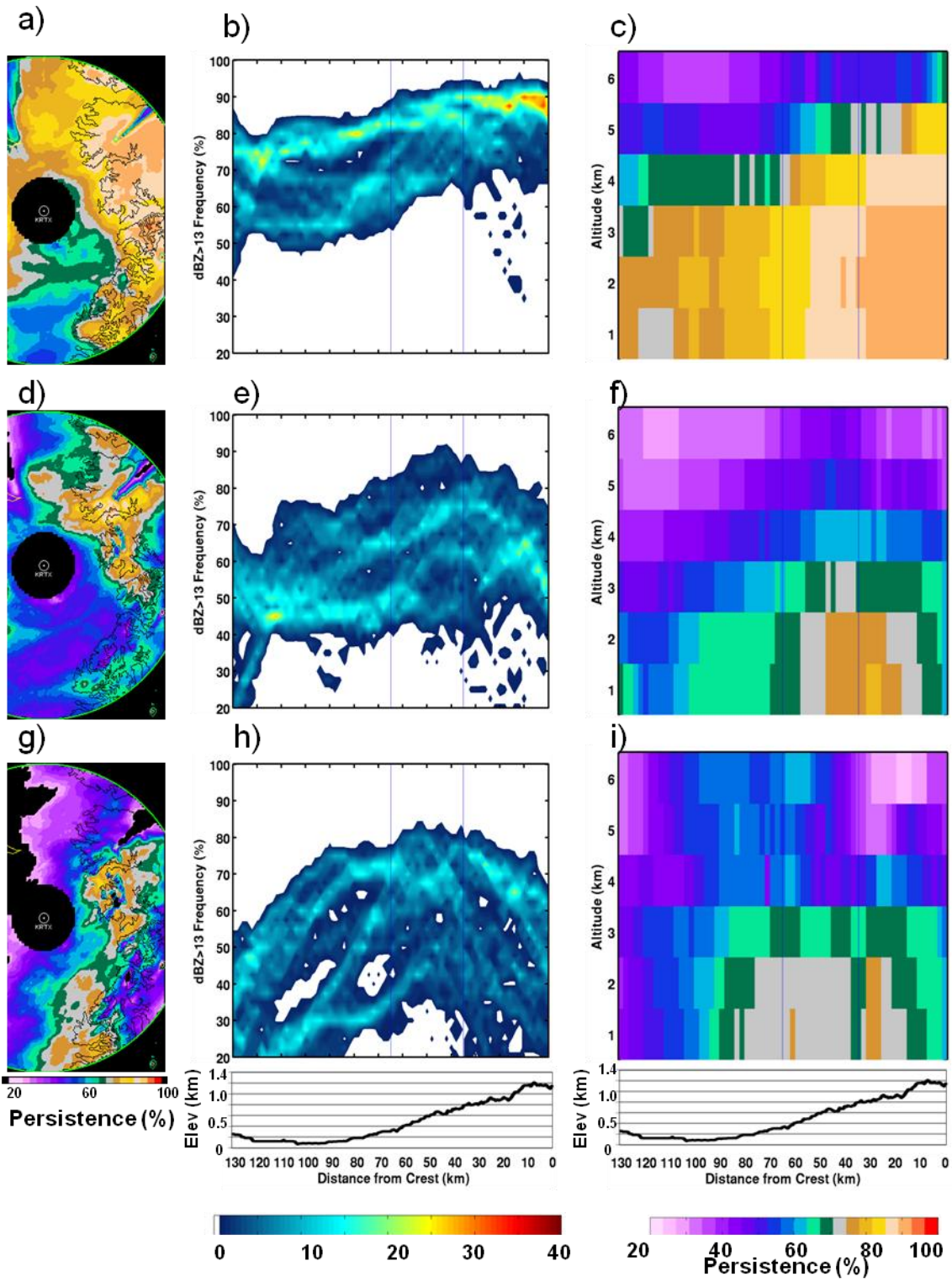


Figure 17. Radar composite of 12-hour period illustrating patterns associated with single layer flow. Data from the period  $\pm 6$  hours from the SLE released March 20, 2007 00Z. (a) Horizontal cross-section of precipitation persistence at 2 km altitude. (b) CFDD of persistence at 2 km altitude. (c) Cross-section of 75<sup>th</sup> percentile values of persistence. (d) Horizontal cross-section of precipitation intensity at 2 km altitude. (e) CFDD of intensity at 2 km altitude. (f) Cross-section of 75<sup>th</sup> percentile values of intensity.

Figure 18. Radar composites of 12 hour periods  $\pm$  6 hours from SLE soundings testing the sensitivity of precipitation persistence on derived freezing level and cross-barrier wind speed values. The median terrain elevation is shown for reference. (a) Horizontal cross-section at 2 km altitude for 12-hour periods with freezing level and cross-barrier wind speed greater than their 75<sup>th</sup> percentiles. (b) CFDD at 2 km altitude using same 12-hour periods as (a). (c) Cross-section of 75<sup>th</sup> percentiles using same 12-hour periods as (a). (d) Horizontal cross-section at 2 km altitude for 12-hour periods with freezing level less than the 25<sup>th</sup> percentile and cross-barrier wind speed greater than the 75<sup>th</sup> percentile. (e) CFDD at 2 km altitude using same 12-hour periods as (d). (f) Cross-section of 75<sup>th</sup> percentiles using same 12-hour periods as (d). (g) Horizontal cross-section at 2 km altitude for 12-hour periods with freezing level greater than the 75<sup>th</sup> percentile and cross-barrier wind speed less than the 75<sup>th</sup> percentile (h) CFDD at 2 km altitude using same 12-hour periods as (g). (i) Cross-section of 75<sup>th</sup> percentiles using same 12-hour periods as (g).



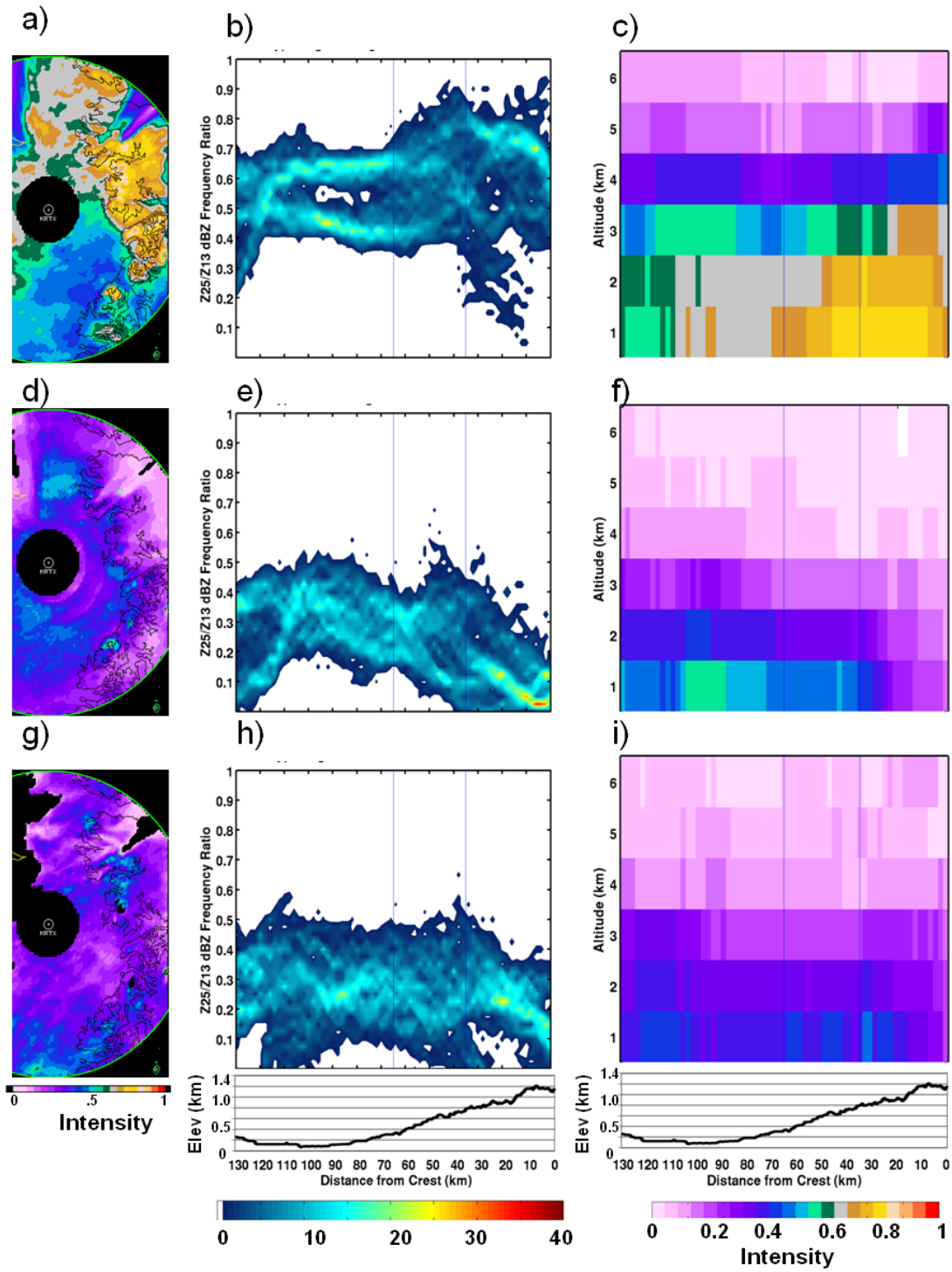
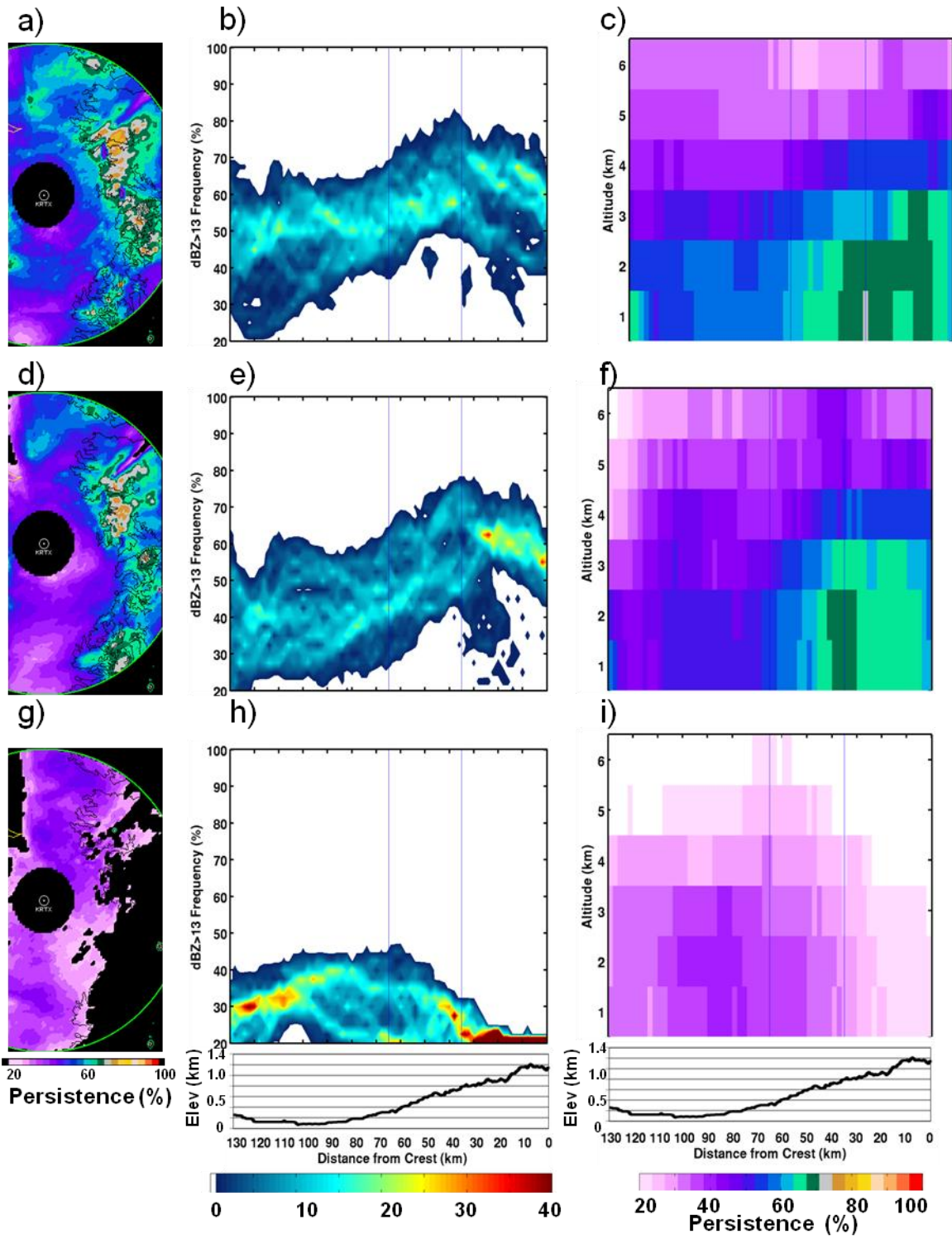


Figure 19. Same as Figure 15 with calculated precipitation intensity.

Figure 20. Radar composites of 12 hour periods  $\pm 6$  hours from SLE soundings testing the sensitivity of precipitation persistence on derived squared moist Brunt-Vaisala frequency and cross-barrier wind speed values. The median terrain elevation is shown for reference. (a) Horizontal cross-section at 2 km altitude for 12-hour periods with the squared moist Brunt-Vaisala frequency and cross-barrier wind speed greater than their 75<sup>th</sup> percentiles. (b) CFDD at 2 km altitude using same 12-hour periods as (a). (c) Cross-section of 75<sup>th</sup> percentiles using same 12-hour periods as (a). (d) Horizontal cross-section at 2 km altitude for 12-hour periods with the squared moist Brunt-Vaisala frequency less than the 25<sup>th</sup> percentile and cross-barrier wind speed greater than the 75<sup>th</sup> percentile. (e) CFDD at 2 km altitude using same 12-hour periods as (d). (f) Cross-section of 75<sup>th</sup> percentiles using same 12-hour periods as (d). (g) Horizontal cross-section at 2 km altitude for 12-hour periods with the squared moist Brunt-Vaisala frequency greater than the 75<sup>th</sup> percentile and cross-barrier wind speed less than the 75<sup>th</sup> percentile (h) CFDD at 2 km altitude using same 12-hour periods as (g). (i) Cross-section of 75<sup>th</sup> percentiles using same 12-hour periods as (g)



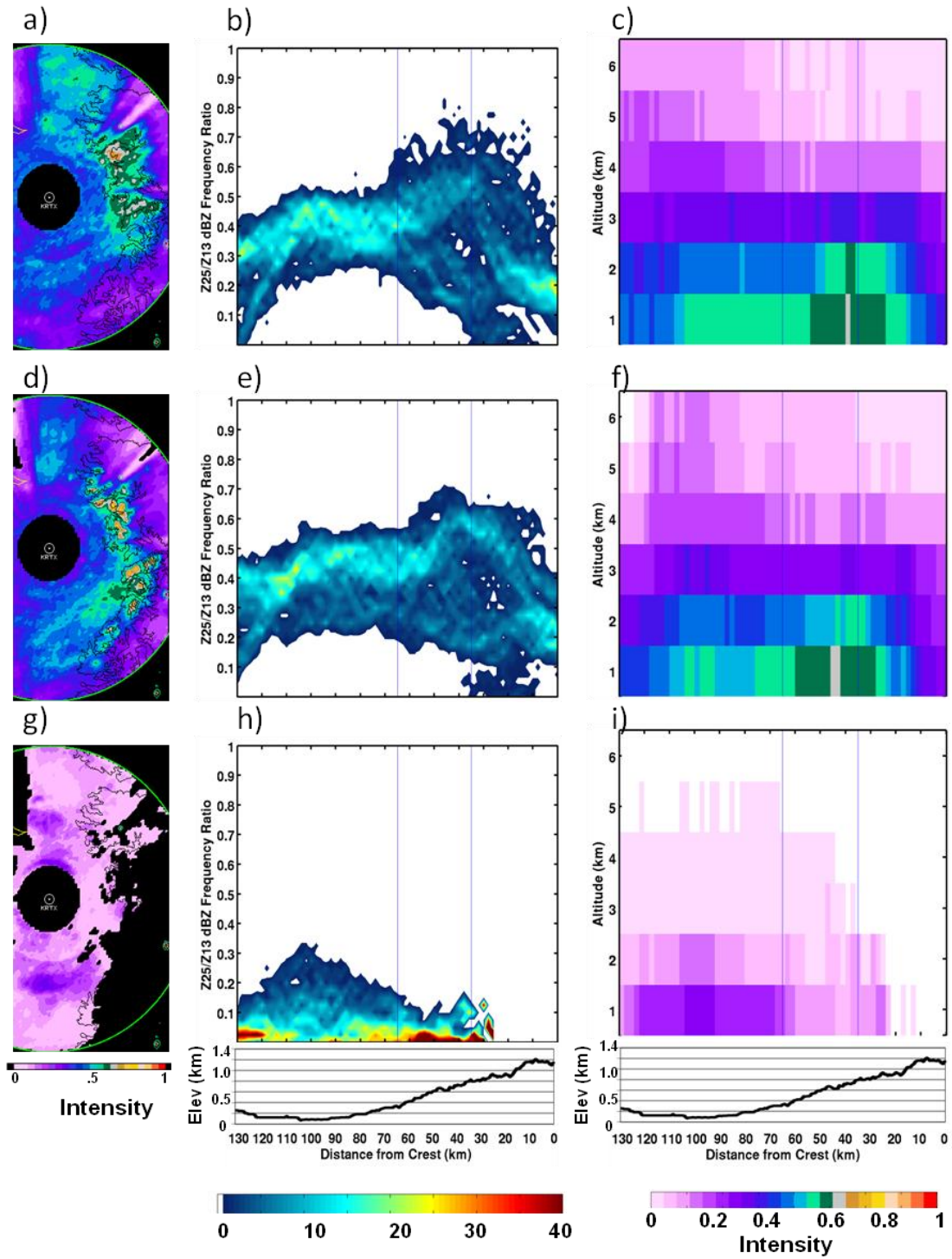


Figure 21. Same as Figure 17 with calculated precipitation intensity.

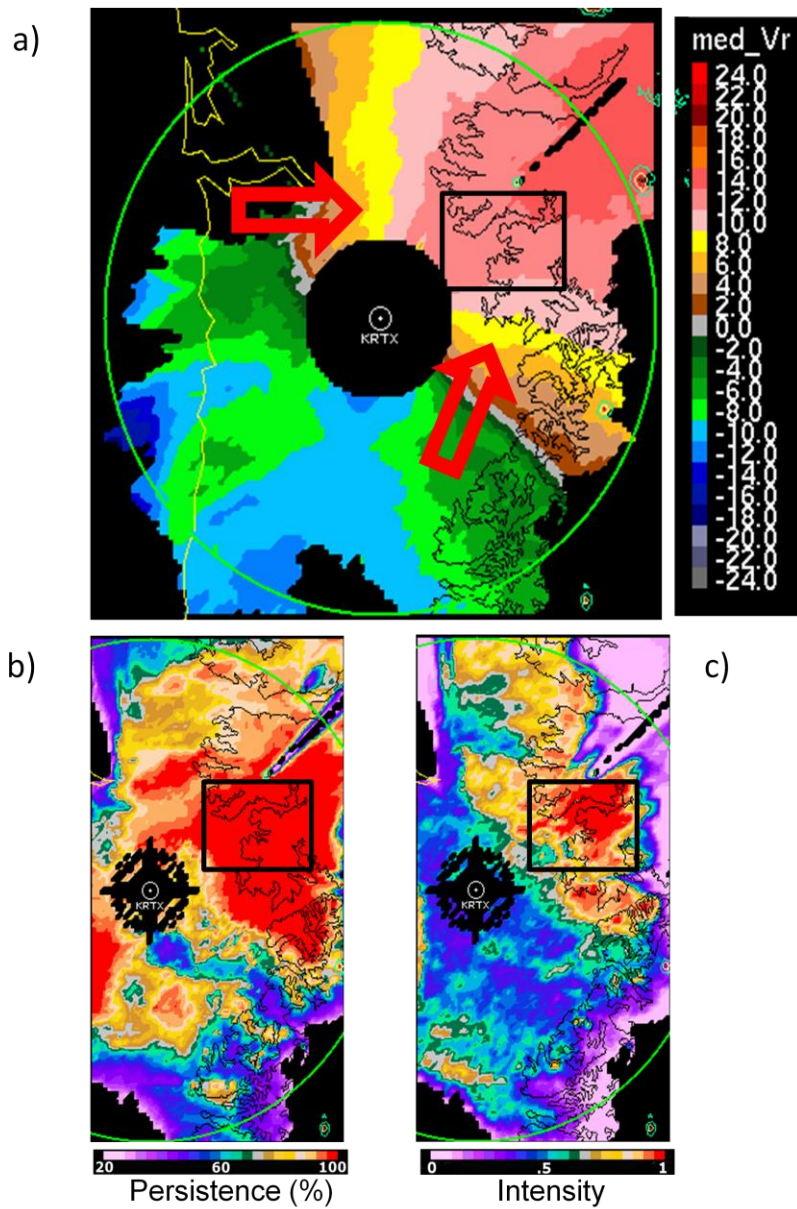


Figure 22. Radar composite of single 12-hour period  $\pm$  6 hours from the SLE released January 8, 2007 00Z illustrating precipitation enhancement over the Lewis River Valley. Black box indicates area of the Lewis River Valley (a) Horizontal cross-section of the median radial velocity at 1 km altitude. The red arrows indicate airflow direction. (b) Horizontal cross-section of precipitation persistence at 1 km altitude. (c) Horizontal cross-section of precipitation intensity at 1 km altitude.

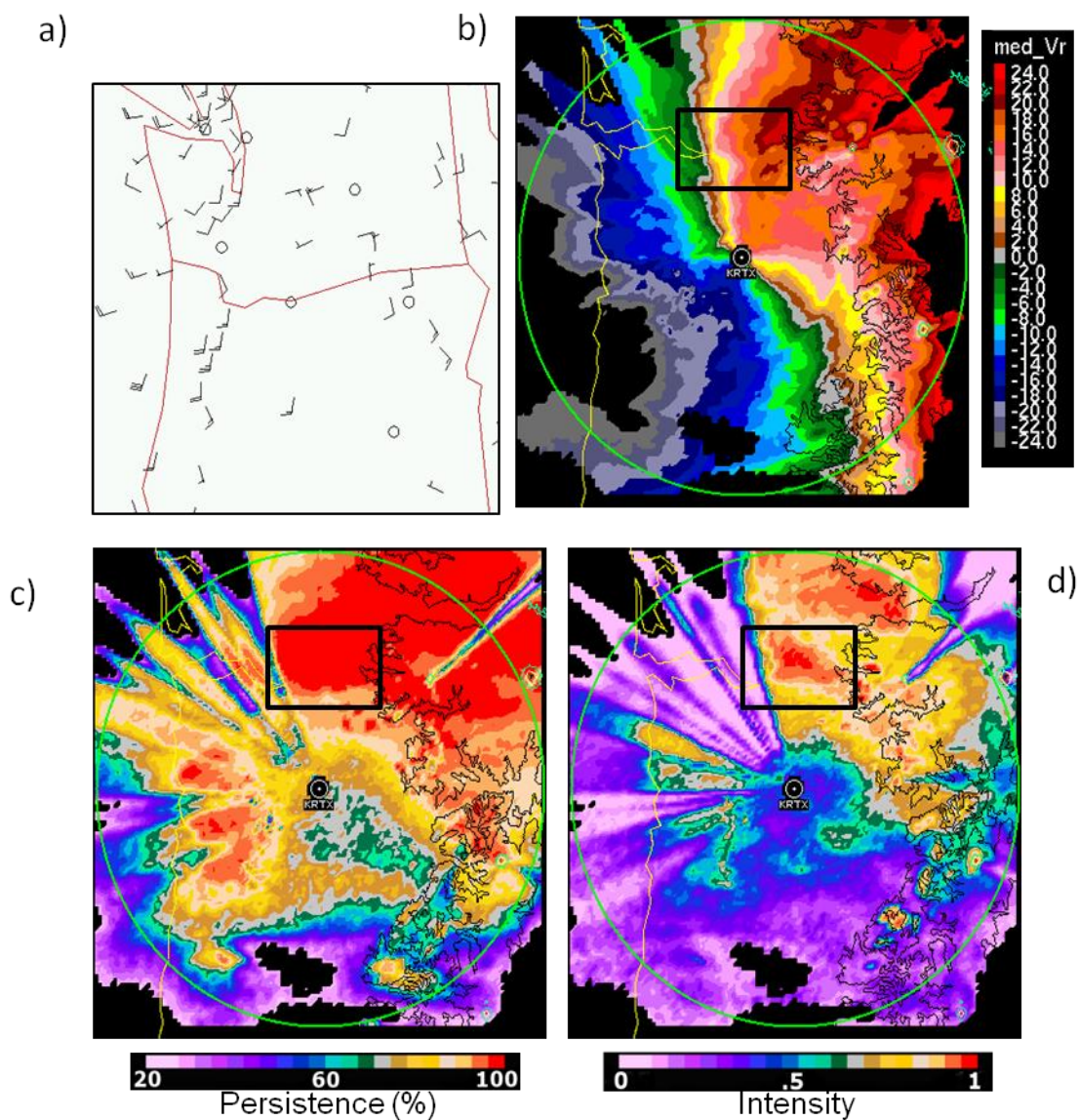


Figure 23. Radar composite of single 12-hour period  $\pm$  6 hours from the SLE released October 31, 2005 12Z illustrating precipitation enhancement over Kelso, Washington. Black box indicates area of Kelso, Washington (a) Surface winds (knots) at 15Z on October 31, 2005 in the Pacific Northwest (b) Horizontal cross-section of the median radial velocity at 1 km altitude. The red arrows indicate airflow direction. (c) Horizontal cross-section of precipitation persistence at 1 km altitude. (d) Horizontal cross-section of precipitation intensity at 1 km altitude.

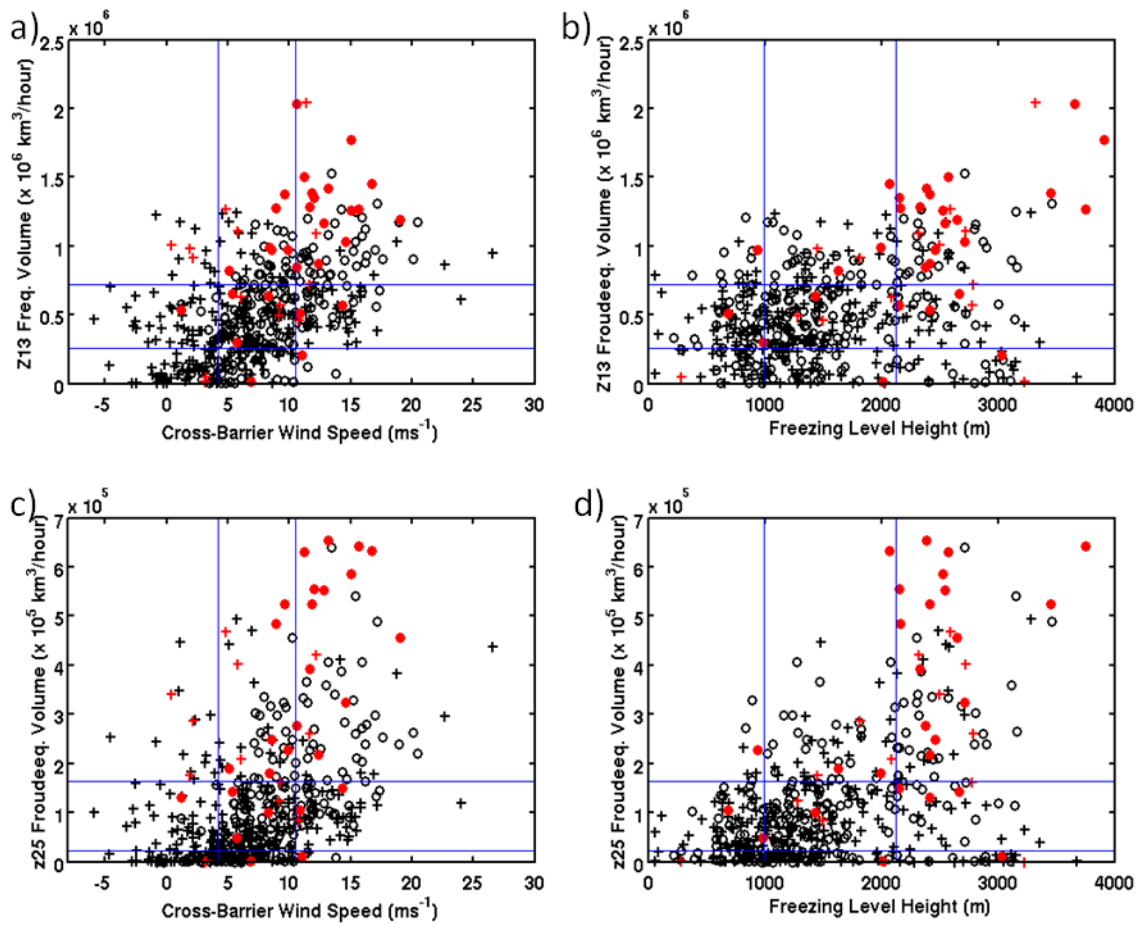


Figure 24. Scatter plots of SLE cross-barrier wind speed and freezing level versus storm volumes per hour. 12-hour periods when the wind direction was between the 25<sup>th</sup> and 75<sup>th</sup> percentile of the wind direction ( $202^{\circ}$ - $242^{\circ}$ ) are indicated by circular points. Wind directions outside this subset are shown by crosses. Red markers indicate times when flooding occurred. (a) Cross-barrier wind speed versus storm volume per hour of  $Z > 13$  dBZ. (b) Freezing level versus storm volume per hour of  $Z > 13$  dBZ. (c) Same as (a) with storm volume per hour of  $Z > 25$  dBZ. (d) Same as (b) with storm volume per hour of  $Z > 25$  dBZ.

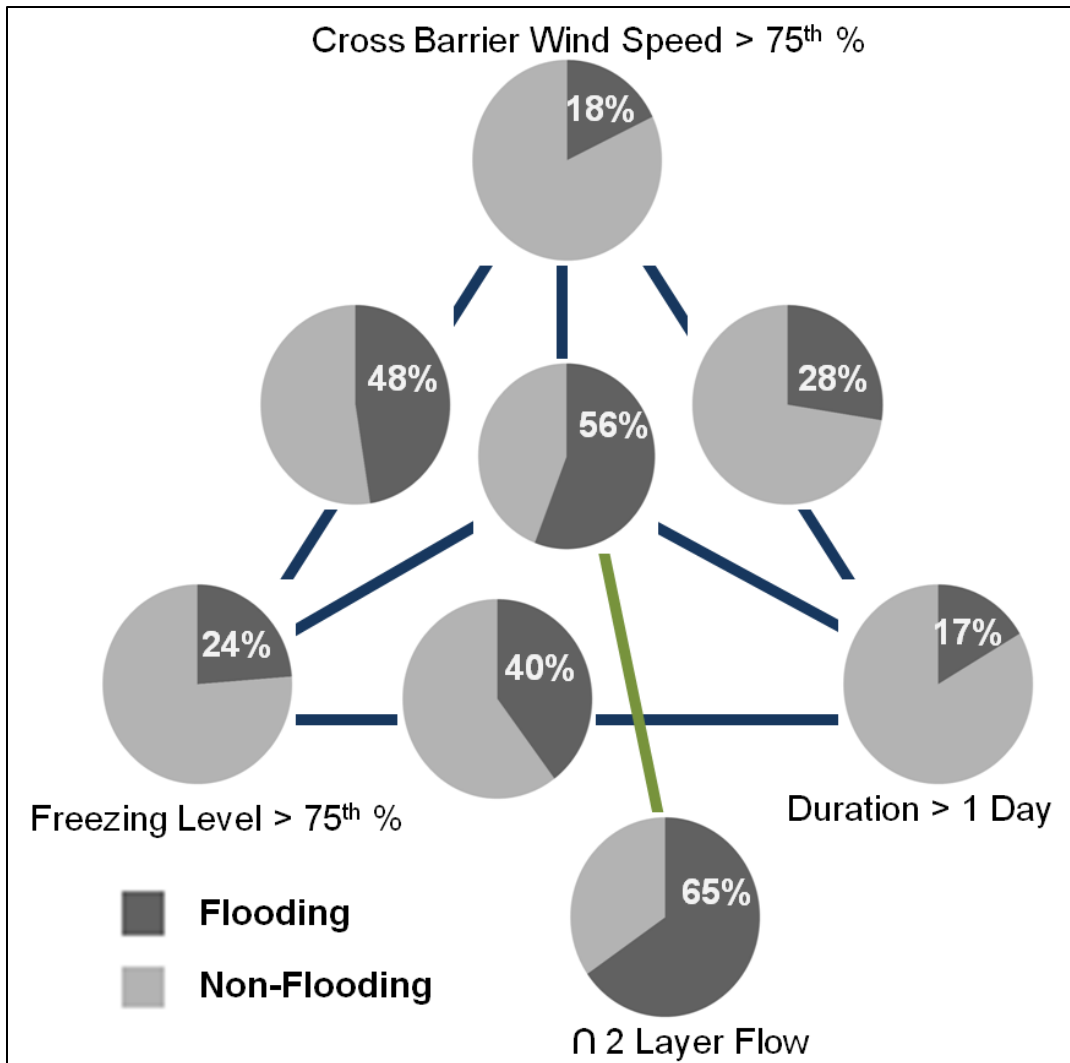


Figure 25. Single and combined conditional probabilities of flooding. Each point is associated with a pie chart, the darker shade of grey and number indicate the probability of flooding with that condition. Each pie chart at a vertex indicates the probability of flooding when the single variable it represents exceeds the stated threshold. The top vertex represents periods when the cross-barrier flow is greater than its 75<sup>th</sup> percentile (10.5 m/s). The bottom left vertex represents periods when the freezing level is greater than its 75<sup>th</sup> percentile (2130 m). The bottom right vertex represents periods when the storm duration is greater than 24 hours. Each side represents the probability of flooding when both conditions of the adjacent vertices are true. The center pie chart represents the probability of flooding when all three conditions are met. The bottom outlying vertex represents the probability when all three conditions are met and flow measured by the SLE sounding is two-layered.

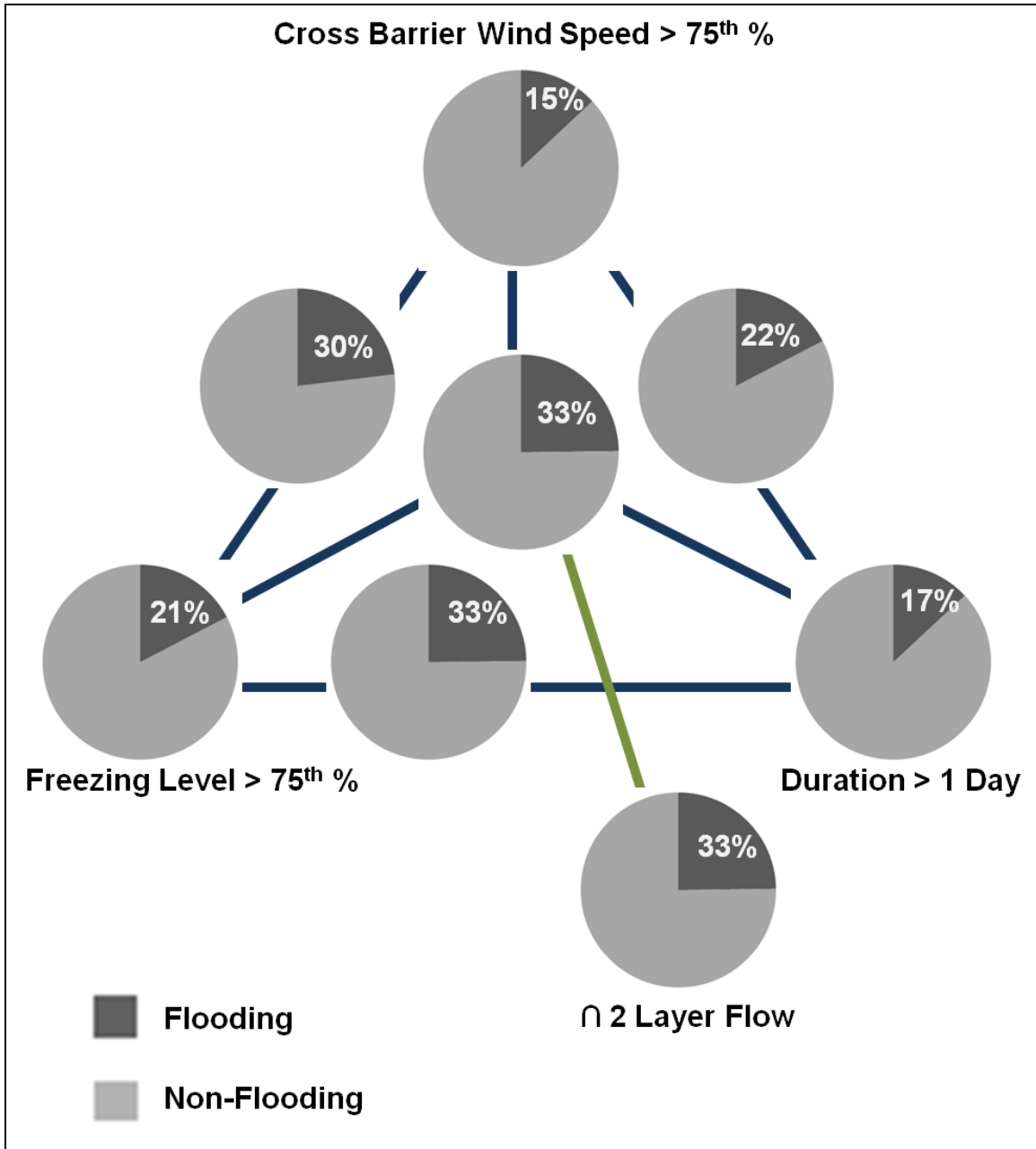


Figure 26. Same as Figure 22, showing critical score index (CSI) for each environmental condition.

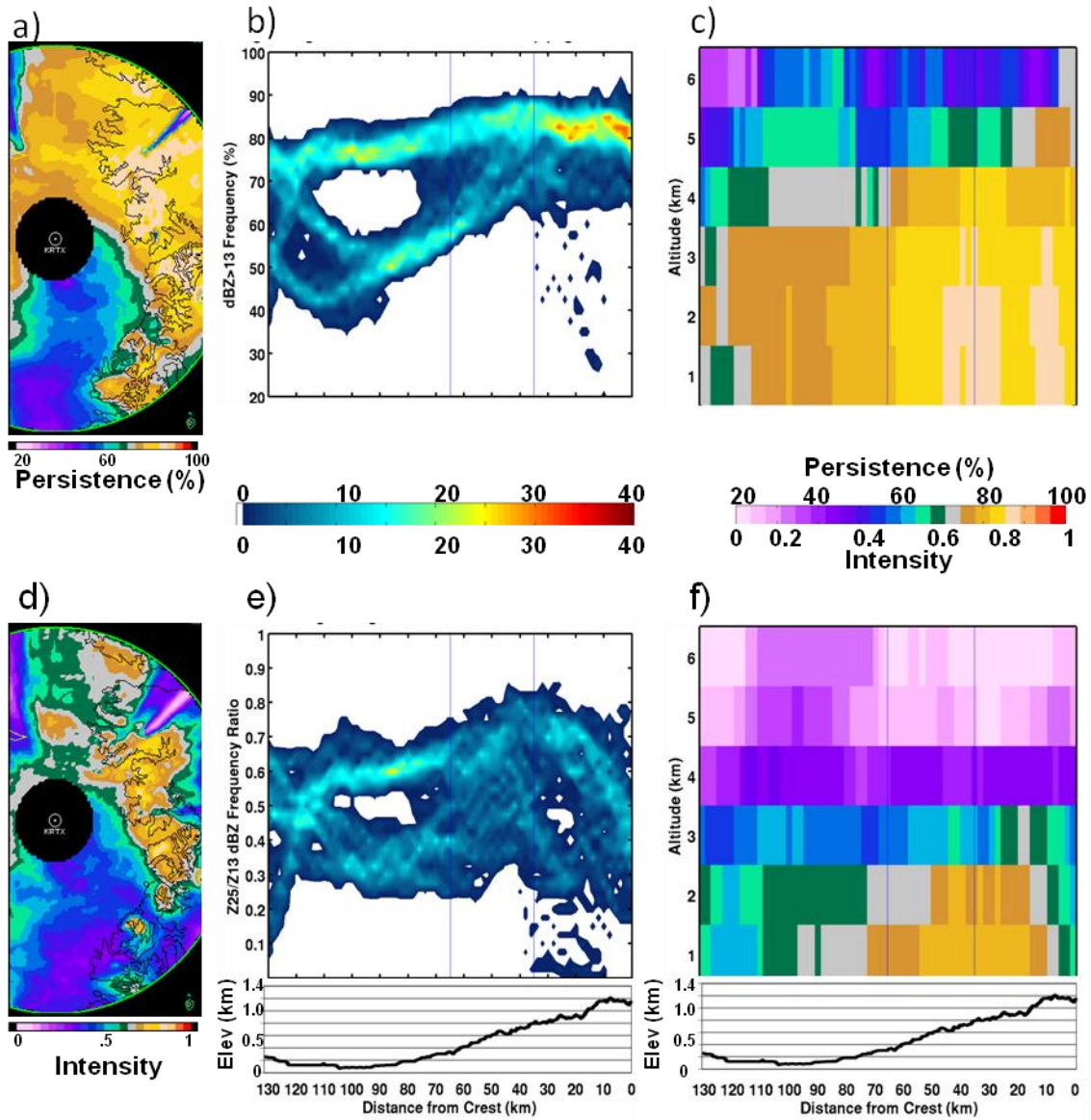


Figure 27. Radar composite of 12-hour periods that did not flood and were associated with cross-barrier winds and freezing level greater than their 75<sup>th</sup> percentiles and having storm durations greater than 24 hours. The median terrain elevation is shown for reference. (a) Horizontal cross-section of precipitation persistence at 2 km altitude. (b) CFDD of precipitation persistence at 2 km altitude. (c) Cross-section of 75<sup>th</sup> percentile values of persistence. (d) Same as (a) for precipitation intensity. (e) Same as (b) for precipitation intensity. (f) Same as (c) for precipitation intensity.

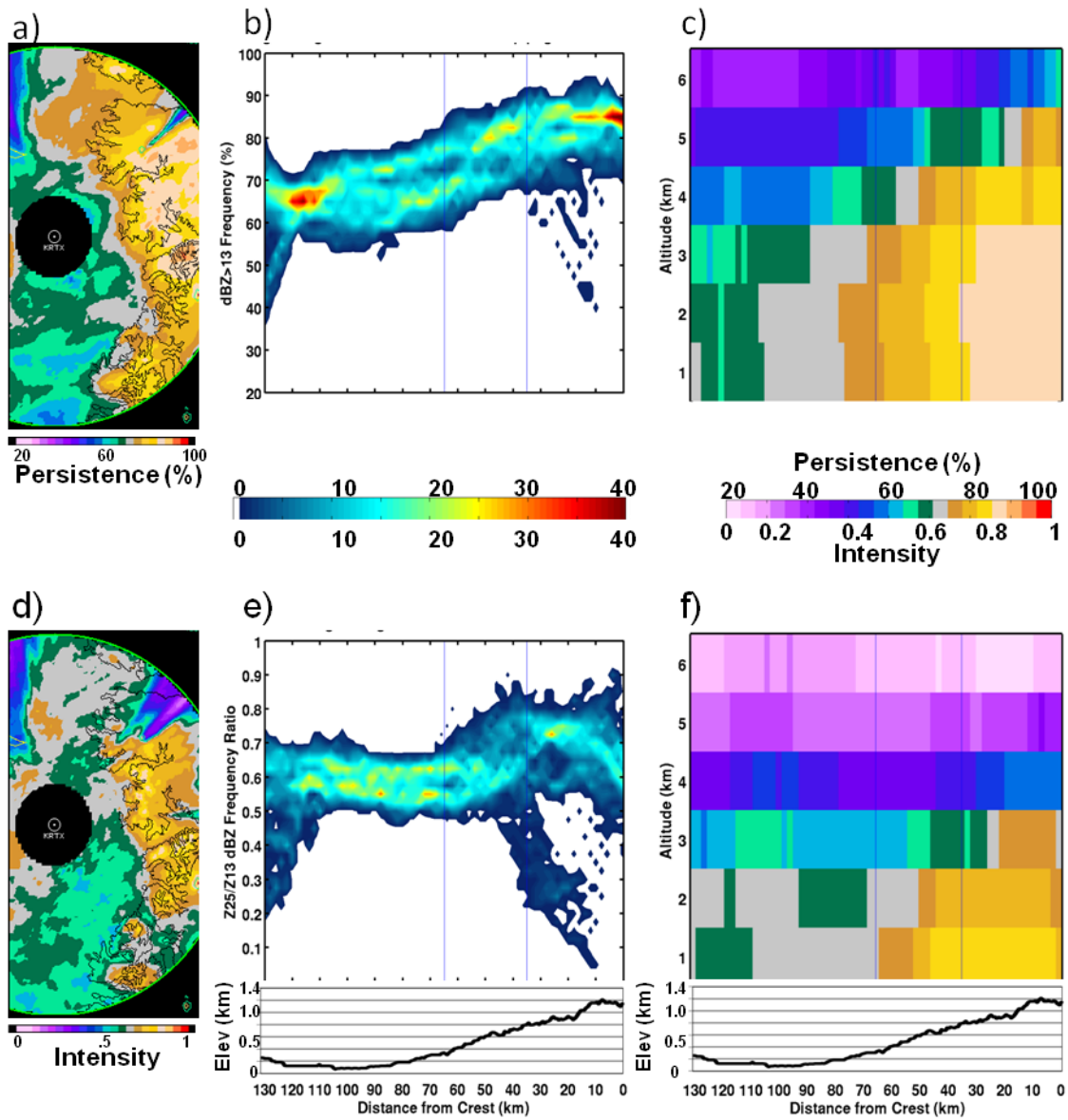


Figure 28. Same as Figure 23, for 12-hour periods that did flood and were associated with cross-barrier winds and freezing level greater than their 75<sup>th</sup> percentiles and having storm durations greater than 24 hours. The median terrain elevation is shown for reference.

## BIBLIOGRAPHY

- Bao, J.W., S.A. Michelson, P.J. Neiman, F.M. Ralph, and J.M. Wilczak,  
2006: Interpretation of Enhanced Integrated Water Vapor Bands Associated with  
Extratropical Cyclones: Their Formation and Connection to Tropical  
Moisture. *Mon. Wea. Rev.*, **134**, 1063–1080.
- Barnes S. L., 1980: Report on a meeting to establish a common Doppler radar data  
exchange format. *Bull. Amer. Meteor. Soc.*, 61, 1401–1404.
- Bougeault, P., P. Binder, A. Buzzi, R. Dirks, R. Houze, J. Kuettner, R. B. Smith, R.  
Steinacker, and H. Volkert, 2001: The MAP Special Observing Period. *Bull.*  
*Amer. Meteor. Soc.*, **82**, 433–462.
- Cayan, D.R., and J.O. Roads, 1984: Local Relationships between United States West  
Coast Precipitation and Monthly Mean Circulation Parameters. *Mon. Wea.*  
*Rev.*, **112**, 1276–1282.
- Colle, B. A., 2004: Sensitivity of orographic precipitation to changing ambient conditions  
and terrain geometries: An idealized modeling perspective. *J. Atmos. Sci.*, **61**,  
588–606.
- Colle, B. A., M. F. Garvert, J. B. Wolfe, C. F. Mass, and C. P. Woods, 2005: The 13– 14  
December 2001 IMPROVE-2 Event. Part III: Simulated microphysical budgets  
and sensitivity studies. *J. Atmos. Sci.*, **62**, 3535–3558.

- Colle, B. A., S. E. Yuter, 2007: The impact of coastal boundaries and small hills on the precipitation distribution across southern Connecticut and Long Island, NY. *Mon. Wea. Rev.*, **135**, 933-954.
- Colle, B.A., 2008: Two-Dimensional Idealized Simulations of the Impact of Multiple Windward Ridges on Orographic Precipitation. *J. Atmos. Sci.*, **65**, 509–523.
- Colle, B.A., M.F. Garvert, J.B. Wolfe, C.F. Mass, and C.P. Woods, 2005: The 13–14 December 2001 IMPROVE-2 Event. Part III: Simulated Microphysical Budgets and Sensitivity Studies. *J. Atmos. Sci.*, **62**, 3535–3558.
- Daly, C., R. P. Neilson, and D. L. Phillips, 1994: A statistical-topographic model for mapping climatological precipitation over mountainous terrain. *J. Appl. Meteor.*, **33**, 140–158.
- Durrant D. R., and J. B. Klemp, 1982: On the effects of moisture on the Brunt–Väisälä frequency. *J. Atmos. Sci.*, **39**, 2152–2158.
- Garvert, M. F., B. A. Colle, and C. F. Mass, 2005: The 13–14 December 2001 IMPROVE-2 Event. Part I: Synoptic and mesoscale evolution and comparison with a mesoscale model simulation. *J. Atmos. Sci.*, **62**, 3474–3492.
- Garvert, M. F., B. Smull, and C. Mass, 2007: Multiscale mountain waves influencing a major orographic precipitation event. *J. Atmos. Sci.*, **64**, 711–737.

- Garvert, M. F., C. P. Woods, B. A. Colle, C. F. Mass, P. V. Hobbs, M. T. Stoelinga, and J. B. Wolfe, 2005: The 13–14 December 2001 IMPROVE-2 Event. Part II: Comparisons of MM5 model simulations of clouds and precipitation with observations. *J. Atmos. Sci.*, **62**, 3520–3534.
- Guirguis, K.J., and R. Avissar, 2008: A Precipitation Climatology and Dataset Intercomparison for the Western United States. *J. Hydrometeor.*, **9**, 825–841.
- Guirguis, K.J., and R. Avissar, 2008: An Analysis of Precipitation Variability, Persistence, and Observational Data Uncertainty in the Western United States. *J. Hydrometeor.*, **9**, 843–865.
- Guarente, B. A., B. F. Jewett, G. M. McFarquhar, and R. A. Rauber, 2007: WRF simulations of a severe squall line: Comparison against high-resolution BAMEX observations. Presentation, 12th Conf. on Mesoscale Processes, Amer. Meteor. Soc., Waterville Valley, NH.
- Hagen, M., and S. E. Yuter, 2003: Relations between radar reflectivity, liquid water content, and rainfall rate during the MAP-SOP. *Quart. J. Roy. Meteor. Soc.*, special MAP issue, **129**, 477–493.
- Houze, R. A., Jr., and S. Medina, 2005: Turbulence as a mechanism for orographic precipitation enhancement. *J. Atmos. Sci.*, **62**, 3599–3623.

- Houze, R. A., Jr., C. N. James, and S. Medina, 2001: Radar observations of precipitation and airflow on the Mediterranean side of the Alps: Autumn 1998 and 1999. *Quart. J. Roy. Meteor. Soc.*, **127**, 2537-2558.
- James, C. N. and R. A. Houze Jr., 2001: A real-time four-dimensional Doppler dealiasing scheme. *J. Atmos. Ocean. Tech.*, **18**, 1674–1683.
- James, C. N. and R. A. Houze Jr., 2005: Modification of precipitation by coastal orography in storms crossing Northern California. *Mon. Wea. Rev.*, **133**, 3110–3131.
- James, C. N., S. R. Brodzik, H. Edmon, R. A. Houze Jr., and S. E. Yuter, 2000: Radar data processing and visualization over complex terrain. *Wea. Forecasting*, **15**, 327–338.
- Lundquist, J.D., P.J. Neiman, B. Martner, A.B. White, D.J. Gattas, and F.M. Ralph, 2008: Rain versus Snow in the Sierra Nevada, California: Comparing Doppler Profiling Radar and Surface Observations of Melting Level. *J. Hydrometeor.*, **9**, 194–211.
- Mass, C., 1981: Topographically Forced Convergence in Western Washington State. *Mon. Wea. Rev.*, **109**, 1335–1347.
- Medina S., and R. A. Houze Jr., 2003: Air motions and precipitation growth in Alpine storms. *Quart. J. Roy. Meteor. Soc.*, **129**, 345–371.

- Medina S., B. F. Smull, R. A. Houze Jr., and M. Steiner, 2005: Cross-barrier flow during orographic precipitation events: Results from MAP and IMPROVE. *J. Atmos. Sci.*, **62**, 3580–3598.
- Medina, S., E. Sukovich, and R.A. Houze, 2007: Vertical Structures of Precipitation in Cyclones Crossing the Oregon Cascades. *Mon. Wea. Rev.*, **135**, 3565–3586.
- Mote, P., and P. Salathe, 2009: Chapter 1 – Scenarios in *The Washington Climate Change Impacts Assessment: Evaluating Washington's Future in a Changing Climate*. The Climate Impacts Group University of Washington, 21-43.
- Neiman, P.J., F.M. Ralph, A.B. White, D.E. Kingsmill, and P.O.G. Persson, 2002: The Statistical Relationship between Upslope Flow and Rainfall in California's Coastal Mountains: Observations during CALJET. *Mon. Wea. Rev.*, **130**, 1468–1492.
- Neiman, P.J., F.M. Ralph, G.A. Wick, J.D. Lundquist, and M.D. Dettinger, 2008: Meteorological Characteristics and Overland Precipitation Impacts of Atmospheric Rivers Affecting the West Coast of North America Based on Eight Years of SSM/I Satellite Observations. *J. Hydrometeor.*, **9**, 22–47.
- Neiman, P.J., P.O.G. Persson, F. Martin Ralph, D.P. Jorgensen, A.B. White, and D.E. Kingsmill, 2004: Modification of Fronts and Precipitation by Coastal Blocking

- during an Intense Landfalling Winter Storm in Southern California: Observations during CALJET. *Mon. Wea. Rev.*, **132**, 242–273.
- Peters, G., B. Fischer, H. Münster, M. Clemens, and A. Wagner, 2005: Profiles of Raindrop Size Distributions as Retrieved by Microrain Radars. *J. Appl. Meteor.*, **44**, 1930–1949.
- Ralph, F.M., P.J. Neiman, and G.A. Wick, 2004: Satellite and CALJET Aircraft Observations of Atmospheric Rivers over the Eastern North Pacific Ocean during the Winter of 1997/98. *Mon. Wea. Rev.*, **132**, 1721–1745.
- Ralph, F.M., P.J. Neiman, and R. Rotunno, 2005: Dropsonde Observations in Low-Level Jets over the Northeastern Pacific Ocean from CALJET-1998 and PACJET-2001: Mean Vertical-Profile and Atmospheric-River Characteristics. *Mon. Wea. Rev.*, **133**, 889–910.
- Ralph, F.M., P.J. Neiman, D.E. Kingsmill, P.O.G. Persson, A.B. White, E.T. Strem, E.D. Andrews, and R.C. Antweiler, 2003: The Impact of a Prominent Rain Shadow on Flooding in California's Santa Cruz Mountains: A CALJET Case Study and Sensitivity to the ENSO Cycle. *J. Hydrometeor.*, **4**, 1243–1264.
- Reinecke, P.A., and D.R. Durran, 2008: Estimating Topographic Blocking Using a Froude Number When the Static Stability Is Nonuniform. *J. Atmos. Sci.*, **65**, 1035–1048.

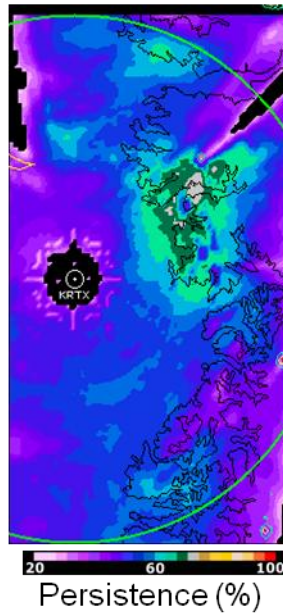
- Rotunno, R. and R. A. Houze Jr., 2007. Lessons on orographic precipitation from the Mesoscale Alpine Programme. *Quart. J. Roy. Meteor. Soc.*, **133**, 811–830.
- Rotunno, R. and R. Ferretti, 2003: Orographic effects on rainfall in MAP cases IOP2b and IOP8. *Quart. J. Roy. Meteor. Soc.*, **129**, 373-390.
- Rotunno, R., and R. Ferretti, 2001: Mechanisms of Intense Alpine Rainfall. *J. Atmos. Sci.*, **58**, 1732–1749.
- Smith, B. L., S. E. Yuter, P. J. Neiman and D. E. Kingsmill, 2009: Water vapor fluxes and orographic precipitation over Northern California associated with a land-falling atmospheric river. *Mon. Wea. Rev.*, accepted.
- Stoelinga, M. T., P. V. Hobbs, C. F. Mass, J. D. Locatelli, B. A. Colle, R. A. Houze Jr., A. L. Rangno, N. A. Bond, B. F. Smull, R. M. Rasmussen, G. Thompson, and B. R. Colman, 2003: Improvement of Microphysical Parameterization through Observational Verification Experiment. *Bull. of Amer. Meteor. Soc.*, **84**, 1807–1826.
- U.S. Army Corps of Engineers, 1956: Snow hydrology: Summary report of the snow investigations. North Pacific Division, U.S. Army Corps of Engineers, 437 pp.
- White, A. B., P. J. Neiman, F. M. Ralph, D. E. Kingsmill, and P. O. G. Persson, 2003: Coastal orographic rainfall processes observed by radar during the California Land-Falling Jets Experiment. *J. Hydrometeor.*, **4**, 264–282.

- White, A.B., D.J. Gattas, E.T. Strem, F.M. Ralph, and P.J. Neiman, 2002: An Automated Brightband Height Detection Algorithm for Use with Doppler Radar Spectral Moments. *J. Atmos. Oceanic Technol.*, **19**, 687–697.
- Whitney, W.M., R.L. Doherty, and B.R. Colman, 1993: A Methodology for Predicting the Puget Sound Convergence Zone and Its Associated Weather. *Wea. Forecasting*, **8**, 214–222.
- Woods, C.P., M.T. Stoelinga, J.D. Locatelli, and P.V. Hobbs, 2005: Microphysical Processes and Synergistic Interaction between Frontal and Orographic Forcing of Precipitation during the 13 December 2001 IMPROVE-2 Event over the Oregon Cascades. *J. Atmos. Sci.*, **62**, 3493–3519.
- Yuter, S. E., and R. A. Houze, Jr., 1995: Three-dimensional kinematic and microphysical evolution of Florida cumulonimbus. Part II: Frequency distribution of vertical velocity, reflectivity, and differential reflectivity. *Mon. Wea. Rev.*, **123**, 1941-1963.
- Yuter, S. E., 2003: Precipitation Radar. *Encyclopedia of Atmospheric Sciences*, (J. R. Holton, J. Pyle, and J. Curry, Eds.), 1833-1851.
- Yuter, S.E., et al. 2009: Observational sensitivity study of the temporal and spatial patterns of orographic precipitation for winter storms near Portland, Oregon. *To be submitted to the Journal of Hydrometeorology*.

Zhu, Y. and R. E. Newell, 1998: A proposed algorithm for moisture fluxes from atmospheric rivers. *Mon. Wea. Rev.*, **126**, 725–735.

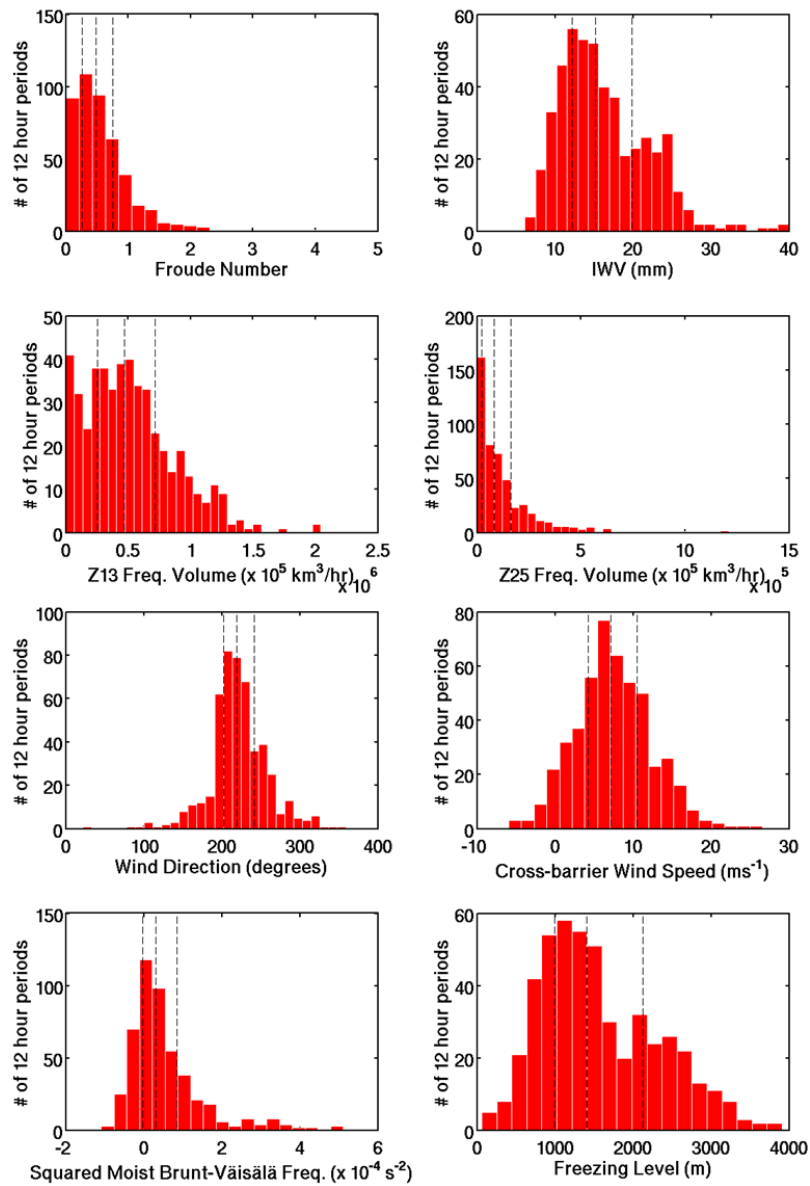
## APPENDIX

## Appendix A



Radar composite of precipitation persistence using 12-hour periods  $\pm 6$  hours of SLE soundings with wind direction, freezing level, and cross-barrier wind speed of typical values (between 25<sup>th</sup> and 75<sup>th</sup> percentiles); and  $Nm^2$  with values greater than the 75<sup>th</sup> percentile (Table 2). Horizontal cross-section is shown at 2 km altitude. This composite indicates upstream enhancement ahead of the Cascade barrier occurring when all conditions are typical and the atmosphere is stable. The increased precipitation persistence extends ~15 km from the Lewis River Valley region out into the Willamette Valley. This is consistent with the findings of MAP, and upstream enhancement occurring when the atmosphere is stable (MH2003).

## Appendix B



Histograms of the environmental parameters calculated from all SLE soundings during the study period and the Z frequency volumes per hour are shown in Appendix B. The

25<sup>th</sup>, 50<sup>th</sup>, and 75<sup>th</sup> percentiles are shown by thin black dotted lines. It should be noted that most do not exhibit a Gaussian distribution. The distributions for this dataset do not differ significantly from the distributions found by Yuter et al. (2009) of the same variables from SLE soundings.

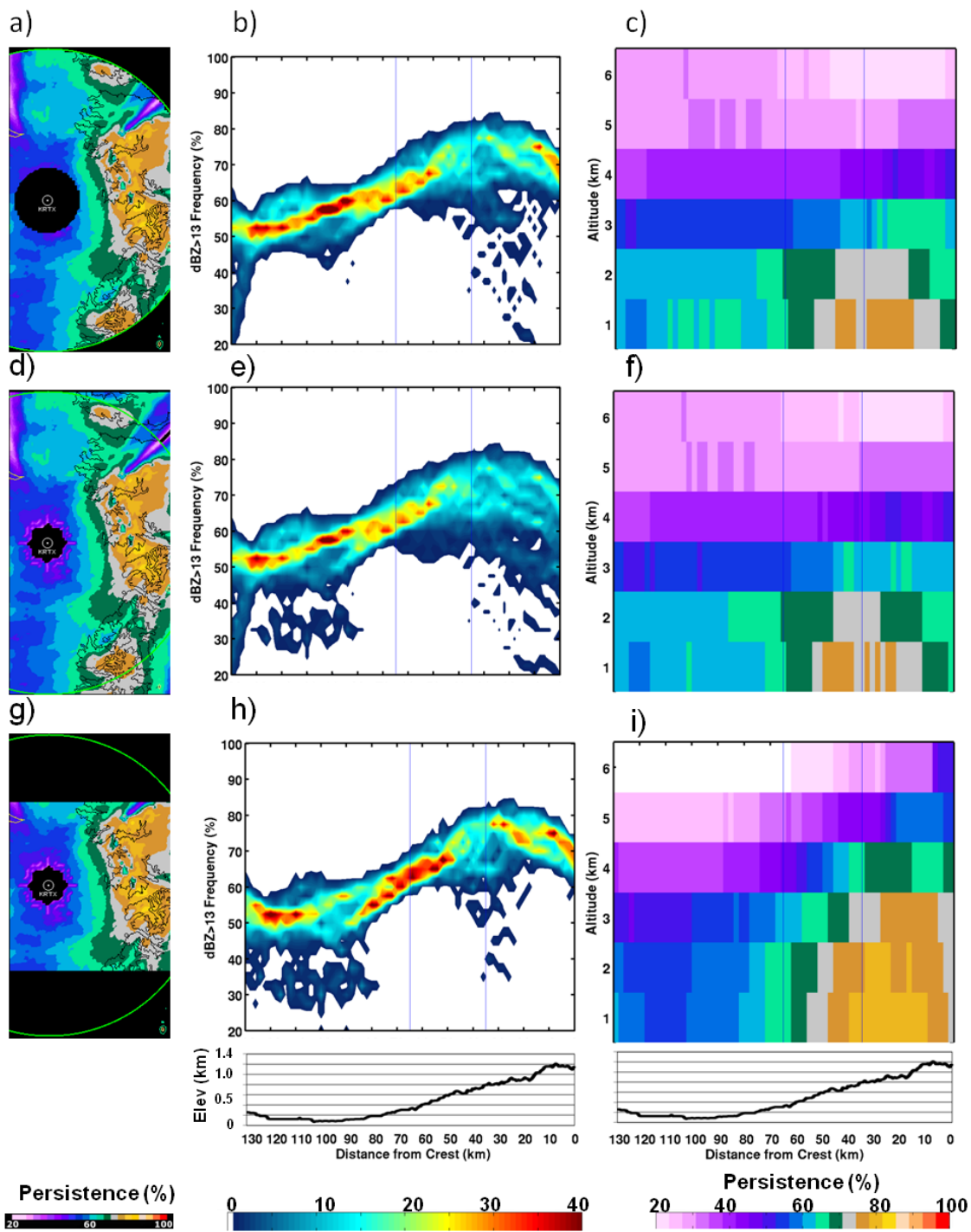
## Appendix C

The domain selection for this study leads to more data being sampled over the Willamette Valley compared to the upper slope of the Cascades. The impact of this could affect the CFDDs and cross-sections of the 75<sup>th</sup> percentiles because they sample the data in north-south swaths. At the eastern extent of the domain, the north to south extent of the domain is over 130 km, while over the Willamette Valley the north to south extent is 240 km. This difference is primarily a product of the range of the radar and us cropping the domain at 120 km distance from KRTX because the beam width is larger than our interpolated grid of 2 km. To test the sensitivity of cropping the radar data beyond this distance, CFDDs and cross-sections of the 75<sup>th</sup> percentiles are created with and without the cropped data. For reference, the radar composites are created for 12-hour periods with a high freezing level with typical (between 25<sup>th</sup> and 75<sup>th</sup> percentile) stability and cross-barrier wind speed.

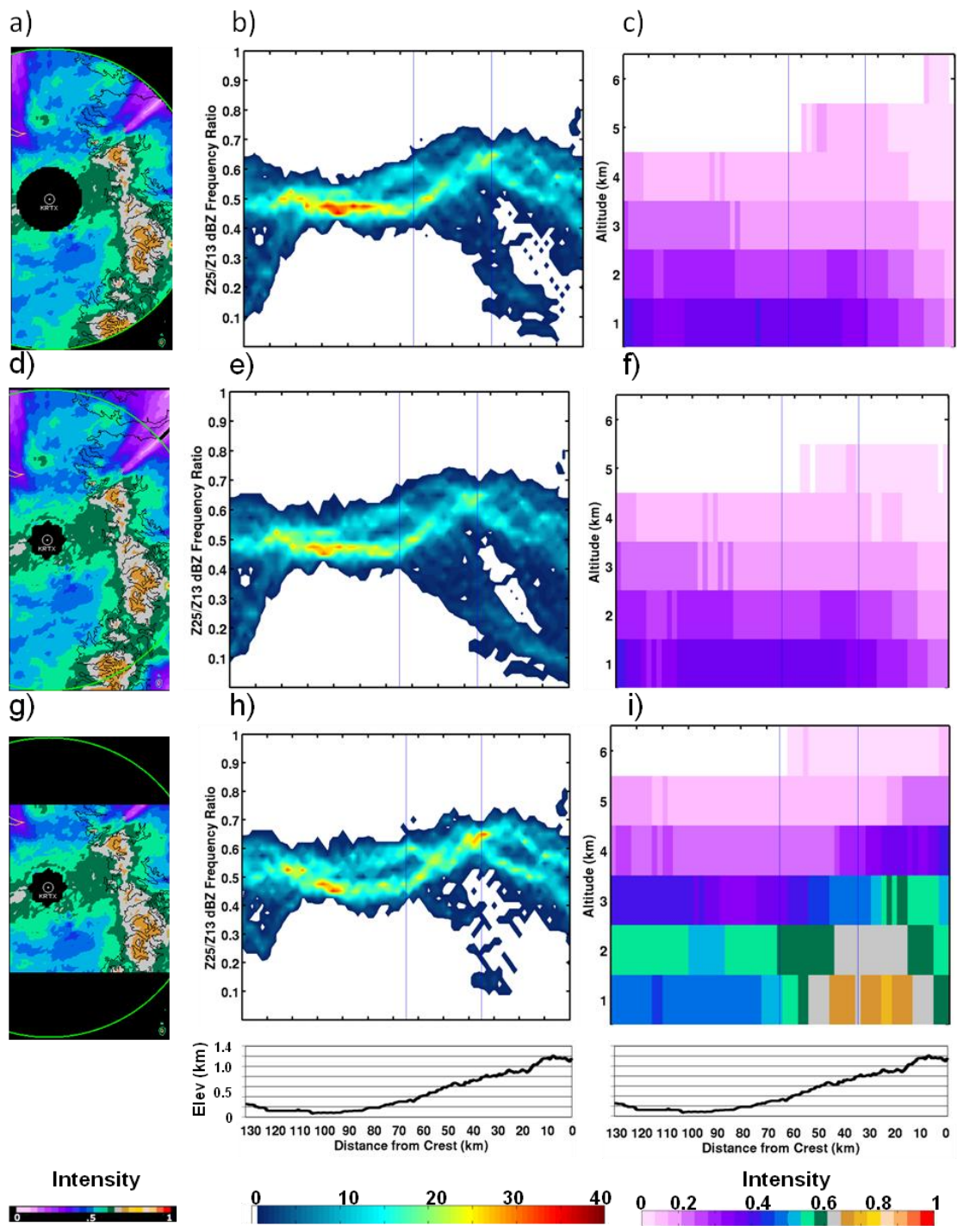
Radar composites and the associated CFDDs and cross-sections were created for the same data sample with cropping of the North-South extent of the data. The data within our already defined domain was confined to 65 km north and south of KRTX. This creates a square of data, with the same amount of data sampled over the Willamette Valley as over the Cascades.

This testing shows that there is not a significant change in the CFDDs and cross-section of 75<sup>th</sup> percentiles when the data is cropped to the 120 km range. There is also not

a significant difference to the CFDDs when the domain is cropped north and south. There is however a large difference in the cross-section of the 75<sup>th</sup> percentiles for the last case. This is most likely due to a smaller sample size leading to a different distribution and 75<sup>th</sup> percentile value. This study wanted to use as much quality data as possible over the domain so we decided to use the data cropped to the 120 km range ring. Investigators wanting a different use for the data might want to use the smaller domain.



Precipitation persistence composite of 12-hour periods with freezing level greater than the 75<sup>th</sup> percentile and stability and cross-barrier flow between 25<sup>th</sup> and 75<sup>th</sup> percentiles. CFDDs and cross-section of 75<sup>th</sup> percentiles shown for data cropped and not cropped at the 120 km range distance. (a) Horizontal cross-section of precipitation persistence at 2 km altitude with radar data cropped at 120 km range from KRTX. (b) CFDD of precipitation persistence at 2 km altitude with radar data cropped at 120 km range. (c) Cross-section of 75<sup>th</sup> percentiles of precipitation persistence with radar data cropped at 120 km range. (d) Horizontal cross-section of precipitation persistence at 2 km altitude with radar data not cropped at 120 km range from KRTX. (e) CFDD of precipitation persistence at 2 km altitude with radar data not cropped at 120 km range. (f) Cross-section of 75<sup>th</sup> percentiles of precipitation persistence with radar data not cropped at 120 km range. (g) Horizontal cross-section of precipitation persistence at 2 km altitude with radar data cropped at 65 km north and south of KRTX. (h) CFDD of precipitation persistence at 2 km altitude with radar data cropped at 65 km north and south of KRTX. (i) Cross-section of 75<sup>th</sup> percentiles of precipitation persistence with radar data cropped at 65 km north and south of KRTX.



Precipitation intensity composite of 12-hour periods with freezing level greater than the 75<sup>th</sup> percentile and stability and cross-barrier flow between 25<sup>th</sup> and 75<sup>th</sup> percentiles. CFDDs and cross-section of 75<sup>th</sup> percentiles shown for data cropped and not cropped at the 120 km range distance. (a) Horizontal cross-section of precipitation intensity at 2 km altitude with radar data cropped at 120 km range from KRTX. (b) CFDD of precipitation intensity at 2 km altitude with radar data cropped at 120 km range. (c) Cross-section of 75<sup>th</sup> percentiles of precipitation intensity with radar data cropped at 120 km range. (d) Horizontal cross-section of precipitation intensity at 2 km altitude with radar data not cropped at 120 km range from KRTX. (e) CFDD of precipitation intensity at 2 km altitude with radar data not cropped at 120 km range. (f) Cross-section of 75<sup>th</sup> percentiles of precipitation intensity with radar data not cropped at 120 km range. (g) Horizontal cross-section of precipitation intensity at 2 km altitude with radar data cropped at 65 km north and south of KRTX. (h) CFDD of precipitation intensity at 2 km altitude with radar data cropped at 65 km north and south of KRTX. (i) Cross-section of 75<sup>th</sup> percentiles of precipitation intensity with radar data cropped at 65 km north and south of KRTX.